NAVAL POSTGRADUATE SCHOOL
Monterey, California

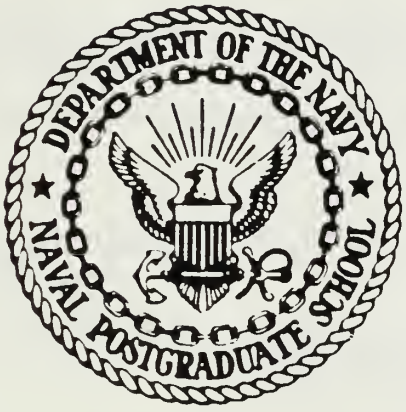

THESIS

AUTOMATED SATELLITE CLOUD ANALYSIS: A MULTISPECTRAL APPROACH TO THE PROBLEM OF SNOW/CLOUD DISCRIMINATION

by

Robert C. Allen, Jr.

June 1987

Co-Advisor Philip A. Durkee
Co-Advisor Carlyle H. Wash

Approved for public release; distribution is unlimited.

SECURITY CLASSIFICATION OF THIS PAGE

REPORT DOCUMENTATION PAGE

1a REPORT SECURITY CLASSIFICATION Unclassified	1b RESTRICTIVE MARKINGS
2a SECURITY CLASSIFICATION AUTHORITY	3 DISTRIBUTION/AVAILABILITY OF REPORT Approved for public release; distribution is unlimited.
2b DECLASSIFICATION/DOWNGRADING SCHEDULE	
4 PERFORMING ORGANIZATION REPORT NUMBER(S)	5 MONITORING ORGANIZATION REPORT NUMBER(S)
6a NAME OF PERFORMING ORGANIZATION Naval Postgraduate School 6b OFFICE SYMBOL (If applicable) 63	7a NAME OF MONITORING ORGANIZATION Naval Postgraduate School
6c ADDRESS (City, State, and ZIP Code) Monterey, CA 93943-5000	7b ADDRESS (City, State, and ZIP Code) Monterey, CA 93943-5000
8a NAME OF FUNDING/SPONSORING ORGANIZATION 8b OFFICE SYMBOL (If applicable)	9 PROCUREMENT INSTRUMENT IDENTIFICATION NUMBER
8c ADDRESS (City, State, and ZIP Code)	10 SOURCE OF FUNDING NUMBERS PROGRAM ELEMENT NO / PROJECT NO / TASK NO / WORK UNIT ACCESSION NO

11 TITLE (Include Security Classification) AUTOMATED SATELLITE CLOUD ANALYSIS: A MULTISPECTRAL APPROACH TO THE PROBLEM OF SNOW/CLOUD DISCRIMINATION

12 PERSONAL AUTHOR(S)
Allen, Robert C. Jr.

13a TYPE OF REPORT	13b TIME COVERED	14 DATE OF REPORT (Year Month Day)	15 PAGE COUNT
Master's Thesis	FROM ____ TO ____	1987 June	114

16 SUPPLEMENTARY NOTATION

17 COSATI CODES			18 SUBJECT TERMS (Continue on reverse if necessary and identify by block number)
FIELD	GROUP	SUB-GROUP	snow/cloud discrimination, AVHRR channel 3, satellite cloud analysis

19 ABSTRACT (Continue on reverse if necessary and identify by block number)

An algorithm is developed and evaluated for discriminating among clouds, snow cover and clear land. The multispectral technique uses daytime images of AVHRR channels 1 (0.63μm), 3 (3.7μm) and 4 (11.0μm). Reflectance is derived for channel 3 by using the channel 4 emission temperature to estimate and remove the channel 3 thermal emission. Separation of clouds from snow and land is based primarily on this derived channel 3 reflectance. Using this technique, observed reflectance in channel 3 is 2 to 4 percent for snow, 3 to 10 percent for land, 2 to 27 percent for ice clouds and 8 to 36 percent for liquid clouds. These values overlap for thin cirrus and snow, so the routine then attempts analysis of cirrus based on its different transmissive properties between channels 3 and 4. Six images were analyzed and the total cloud cover was verified against a total of 110 conventional surface observations using the standard categories of clear, scattered, broken and overcast. The routine was quite successful, with the analyzed sky cover being within category for 55 percent of the stations, one category different for 33 percent, 2 categories different for 9 percent and 3 categories different for 3 percent of the stations. A major remaining problem is discrimination between ice clouds and snow cover due to the great similarity of reflective properties of these two surfaces.

20 DISTRIBUTION/AVAILABILITY OF ABSTRACT	21 ABSTRACT SECURITY CLASSIFICATION	
☒ UNCLASSIFIED/UNLIMITED ☐ SAME AS RPT ☐ DTIC USERS	Unclassified	
22a NAME OF RESPONSIBLE INDIVIDUAL Philip A. Durkee/Carlyle H. Wash	22b TELEPHONE (Include Area Code) 408-646-3465/2295	22c OFFICE SYMBOL 63De/63Wx

DD FORM 1473, 84 MAR — 83 APR edition may be used until exhausted. All other editions are obsolete.

SECURITY CLASSIFICATION OF THIS PAGE

Approved for public release; distribution is unlimited.

Automated Satellite Cloud Analysis: A Multispectral Approach to the Problem of Snow/Cloud Discrimination

by

Robert C. Allen, Jr.
Captain, United States Air Force
B.A., Eastern Illinois University, 1982

Submitted in partial fulfillment of the
requirements for the degree of

MASTER OF SCIENCE IN METEOROLOGY

from the

NAVAL POSTGRADUATE SCHOOL
June 1987

ABSTRACT

An algorithm is developed and evaluated for discriminating among clouds, snow cover and clear land. The multispectral technique uses daytime images of AVHRR channels 1 (0.63μm), 3 (3.7μm) and 4 (11.0μm). Reflectance is derived for channel 3 by using the channel 4 emission temperature to estimate and remove the channel 3 thermal emission. Separation of clouds from snow and land is based primarily on this derived channel 3 reflectance. Using this technique, observed reflectance in channel 3 is 2 to 4 percent for snow, 3 to 10 percent for land, 2 to 27 percent for ice clouds and 8 to 36 percent for liquid clouds. These values overlap for thin cirrus and snow, so the routine then attempts analysis of cirrus based on its different transmissive properties between channels 3 and 4. Six images were analyzed and the total cloud cover was verified against a total of 110 conventional surface observations using the standard categories of clear, scattered, broken and overcast. The routine was quite successful, with the analyzed sky cover being within category for 55 percent of the stations, one category different for 33 percent, 2 categories different for 9 percent and 3 categories different for 3 percent of the stations. A major remaining problem is discrimination between ice clouds and snow cover due to the great similarity of reflective properties of these two surfaces.

TABLE OF CONTENTS

LIST OF TABLES

LIST OF FIGURES

ACKNOWLEDGEMENTS

I would like to thank Dr. James T. Bunting of the Air Force Geophysics Laboratory, Hanscom AFB, MA, for providing the background information used in this thesis, and also for further ideas and encouragement along the way. Mr. Doug Burks of the Naval Postgraduate School Meteorology Department was especially helpful by providing his expertise on the computer system and many ideas on streamlining the processing. Mr. Burks wrote the software that handled data calibration and navigation, and all the graphics-interfacing software used to generate the images presented here. The images were produced on a Digital Equipment Corporation VAX 11/780 computer system and COMTAL Vision One/20 image processing system at the Naval Postgraduate School. I also thank Professors Durkee and Wash for their patience and guidance throughout this project. Finally, without the support of my wife, Jean, and our sons I could not have completed this work.

I. AUTOMATED CLOUD ANALYSIS

A. INTRODUCTION

One of the critical factors in the conduct of military operations is knowledge of the environment in which they are to take place, particularly regarding cloud cover. Clouds can dramatically affect such missions as aerial intelligence gathering, air refueling and tactical employment of weapons that use the visible-infrared portion of the electromagnetic spectrum to designate targets. Cloud cover analyses can be accomplished with synoptic weather observations but data-void areas severely limit their usefulness. Techniques have been developed to produce cloud analyses using satellite imagery, where human image analysts make subjective interpretations of cloud cover based on brightness and texture contrasts. Manual analysis takes a great deal of time to accomplish and quick response for large geographical areas in critical situations is very difficult. The Air Force Global Weather Central (AFGWC) developed an automated cloud analysis system in order to introduce objectivity to the analysis procedure based on sound physical principles, and also to address the Air Force's mission requirement for rapid cloud analyses. The 3-Dimensional Nephanalysis (3DNEPH) system became operational in January 1970. This pioneering effort did not have the benefit of experience from other systems. Various improvements have been made over the years, and in 1984 a second-generation model called the Real-Time Nephanalysis (RTNEPH) became operational. It is the only known automated system capable of processing and interpreting the tremendous volume of satellite data that are available today and integrating them with conventional information to provide a high-resolution, three-dimensional cloud analysis data base for the entire world.

In addition to global analysis models, efforts have been made to develop automated analysis routines for minicomputers that can be used in a theater or battlefield environment. Wash *et al.* (1985) developed a cloud and precipitation analysis program for an interactive minicomputer system which uses geostationary infrared and visual data. This type of analysis package could be used in a weather station or a tactical van to provide cloud cover analyses and forecasts to operational commanders on a real-time basis.

B. SNOW/CLOUD DISCRIMINATION

Various long-term problems have plagued automated systems, one of the most significant being discriminating low clouds from snow cover. Middle and high clouds can be detected against snow cover due to the thermal contrast detectable at infrared wavelengths, but in the regions of the electromagnetic spectrum used most often in satellite analysis, low clouds and snow cover have similar radiometric properties. In the visible portion of the spectrum both have high albedos, and in the infrared portion both have similar thermal properties. Thus there is little contrast in images at these spectral wavelengths.

Bunting *et al.* (1977) discussed the reflectance properties of snow and clouds at visible and near-infrared wavelengths, using data from the Earth Resources Experiment Package which flew aboard Skylab. They analyzed the imagery in pairs: one set in the visible spectrum and the other in the near-infrared spectrum (1.55μm to 1.75μm). The two sets showed high reflectance for snow, water clouds and ice clouds in the visible spectrum, but in the near-infrared the reflectance was high for water clouds, medium for ice clouds and very low for snow. They concluded that these differences could be the basis for an automated routine which makes an analysis decision based on the ratio of visible reflectance to near-infrared reflectance. Bunting and d'Entremont (1982) tested six automated classifiers on data from a special Defense Meteorological Satellite Program (DMSP) sensor in the wavelength band from 1.51μm to 1.63μm, along with visual and infrared data. They used the classifiers successfully to distinguish water clouds, ice clouds, snow cover and other cloud-free surfaces. Their technique was so successful that plans are now being made to add this sensor as an operational component of the DMSP satellite.

Kidder and Wu (1984) showed that there is a contrast in brightness temperature between snow and low clouds in daytime imagery of channel 3 (3.7μm) of the National Oceanic and Atmospheric Administration (NOAA) polar-orbiting Advanced Very High Resolution Radiometer (AVHRR). They related this contrast to solar reflection, which is a substantial component of the channel 3 radiance measurement along with thermal emission. Since low clouds and snow have similar emission temperatures, this contrast is the result of a difference in their solar reflection at 3.7μm which, in theory, is just a few percent for snow and about 20 percent for clouds. This results in a warmer brightness temperature for clouds (darker image) than for snow (whiter image).

Fye (1978) documented the 3DNEPH system and discussed the problem of snow/cloud discrimination. Cloud cover is overestimated in areas of new snow and in areas where the ice analysis contains too little ice. Underestimation or no analysis of clouds results when snow melts rapidly or the ice analysis contains too much ice. Presently, the system uses the AFGWC Snow Cover Model and grid points that have snow or ice as a background are treated as missing for the cloud analysis routine. A solution to this problem has not yet been implemented on the RTNEPH system. This has a significant effect on the analysis in the late fall through early spring because about 30 to 35 percent of all the model grid points in the northern hemisphere are snow and/or ice covered.

C. THESIS OBJECTIVES

The first objective of this thesis is to calculate and report solar reflectance in AVHRR channel 3 using a method that estimates the thermal emission from channel 4 and removes this portion from the channel 3 radiance measurement. Derived values will be compared to theoretical 3.7μm reflectance for snow cover, land and clouds. During the 1990's both NOAA and the Department of Defense plan to launch satellites with a 1.6μm sensor for daytime snow/cloud discrimination, and the NOAA satellite will have a 3.7μm sensor for use at night. Even with this change, there are good reasons to pursue this work now. First, by the time the new sensor flies there will be over 10 years of archived daytime 3.7μm imagery. Second, since snow and cloud reflectances are similar at 1.6μm and 3.7μm, a data set of reflectances from channel 3 would be very useful in testing software for the new sensor.

The second objective of this thesis is to use calculated channel 3 reflectance to develop an automated cloud analysis routine that separates snow cover, clouds and snow-free land. It will be designed to handle various combinations of cloud and surface features, but the focus is on the separation of low clouds and snow. The routine will not rely on sophisticated statistical analysis or on artificial image enhancement techniques, but rather on basic physical principles of radiative transfer in the earth's atmosphere. In addition to similar visible reflective properties, low clouds and snow have nearly identical infrared thermal properties. Because of this and the results of the previously mentioned studies, the routine is based primarily on the reflective properties of these surfaces in AVHRR channel 3. A multispectral technique is developed and evaluated using visible and infrared data along with channel 3 to process daytime AVHRR images.

In Chapter II the necessary theoretical background is presented. The details of satellite data processing are presented along with a theoretical discussion of the reflection and emission characteristics of the cloud and surface features to be analyzed. A discussion of the satellite data and the techniques of data analysis are presented in Chapter III along with observed values of channel 1 and channel 3 reflectance for these surfaces. Finally, the analysis routine is developed using these measured reflectance values. Chapter IV discusses the performance of the analysis routine when applied to six images containing various combinations of snow and cloud cover, and sun-satellite geometry. Data were taken from two different NOAA satellites to illustrate the general utility of the routine and to provide additional statistical independence to the verification of the analyses. Total sky cover on the analyses is verified against the available surface observations using the standard conditions of clear, scattered, broken and overcast. The reported statistics include the percentage of stations where the analyzed sky cover matched the observed sky cover, and the percentage of stations with a one-category, a two-category and a three-category difference between the analyzed and observed sky cover.

II. THEORETICAL FOUNDATION

A. DISCUSSION

In general terms, detection of cloud cover on a satellite image depends on the contrast between the clouds and their background. At visible wavelengths this contrast is in terms of reflectance differences, and at infrared wavelengths this contrast is in terms of differences in brightness temperature. At middle infrared wavelengths (AVHRR channel 3) the contrast is a mixture of difference in reflectance and difference in brightness temperature. This chapter presents the theoretical foundation for the algorithm developed in this thesis. Included here is a theoretical discussion of the reflective and thermal characteristics of the features to be analyzed, the satellite data processing to derive these properties and a preliminary assessment concerning how the routine might work based on the theoretical characteristics of the features. See Appendix A for a list of symbols and constants used.

Two visible and two thermal infrared channels are available on the AVHRR instrument. In addition to these, channel 3 is at a wavelength (3.7μm) that has contributions from both thermal emission and solar reflection. Channel 1 (0.63μm) is completely in the visible spectrum while channel 2 (0.87μm) extends into the near-infrared portion of the spectrum. Channel 1 is the visible channel used in this study. It will be shown later that the method of deriving the reflectance in channel 3 depends on channel 4 (11.0μm), so it is the infrared channel used in this study.

Throughout this thesis, the satellite-measured radiance during daytime is approximated as follows:

$$L = \varepsilon B(T) + r(\theta_o,\theta,\varphi)I\cos\theta_o \qquad (2.1)$$

The first term on the right hand side is the contribution to the measured radiance from thermal emission of the viewed surface assuming the transmissivity between it and the satellite is 1.0. The amount of radiance from thermal emission reaching the satellite is determined by the emissivity (ε) of the viewed surface. The Planck function relates the emitted monochromatic intensity with the wavenumber and temperature of the emitting surface as follows:

$$B(\nu,T) = \frac{2hc^2\nu^3}{\exp(hc\nu/KT) - 1} \qquad (2.2)$$

The second term on the right hand side of Eq. 2.1 is the contribution to the measured radiance due to solar reflection. The amount of reflected solar radiance reaching the satellite is determined by the incident solar radiance (I) which is weighted by the cosine of the solar zenith angle (θ_o), and the reflectance (r) of the viewed surface. The directional reflectance is a function of the solar zenith angle, the satellite zenith angle (θ) and the horizontal angle between them (φ). This sun-satellite geometry is illustrated in Fig. 2.1. Isotropic reflectance is related to the directional reflectance by the anisotropic reflectance factor (f). This relationship is expressed as (Taylor and Stowe, 1984):

$$r_3 = \frac{r_3(\theta_o,\theta,\varphi)}{f} \qquad (2.3)$$

The anisotropic reflectance factor arises due to the directional dependence of the scattering mechanisms. It is the ratio between the radiant exitance in a given direction assuming the surface reflects isotropically, and the actual radiant exitance. For example, a radiance measurement in a given direction with a factor of 1.0 gives the correct radiant exitance, while a factor of 1.5 with the same measurement means the isotropic assumption would yield a 50 percent overestimate of radiant exitance.

It is assumed that any viewed clouds are optically thick so that upwelling radiance from below them does not reach the satellite. This assumption breaks down when considering thin cirrus clouds and this will be discussed later.

B. REFLECTANCE

This section reviews the results of various theoretical studies concerning the reflective properties of the surfaces to be analyzed. These values then will be used for comparison to observed values in the data analysis section of Chapter III.

1. Liquid Clouds

The reflectance of liquid clouds is dependent upon cloud optical thickness and sun-satellite geometry. Tables 1 and 2 show the results of reflectance calculations from the model of Shettle and Weinman (1970), which is based on Mie theory and the delta-Eddington approximation. The values show the expected extremes of reflectance for clouds of various physical properties which are coded in the tables as follows:

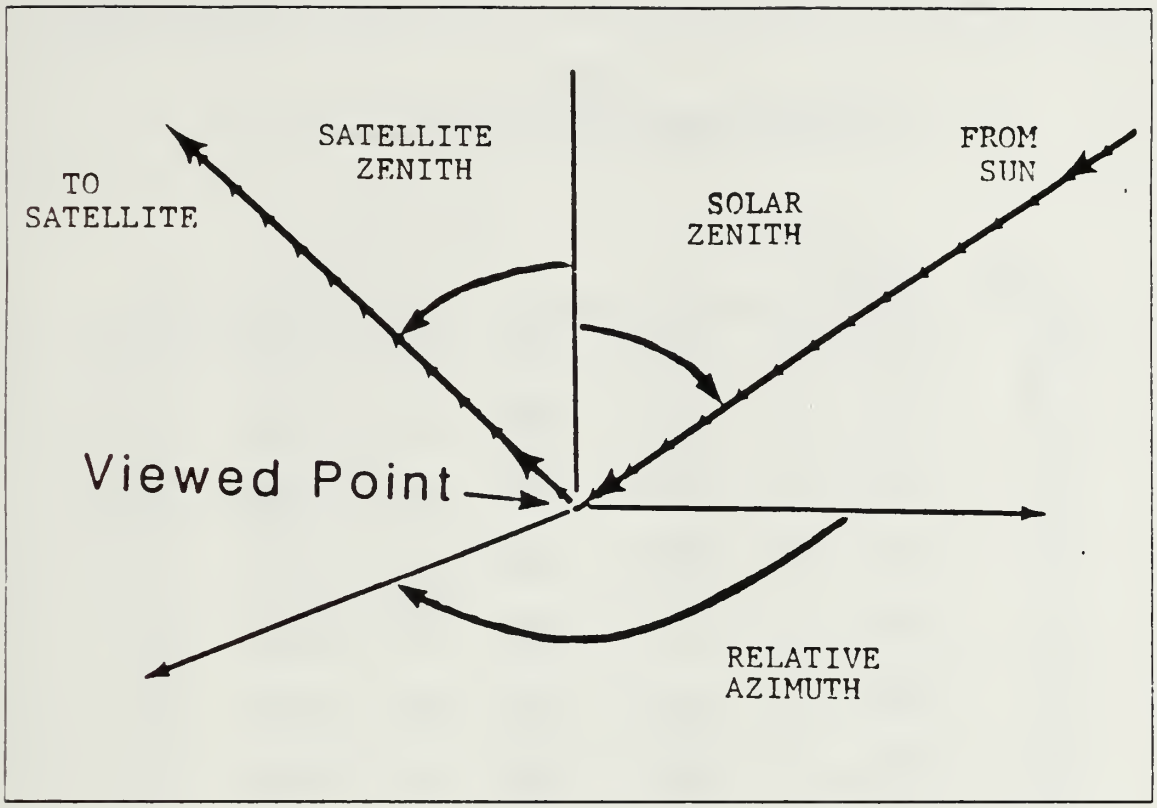

Fig. 2.1 Earth-sun-satellite geometry.

1. First digit = liquid water content ($\times 10^{-1}$ g/m^3).
2. Second digit = droplet mode radius ($\times 10^{-1}$ μm).

For example, a code of 66 means the liquid water content is 0.6g/m^3 and the droplet mode radius is 0.6μm. The extinction coefficient, asymmetry factor and the single scattering albedo were used as input to the computer program along with the cloud optical depth and solar zenith angle to calculate the reflectance.

Table 1 shows the strong dependence of reflectance at visible wavelengths on cloud thickness. To a lesser degree this reflectance is dependent on liquid water content and solar zenith angle. The same general characteristics for 3.7μm are apparent in Table 2, but in this case the dependence on liquid water content and cloud thickness is not as great as the dependence on solar zenith angle. Absorption by liquid water at 3.7μm is so great that a cloud has essentially an infinite optical depth with a thickness of just a few tens of meters. These values agree closely with those reported by Hansen and Pollack (1970), and Welch *et al.* (1980). The major differences in the values listed in Table 2.6 of Welch *et al.* and the values listed here in Tables 1 and 2

TABLE 1

Calculated reflectance of water clouds at 0.63μm.

Code	Cloud Thickness	Solar Zenith 45	55	65	75	85
34	100m	0.375	0.431	0.500	0.577	0.656
	1000m	0.861	0.875	0.890	0.907	0.924
36	100m	0.269	0.327	0.404	0.499	0.596
	1000m	0.794	0.814	0.836	0.861	0.887
38	100m	0.209	0.262	0.340	0.446	0.561
	1000m	0.735	0.760	0.790	0.821	0.854
64	100m	0.549	0.593	0.642	0.696	0.753
	1000m	0.926	0.933	0.941	0.950	0.959
66	100m	0.428	0.482	0.545	0.614	0.686
	1000m	0.885	0.897	0.909	0.923	0.937
68	100m	0.349	0.406	0.478	0.559	0.641
	1000m	0.848	0.863	0.879	0.897	0.916
94	100m	0.648	0.682	0.721	0.763	0.807
	1000m	0.949	0.954	0.960	0.966	0.972
96	100m	0.532	0.577	0.628	0.684	0.743
	1000m	0.921	0.928	0.937	0.947	0.956
98	100m	0.448	0.500	0.561	0.628	0.697
	1000m	0.893	0.904	0.915	0.928	0.941

are due to the different solar zenith angles and a slight difference in wavelength. These calculated values, along with the measured values which will be reported in Chapter III, are used to determine the thresholds for separating liquid cloud surfaces from other surfaces.

2. **Ice Clouds**

The reflectance of ice clouds is not only dependent on the optical thickness and sun-satellite geometry as with liquid clouds, but also on complicating factors of ice particle shape and size distribution. Modeling the reflectance of ice crystals is an extremely difficult task because of these complications. Welch *et al.* (1980) discussed the physical characteristics and properties of ice crystals. They reported reflectance at 3.3μm, which is slightly outside the channel 3 spectral band, for a wide range of shape and particle size distributions. They indicated a range of values of reflectance at 3.3μm

TABLE 2

Calculated reflectance of water clouds at 3.7μm.

Code	Cloud Thickness	Solar Zenith 45	55	65	75	85
34	100m	0.244	0.280	0.326	0.384	0.456
	1000m	0.250	0.285	0.330	0.387	0.459
36	100m	0.159	0.192	0.235	0.290	0.361
	1000m	0.170	0.201	0.242	0.295	0.365
38	100m	0.112	0.141	0.180	0.232	0.298
	1000m	0.125	0.152	0.189	0.237	0.302
64	100m	0.250	0.285	0.330	0.387	0.459
	1000m	0.250	0.285	0.330	0.387	0.459
66	100m	0.169	0.200	0.241	0.295	0.364
	1000m	0.170	0.201	0.242	0.295	0.365
68	100m	0.124	0.151	0.188	0.237	0.302
	1000m	0.125	0.152	0.189	0.237	0.302
94	100m	0.250	0.285	0.330	0.387	0.459
	1000m	0.250	0.285	0.330	0.387	0.459
96	100m	0.170	0.201	0.242	0.295	0.365
	1000m	0.170	0.201	0.242	0.295	0.365
98	100m	0.125	0.152	0.189	0.237	0.302
	1000m	0.125	0.152	0.189	0.237	0.302

of 0.001 to 0.007 with a solar zenith angle of 0°. They also calculated reflectance at 0.55μm and 0.76μm. The values at both of these wavelengths are similar and can be used as an estimate of reflectance in channel 1 which is between these two wavelengths. They reported a range of reflectance values for 0.55μm and 0.76μm between 0.01 and 0.93 with most values in the range from 0.60 to 0.90. Arking and Childs (1985) reported channel 3 reflectance of ice clouds as a function of optical thickness between 0.1 and 100.0, and of ice particle size between 2μm and 32μm. Their values of channel 3 reflectance range between 0.01 and 0.30 for a solar zenith angle of 60°, a satellite zenith angle of 41.2°, and a relative azimuth angle of 110°. Finally, Bunting (personal communication, 1986) reported an average channel 3 reflectance of 0.05 for ice clouds. Reflectance of ice clouds will be measured and reported in Chapter III, and the measured and theoretical values will be used to establish thresholds for separating ice clouds from the other surfaces.

3. **Clear Land**

The reflectance of clear land is dependent upon soil type, vegetation type and coverage, and moisture content. Bunting and Hardy (1984) reported the albedo of snow-free land at visible wavelengths to be approximately 0.10. Bunting (personal communication, 1986) reported an average value of 0.15 at 3.7μm.

4. **Snow Cover**

The reflectance of snow is dependent upon a variety of factors: snow grain size, liquid water content, solar zenith angle, cloud cover, snowpack thickness and impurities. Wiscombe and Warren (1980) developed a model for the spectral albedo of snow and considered these factors:

1. Snow grain size or age. The albedo of snow decreases as it ages due to an increase in absorption and more forward scattering of larger grains which develop from the aging process. At visible wavelengths, the reduction is only about 10-15 percent, but at 3.7μm this reduction is a factor of 2 or more for grain radii larger than 100μm.
2. Liquid water content. Snow melt affects albedo because water replaces air between individual snow grains. This has the effect of increasing the effective snow grain size. The reduction in albedo is not as great as the effect due to aging.
3. Solar zenith angle. Albedo increases at all wavelengths as the zenith angle increases. Relative to an overhead sun, the albedo increases only by a few percent at visible wavelengths, but at 3.7μm the albedo increases from less than 0.005 to 0.025. These calculations are for a flat snow surface. When the snow pack is uneven due to hills and valleys, the solar zenith angle is a function of location, causing the albedo to vary within a small area. This may occur on a large enough scale to appear as a variation of brightness from pixel to pixel on a satellite image.
4. Effects of cloud cover. Cloud cover influences spectral albedo by changing direct radiation into diffuse radiation. This should be important only when there is thin cloud cover through which a satellite can see snow cover.
5. Snowpack thickness. If the snow cover is thin, the underlying surface affects the albedo. This effect is wavelength dependent and also dependent on the snow grain size. Because of the strong absorption at 3.7μm, less than 1 mm of depth is required to make the snow cover optically semi-infinite. At visible wavelengths the radiation can penetrate to greater depths and in general, a depth of 20 cm is required in order not to "see" the ground.

Wiscombe and Warren (1980) used Mie theory for single scattering and the delta-Eddington approximation for multiple scattering. Their model allows snow albedo calculations for the entire solar spectrum ($0.3\mu m \leq \lambda \leq 5.0\mu m$) for diffusely or directly

incident radiation at any zenith angle. Calculations of snow albedo were made using this model and compared with observations, and there is good agreement at 3.7μm. Values used for comparison with observations in this study are 0.005-0.025. This range of values is applicable for a semi-infinite snow pack with a grain radius of 50μm to 200μm, and a range of solar zenith angles between 40° and 80°. At visible wavelengths, there is a considerable difference between calculated and measured values which they attributed to impurities in the snow. This is an important consideration for this study since the cases are taken sufficiently close to the industrialized regions of the United States and Canada. The value for 0.63μm should be 0.75 to 0.80 for semi-infinite snow cover with a solar zenith angle of 60°. This value is less for a smaller zenith angle or snow cover of less than 20 cm in depth, and higher for a greater solar zenith angle.

C. INFRARED TRANSMISSIVE PROPERTIES

As shown above, snow and optically thin ice clouds have similar reflective properties, thus another method must be used to separate them. It is expected that, since the channel 3 reflectance of optically thick ice clouds is greater than that of snow, the thresholds in the analysis routine can be tuned finely enough to correctly analyze most of the ice clouds, but there will be cases for which this fails. The easiest approach would be to analyze as much of the data as possible in an effort to find a threshold emission temperature between snow and ice clouds. However, this does not allow for the fact that snow is warmer in the fall and spring than in the middle of winter, and also for the fact that snow temperature is a function of latitude. In reality, the snow temperature is too variable to allow an analysis routine to use a single threshold value. One could get around this problem if the surface temperature for each pixel were known, but the analysis routine will be designed to work with the satellite data alone so this is not possible.

Another possibility is to take advantage of the difference in the transmissive properties of ice clouds between channel 3 and channel 4. The assumption made at the beginning that no radiance from below the clouds reaches the satellite breaks down in the case of thin cirrus. However, this can be exploited to differentiate between cirrus and snow because of a difference in transmissivity between channels 3 and 4. Eq. 2.1 for the channels 3 and 4 radiance measurement becomes:

$$L_3 = \tau_3\varepsilon_3(s)B_3(T_s) + \varepsilon_3(c)B_3(T_c) + r_3(\theta_o,\theta,\varphi)I\cos\theta_o \qquad (2.4)$$

and

$$L_4 = \tau_4 \varepsilon_4(s) B_4(T_s) + \varepsilon_4(c) B_4(T_c), \qquad (2.5)$$

where τ is the transmissivity of the cirrus cloud.

Neglecting solar reflection and assuming the clouds are optically thick, the measured radiance for both channels includes only the thermal emission from the cloud, and inverting Eq. 2.2 to get a brightness temperature yields the same result for both channels. In the case of thin cirrus, and again neglecting solar reflection, there is a difference in its transmissive properties between channels 3 and 4, which results in a different amount of surface radiance for each channel getting through the clouds to be sensed by the satellite. Stephens (1981) argued that, first, the Planck blackbody emission as a function of temperature varies differently for these two channels and, second, cirrus transmits more surface radiation at 3.7μm than at 11μm. When cirrus is present, the channel 3 cloud emission is small compared to surface emission, making the satellite-measured radiance for this channel primarily due to surface radiation transmitted through the cirrus cloud. In channel 4 there is significant emission from within the cloud compared to surface emission and the cloud transmits less of the surface radiation. The satellite-measured radiance in channel 4 is then primarily due to emission from the cloud. Both of these effects combine to produce a difference in brightness temperature.

In reality, the effects of solar reflection cannot be neglected. Solar reflection is larger in channel 3 than in channel 4 and this contributes to the difference in brightness temperature. The magnitude of solar reflection for cirrus is comparable to the magnitude of thermal emission, thus solar reflection contributes a great deal to the difference in brightness temperature. However, there are certain conditions under which the reflectance of snow cover and ice clouds is equal, so when comparing Eq. 2.4 for these surfaces, the third term is the same for both. Under these conditions the distinction between them arises because τ_3 is not equal to τ_4 for cirrus, but τ_3 is very nearly equal to τ_4 for the clear sky case. Fig. 2.2 shows this difference in brightness temperature for cirrus clouds from model calculations of Stephens (1981). The dotted line is a nighttime case, which shows the effects of thermal emission alone, and the solid line is a daytime case with an overhead sun. In this study the solar zenith angle is greater than 45° so the temperature difference due to reflection is less, but still

significant. At very low optical depths the temperature difference is nearly all due to solar reflection and the upwelling radiance is essentially all from the surface. The temperature difference increases as optical depth increases and, for the nighttime case, reaches maximum at an optical depth of about 2.0. At higher optical depths the temperature difference continues to increase, but the effect of transmissivity differences decreases to zero. At optical depths higher than 10.0 the difference in brightness temperature is due only to solar reflection.

The distinction between cirrus and snow cover (clear sky) can be made only when the effect of the difference in its transmissive properties between channels 3 and 4 outweighs the effect of solar reflection. For example, assume a cirrus cloud is to be analyzed that has a channel 3 reflectance of 0.03. There is a total difference in brightness temperature of 10K, half due to reflection and half due to to transmissive differences between channels 3 and 4. Snow cover with the same reflectance produces a temperature difference of 5K so in this case it is distinguished from cirrus. If the snow reflectance is higher than the cloud reflectance, the temperature difference is also higher and this would eliminate some or all of the distinction present when the snow reflectance is the same as that of cirrus. If the effect of transmissivity differences had contributed 8K to the total temperature difference in this example, only 2K would be subject to being eliminated by variability of solar reflection. As seen in Fig 2.2, the effect of transmissivity differences is larger than the effect of solar reflection only for optical depths between about 0.5 and 2.0. It remains to be seen how many cirrus cloud pixels will be handled correctly based on channel 3 reflectance alone and thus how many of the remaining cirrus clouds will fall within this optical depth range.

For this study, a unitless factor is derived from this difference in brightness temperature for use by the analysis routine. Development of this temperature factor begins with normalizing the temperature difference by the channel 4 brightness temperature:

$$F_T = \frac{T_3 - T_4}{T_4} \tag{2.6}$$

It follows that, using this approach, the temperature factor is proportional to the ratio of the channels 3 and 4 brightness temperatures:

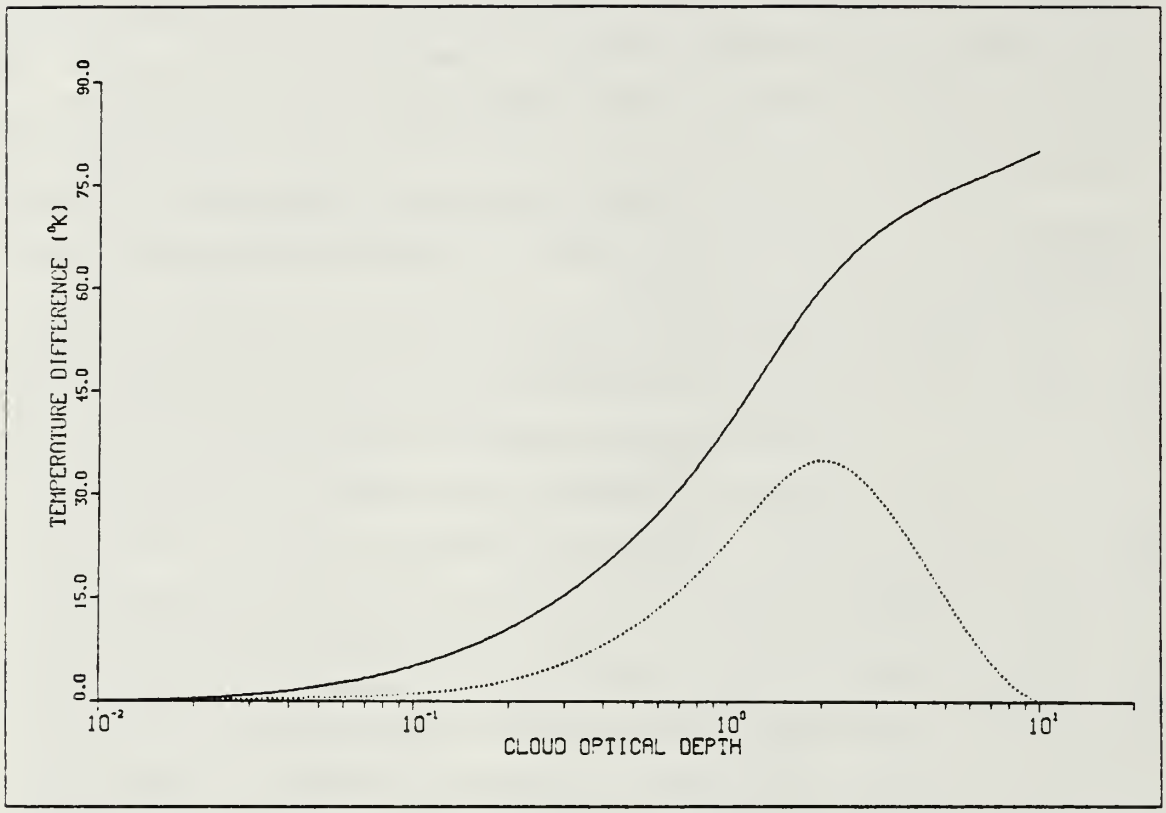

Fig. 2.2 Difference in channel 3 and channel 4 brightness temperature as a function of cloud optical depth. Solid line is daytime case with overhead sun, dotted line is nighttime case (adapted from Stephens, 1981).

$$F_T = \frac{T_3}{T_4} - 1 \qquad (2.7)$$

These numbers range from approximately zero for the clear sky case to values between zero and 1.0 when thin cirrus is present. It is nearly impossible to choose a threshold from this small range of values, so the reciprocal of Eq. 2.7 was used to choose a threshold. This means that, in qualitative terms, for the clear sky case the temperature difference is small, making the factor large. For thin cirrus the temperature difference is larger, making the factor smaller than with the clear sky case.

D. SATELLITE DATA PROCESSING

This section discusses how the satellite data were processed in order to derive the reflective and thermal properties presented above.

1. Channel 1

AVHRR Channel 1 data are preflight calibrated in terms of albedo (Lauritson *et al.*, 1979). The measured directional reflectance was converted to isotropic reflectance by weighting the measurement by the cosine of the solar zenith angle and the anisotropic reflectance factor as discussed above. This reflectance is very similar for snow cover and clouds, but it can be used to separate land from clouds and snow cover.

2. Channel 3

Channel 3 AVHRR data are calibrated in units of $mW/m^2 \cdot sr \cdot cm^{-1}$, and during daytime the radiance measurement in this channel is comprised of both solar reflection and thermal emission. Fig. 2.3 illustrates the relative contributions of each using incident solar irradiance measurements of Thekaekara *et al.* (1969), assuming a typical cloud reflectance of 0.05 to 0.40 and assuming a Planck blackbody emission temperature of 260K. The dashed vertical lines in the figure define the approximate location of the 50 percent response function boundaries of NOAA-9 channel 3. Fig. 2.3 shows that solar reflection is the greatest contributor for most clouds, while for the lowest reflecting surfaces of ice clouds, land and snow cover the two contributions are nearly equal. Bunting (1986, personal communication) suggested the method discussed here for removing the thermal emission in channel 3. There are two major assumptions involved in using this technique (Ruff and Gruber, 1983). First, atmospheric transmission effects are neglected. The most important absorbing constituent in the atmosphere in this portion of the spectrum is water vapor and in this study the data were taken from high latitude, cold air masses where there is little water vapor present. Second, it was assumed that the emissivity of a viewed scene is 1.0. Thermal emission for the scene was then determined directly from the channel 4 radiance measurement. Error results from this assumption due to the fact that the emissivity of any surface is variable between channels 3 and 4 and not equal to 1.0. It is impractical to try to determine the emissive properties of the viewed scene so this effect was not corrected. The error resulting from these assumptions should have the greatest effect when deriving the reflectance for snow cover, land, or ice clouds because the magnitude of thermal emission for these surfaces is comparable to that of solar reflection. The least effect from the resultant error should occur with liquid clouds since for these surfaces the magnitude of solar reflection is much greater than that of thermal emission (see Fig. 2.3).

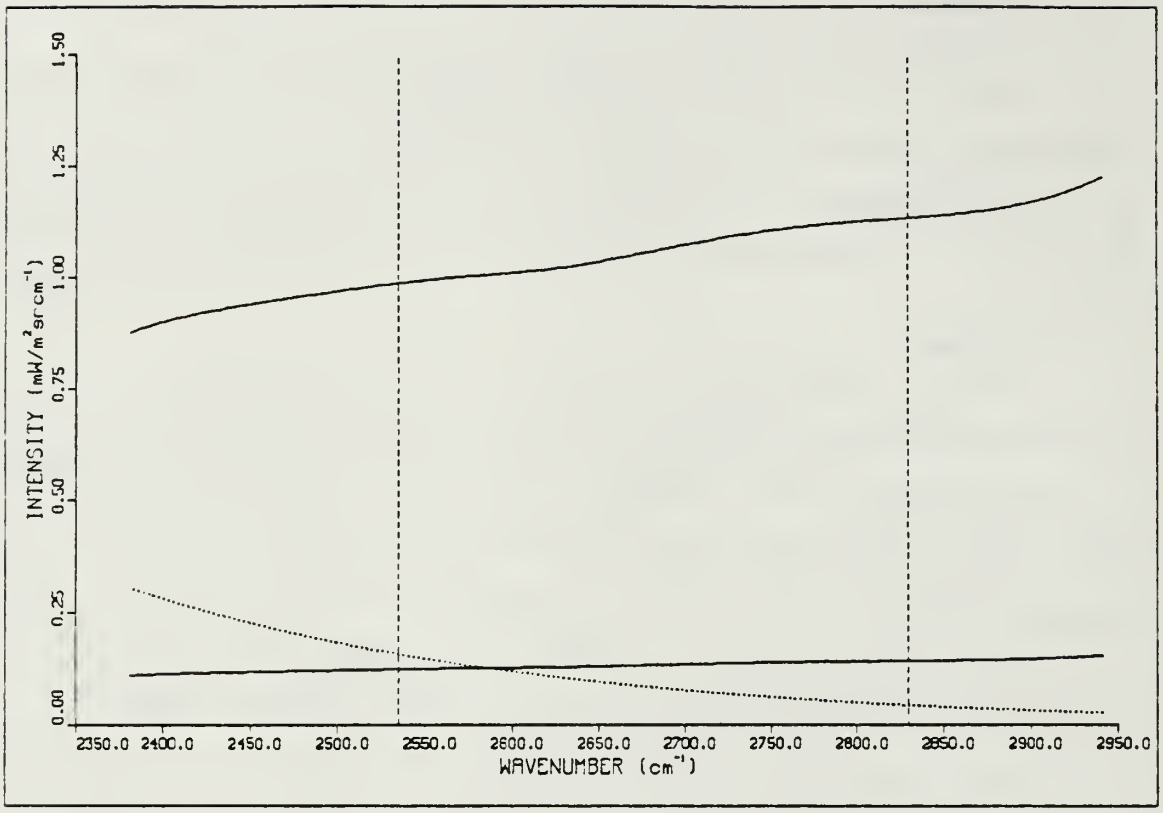

Fig. 2.3 Reflected solar intensity and terrestrial thermal intensity for channel 3. Reflectance is 5 and 40 percent, solar zenith is 60° (solid lines), blackbody temperature is 260K (dotted line).

For channel 3, Eq. 2.1 becomes:

$$L_3 = \varepsilon_3 B_3(T) + r_3(\theta_o,\theta,\varphi) I_3 \cos\theta_o \qquad (2.8)$$

See Appendix B for the calculation of the channel 3 incident solar radiance. Thermal emission for channel 3 was estimated by solving Eq. 2.1 for the Planck function based on the channel 4 measured radiance:

$$B_4(T) = L_4/\varepsilon_4 \qquad (2.9)$$

The temperature was found by inverting the Planck function, and was then used in Eq. 2.2 to find the thermal emission in channel 3.

Ignoring atmospheric absorption, emittance for channel 3 is related to reflectance by:

$$\varepsilon_3 = 1 - r_3 \tag{2.10}$$

In Eq. 2.10 isotropic radiation was assumed. Substituting Eqs. 2.3 and 2.10 into Eq. 2.8 gives:

$$L_3 = (1 - r_3)B_3(T) + r_3(I_3\cos\theta_o)f \tag{2.11}$$

Finally, solving for reflectance:

$$r_3 = \frac{L_3 - B_3(T)}{(I_3\cos\theta_o)f - B_3(T)} \tag{2.12}$$

Eq. 2.12 was used to derive the channel 3 reflectance and this calculation is the central component of the analysis routine.

To calculate the brightness temperature, the data were calibrated and then Eq. 2.2 was inverted to solve for temperature. The central wavenumber used in this calculation is based on a range of temperature values between 225K and 320K (Lauritson *et al.*, 1979), which should be a valid range of temperatures for the time of year from which the data were taken.

3. **Channel 4**

Channel 4 AVHRR data are calibrated in units of $mW/m^2 \cdot sr \cdot cm^{-1}$. A non-linear correction (Lauritson *et al.*, 1979) must be added when converting from radiance to temperature. A polynomial was fit to the published corrections for NOAA-9 for use in the computer program (Gerald and Wheatley, 1984). The polynomial derived for the NOAA-10 corrections was unstable so linear interpolation was used instead. For ease in computer processing all channel 4 temperatures were assumed to be in the range from 225K to 275K so that only one central wavenumber need be used in the calculations (Lauritson *et al.*, 1979). This range of temperatures provides adequate separation of the various features to be analyzed. Temperatures less than or greater than these were set to 225K and 275K respectively. This assumption is valid for the images processed in this study since they were from the fall and winter, and it is

unlikely that an emitting surface has a temperature outside this range at that time of year.

E. SEPARATION ALGORITHM

Based on the theoretical reflectances discussed above, an automated routine can be developed that separates the cloud and surface features. The most important separation is between clouds and snow cover and this can be accomplished by evaluating the channel 3 reflectance. The lowest theoretical channel 3 reflectance for liquid clouds is 0.11 while for snow the values range from 0.005 to 0.025. There is some overlap between ice clouds and snow but a significant number of ice cloud pixels can be correctly analyzed along with all liquid clouds. Land can be easily separated since its channel 1 reflectance is about 0.10, well below that of the remaining surfaces. When attempting to make a distinction between the remaining ice clouds and snow the routine will have to use the channel 3-channel 4 temperature factor. In this case the reflective properties are nearly identical in both channels 1 and 3 and it is hoped that their different transmissive properties between channels 3 and 4 will improve the analysis.

The ability of an automated routine to separate these surfaces depends on the amount of each of them present in a single pixel and this must be considered when the separation thresholds are derived. For example, liquid clouds and land covering a pixel together may combine to give a reflectance value that is recognized as either liquid cloud or land, or possibly neither of these. In the case of clear skies over snow cover, the measured reflectance may be significantly less than 0.75 to 0.80 because even with deep snow, buildings, roads and trees protrude above the snow cover. This is especially important in thin snow cover where the underlying surface and adjacent areas of no snow affect the measured reflectance. For a single pixel, the measured reflectance is expressed by:

$$r_1 \sim 0.70\rho_c + 0.60\rho_i + 0.10\rho_l + 0.80\rho_s \qquad (2.13)$$

and

$$r_3 \sim 0.25\rho_c + 0.05\rho_i + 0.05\rho_l + 0.02\rho_s \qquad (2.14)$$

The following examples illustrate how the pixel coverage must be taken into account when deciding on the separation thresholds:

1. If, for example, a decision were to be made between land and thin cirrus based on the channel 1 reflectance, Eq. 2.13 becomes:

$$r_1 \sim 0.60\rho_i + 0.10\rho_l$$

If the threshold channel 1 reflectance were set at 25 percent, a pixel would have to be covered by at least 30 percent of cloud in order to be recognized as such. If the pixel coverage were less, it would be analyzed as land.

2. If a decision were to be made between snow and liquid clouds based on the channel 3 reflectance, Eq. 2.14 becomes:

$$r_3 \sim 0.25\rho_c + 0.02\rho_s$$

If the threshold channel 3 reflectance were set at 10 percent, the pixel would have to be covered by at least 35 percent of cloud in order to be recognized as such. If the coverage were less, it would be analyzed as snow.

Thus when a pixel is covered by more than one of the surfaces to be analyzed, the classification that is made depends not only on the surface that dominates but also on the combined reflectance of the scene as sensed by the satellite. This is an important consideration when one is interested in analyzing thin clouds correctly and also in cases covered by this study where the difference between snow-covered and snow-free land is to be analyzed correctly. It is particularly important when using coarse-resolution geostationary data where a variable pixel composition is more likely due to the larger area covered by the individual pixels.

III. DEVELOPMENT OF THE ANALYSIS ALGORITHM

A. OVERVIEW

This chapter discusses development of the analysis algorithm. Although the primary objective was the separation of low clouds and snow cover, the thresholds were developed so the routine would also work well when snow is not present, and in the presence of high-level clouds including cirrus. First, observed reflectances from channels 1 and 3 were compared with the theoretical values from Chapter II. Then the observed values of reflectance were used to determine the separation thresholds. Using an image analysis work station, land pixels were assigned grayshade values between 0 and 25, and snow pixels were assigned grayshade values between 26 and 50. This darkened the snow pixels in relation to the cloud pixels, and this range was enough to show the boundary between snow-free land and snow-covered land, and to show some texture within each classification. Clouds were displayed as in an infrared image on a grayshade scale between 75 and 255. The temperature scale is 225K to 275K and this range allows distinction between low-level warm clouds and high-level cold clouds. Clouds were the most important part of the analysis so they were given the greatest range of grayshades. However, it is hoped that the land and snow grayshade ranges are large enough so various enhancement techniques can be employed to analyze them in greater detail if necessary.

B. SATELLITE DATA DESCRIPTION

Data for the benchmark cases were taken from the 2000-2100 GMT pass of NOAA-9 on November 9 and 10, 1986 (see Figs. 3.1 through 3.4). A winter storm passed through the upper midwestern United States and south-central Canada producing the first major snowfall of the 1986-87 season, and both of these passes cover that area. The storm left 3-10 inches of snow on the ground in North Dakota and South Dakota, and 1-3 inches in Minnesota and western Wisconsin. A typical frontal-band cloud pattern is present in the 10 November pass, with low- to mid-level enhanced cumulus clouds streaming in behind the frontal system, along with scattered snow showers (Fig. 3.3). The images have a combination of clouds over both clear land and over snow, and clear conditions with clear land and snow cover. The passes cover the area from 40° north latitude to 60° north latitude, and 80° west longitude to 115° west longitude.

Two subscenes were chosen from each pass, each of which covers an area of about 500 square kilometers. Subscene 1 of November 9 (Figs. 3.5 and 3.6) shows most of Wisconsin and Lake Michigan, western Michigan and the extreme northern portions of Illinois and Indiana. This area was covered by mainly clear land and low clouds and was sampled for these surfaces. Subscene 2 of November 9 (Figs. 3.7 and 3.8) shows the eastern half of Nebraska, western Iowa, and southeastern South Dakota. This area was chosen for the cirrus clouds that are present; there was an abundance of both thick and thin cirrus here. There was no snow on the ground in either of these November 9 subscenes. Subscene 1 of November 10 (Figs. 3.9 and 3.10) has Lake Huron in the center with most of Michigan and the southernmost portion of Canada. This area had thick and thin cirrus along with low level clouds available for sampling, but no snow on the ground. Subscene 2 of November 10 (Figs. 3.11 and 3.12) shows most of Minnesota and the eastern portions of North and South Dakota. This area had clear skies and snow cover in eastern North and South Dakota and western Minnesota, with low-level convective clouds in eastern Minnesota. There were a few of these cloud elements over the snow cover in southwestern Minnesota.

Figs. 3.1 through 3.4 show the November 9 and November 10 passes in what will be referred to as the overview format. These figures show channel 1 of both passes along with an image of derived channel 3 reflectance. There are 2048 pixels in each of approximately 2500 lines in these passes, but only every eighth line and every eighth pixel were processed and displayed. The overviews were then enlarged to cover a full 512 by 512 screen. Data were taken from seven groups of 10 by 10 pixels on the November 9 pass and six groups of 10 by 10 pixels on the November 10 pass, and these boxes are labeled in Figs. 3.2 and 3.4. Due to the way the overview for each pass was processed, these groups are actually every eighth line and pixel of an 80 by 80 box. Care was taken to insure that all of the surfaces to be analyzed were sampled in nearly equal numbers, and also that the areas chosen were comprised only of either snow, snow-free land, ice clouds or liquid clouds. Uniformity of these areas was determined subjectively by evaluating the visible and infrared images along with plotted surface observations for the area. From both passes a total of 300 land pixels, 400 ice cloud pixels, 300 liquid cloud pixels, and 300 snow pixels were sampled and the following information calculated:

1. Channel 1 reflectance.
2. Channel 3 reflectance.
3. Channel 4 brightness temperature.

Fig. 3.1 9 Nov 86 overview - NOAA-9 AVHRR channel 1.

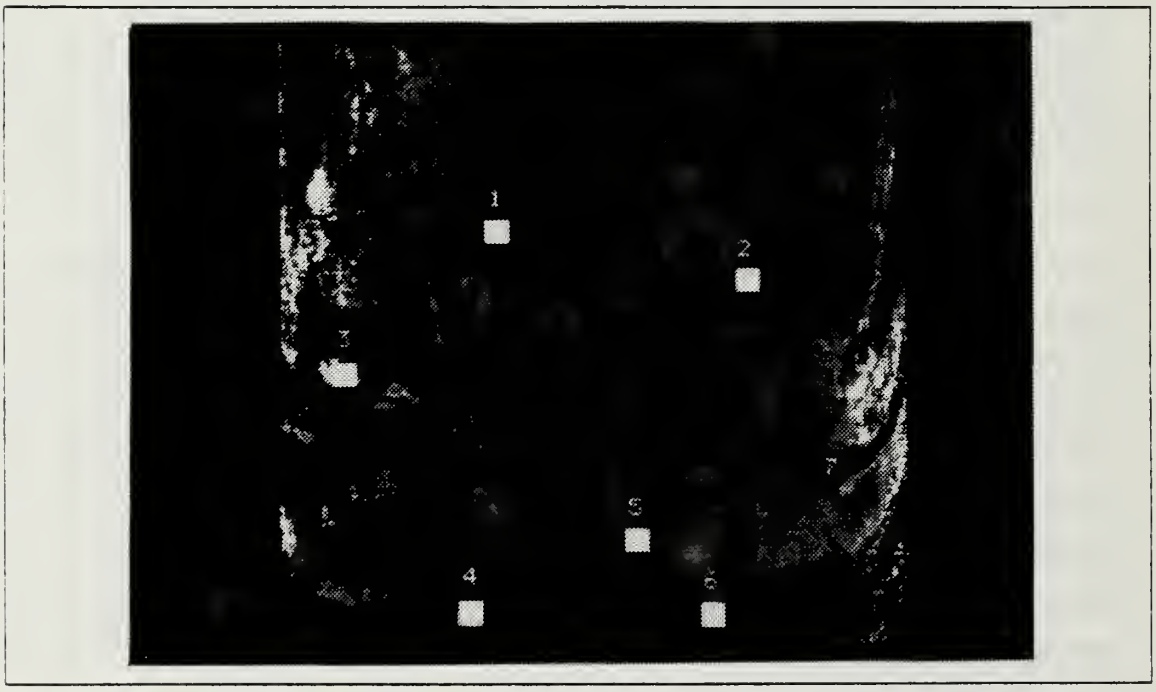

Fig. 3.2 Same as Fig. 3.1 except for derived channel 3 reflectance with data samples.

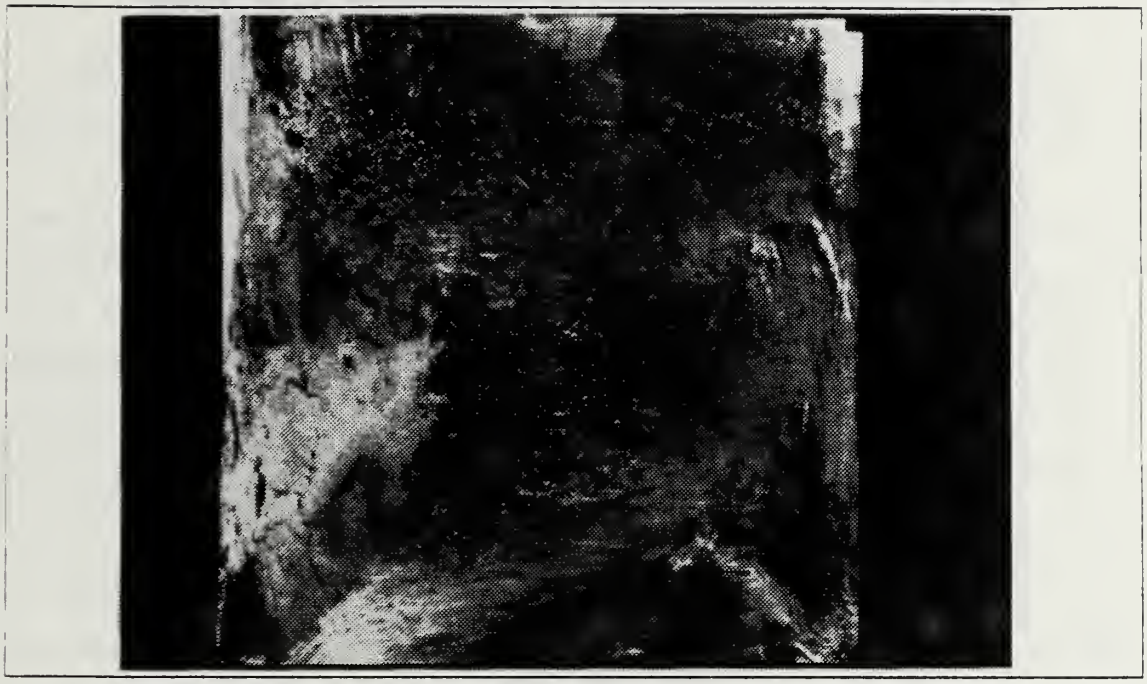

Fig. 3.3 10 Nov 86 overview - NOAA-9 AVHRR channel 1.

Fig. 3.4 Same as Fig. 3.3 except for derived channel 3 reflectance with data samples.

4. Channel 3-channel 4 temperature factor.
5. Channel 3 reflectance not including the anisotropic reflectance factor.

Additionally, the averages and standard deviations of all of these were calculated for each 10 by 10 box.

Figs. 3.5 through 3.12 show channel 1 of the subscenes along with images of the derived channel 3 reflectance. The 10 by 10 boxes of data samples are labeled on the images of derived channel 3 reflectance for easy reference to the tables of reported values in the following section. For all four subscenes, a total of 600 land pixels, 600 thin/warm ice cloud pixels, 600 cold/thick ice cloud pixels, 1000 liquid cloud pixels and 700 snow pixels were sampled. Separation of the ice clouds in this manner was due to the need to more accurately specify thresholds that will separate them from everything else. The information calculated was the same as with the overviews except the channel 3 reflectance not including the anisotropic factor. This was calculated only for the overviews and its significance will be discussed later. The averages and standard deviations were calculated for each individual box as was done with the overviews.

C. DATA SAMPLES

Tables 3 through 8 show the observed reflectance and the channel 3-channel 4 temperature factor for the sampled areas from the overviews and subscenes. The range of values reported for each box includes one standard deviation either side of the average. The solar zenith angle reported with each group is for the center of the box. Figs. 3.13 and 3.14 summarize these values in graphical form to illustrate how the separation thresholds are selected. Theoretical values reported in Chapter II for this range of solar zenith angles (64° to 79°) are 0.18-0.42 for liquid clouds, 0.01-0.30 for ice clouds, 0.005-0.025 for snow cover and about 0.10 for snow-free land. The major differences between theory and observation are with liquid clouds and snow cover. With liquid clouds the discrepancy is possibly due to a difference between parameters used in model calculations and what was actually observed. The higher values of the liquid cloud observations verified quite well. With snow cover the discrepancy is likely due to error in the method of calculating the channel 3 reflectance. The assumptions affect only the thermal emission portion of the channel 3 radiance measurement which, in the case of snow cover, has a magnitude comparable to that of solar reflection. Thus a larger error should be expected in the reflectance calculation. These observed values verify that there are sufficient differences on which to base an automated

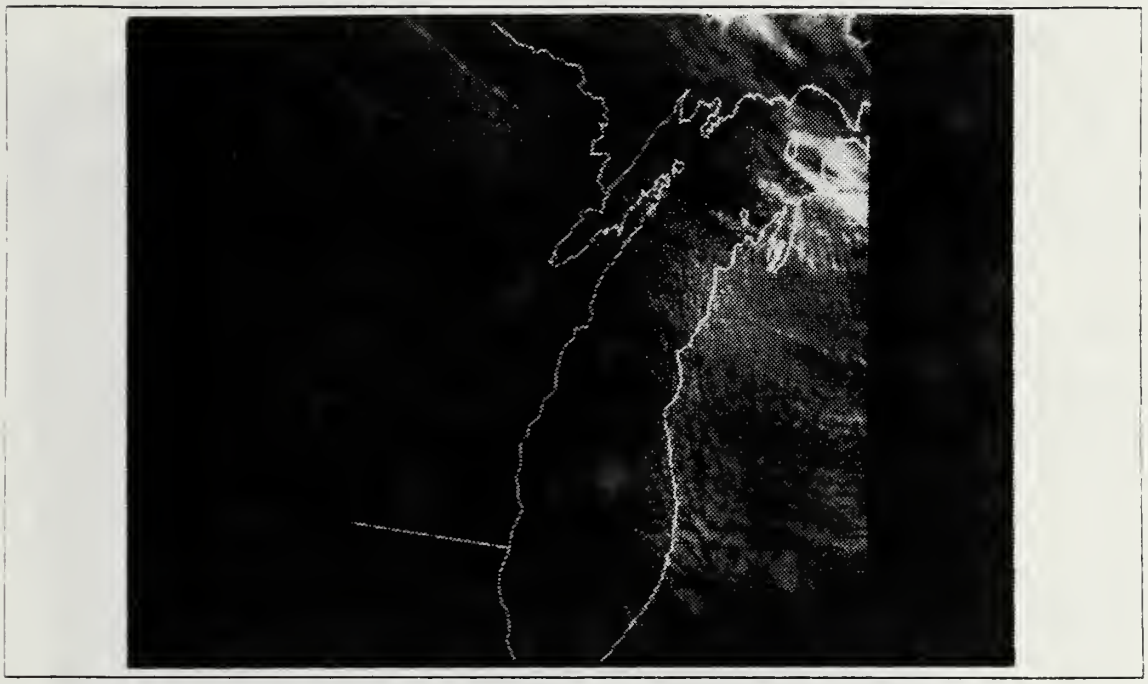

Fig. 3.5 9 Nov 86 subscene 1 - NOAA-9 AVHRR channel 1, full resolution image.

Fig. 3.6 Same as Fig. 3.5 except for derived channel 3 reflectance with data samples.

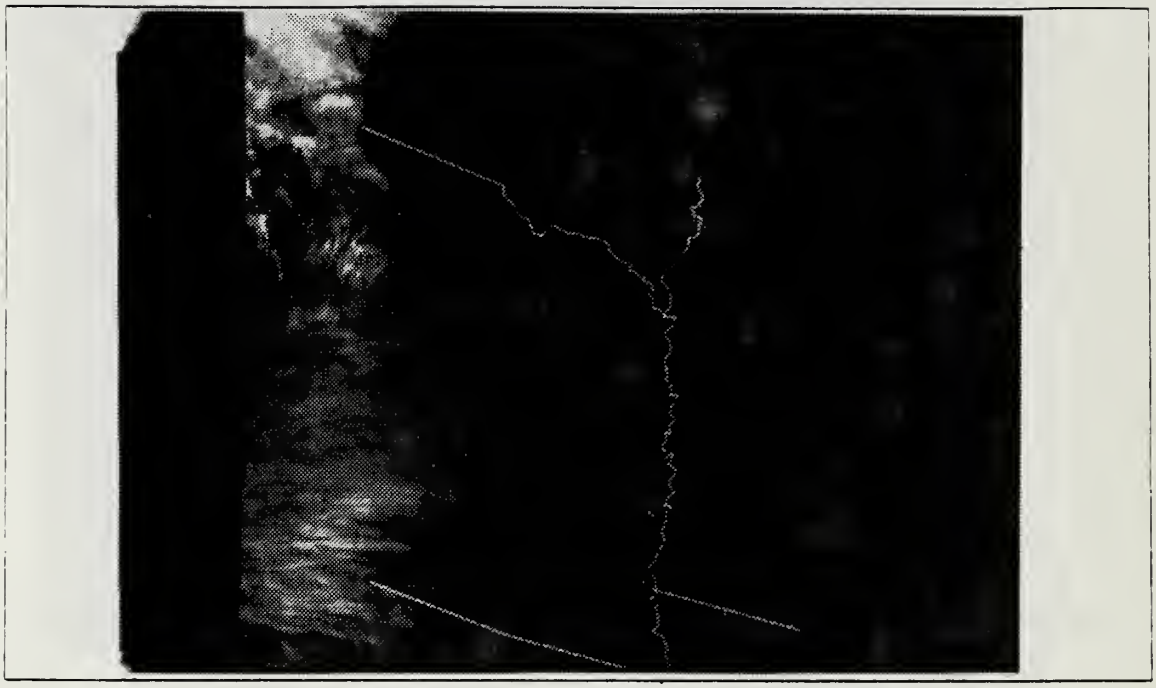

Fig. 3.7 9 Nov 86 subscene 2 - NOAA-9 AVHRR channel 1, full resolution image.

Fig. 3.8 Same as Fig. 3.7 except for derived channel 3 reflectance with data samples.

analysis routine. The importance of channel 3 in developing this routine is evident from Figs. 3.13 and 3.14. Without channel 3, a routine would have to rely on distinctions in channel 1 reflectance and/or the channel 4 temperature. The only distinct surface in channel 1 is land, and the channel 4 temperature could be used only if the ground temperature were known from a conventional observation. Channel 3 is the key to providing the distinction necessary for the automated routine to separate these surfaces successfully.

Fig 3.15 shows the observed channel 3-channel 4 temperature factor for the sampled snow cover and cirrus, and there is a great deal of overlap at values greater than 20.0. It is likely that most of the cirrus with a lower factor will be analyzed correctly because the channel 3 reflectance is high, thus leaving very few to be unambiguously separated from snow cover based only on this factor.

Taylor and Stowe (1984) report the anisotropic reflectance factor for clear land, clear snow, ocean and low, middle and high clouds as derived from the NIMBUS-7 Earth Radiation Budget instrument. These factors are for spectrally-integrated albedo between 0.2μm and 50μm. They specify the factor as a function of solar zenith angle and what they refer to as the angular bin, which is determined by the satellite zenith angle and the relative azimuth angle. Each bin spans approximately 12-15 degrees of satellite zenith angle and 10-20 degrees of relative azimuth angle, while the solar zenith angles are stratified into ten categories from 0 to 90 degrees with an interval of 6 to 25 degrees.

Two major assumptions concerning this factor which were applied to this study are:

1. The factor for the low cloud category adequately describes the factor for all clouds.
2. Since the factor is used to determine the scene classification, its variation among the different surfaces is neglected.

These assumptions were made primarily to ease the burden of computer storage and processing. The values of this factor reported by Taylor and Stowe were determined with prior knowledge of the scene classification; however, this routine needed the factor first in order to make its classification decision. For a particular bin and solar zenith angle, the factors for land, snow and clouds are close enough so that the average is a reasonable estimate for any of the three features. For this reason it was decided to use the average anisotropic factor to classify the scene. A single array of factors was used in the computer program, with 49 bins and 7 categories of solar zenith angle. The

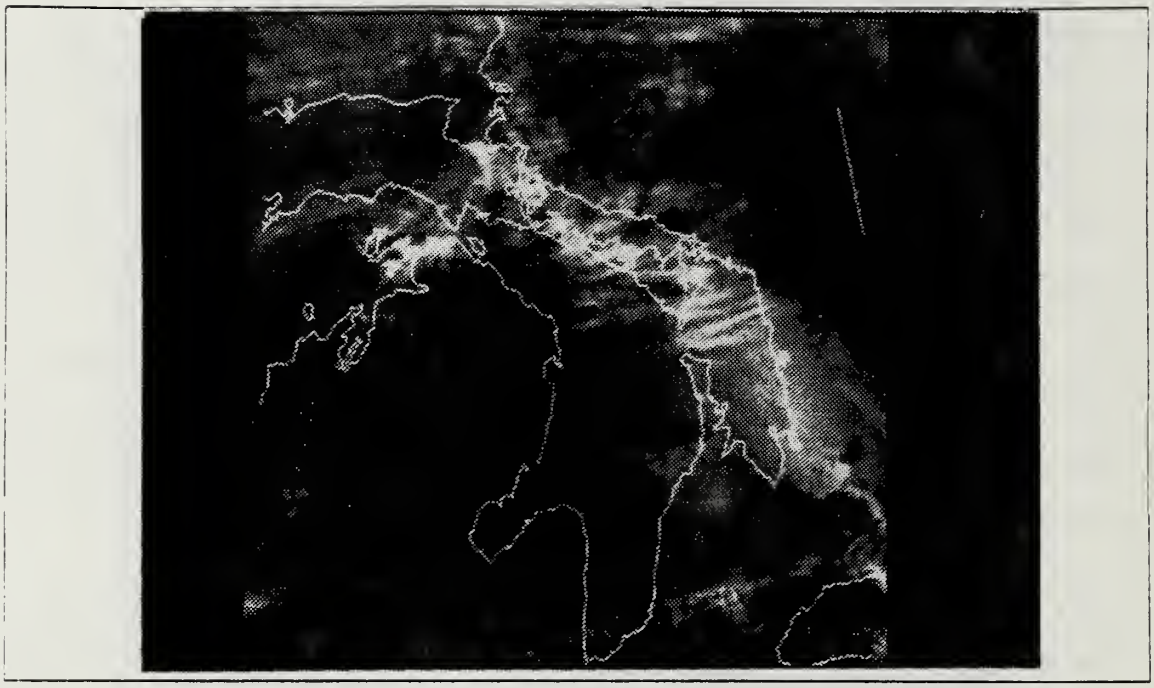

Fig. 3.9 10 Nov 86 subscene 1 - NOAA-9 AVHRR channel 1, full resolution image.

Fig. 3.10 Same as Fig. 3.9 except for derived channel 3 reflectance with data samples.

Fig. 3.11 10 Nov 86 subscene 2 - NOAA-9 AVHRR channel 1, full resolution image.

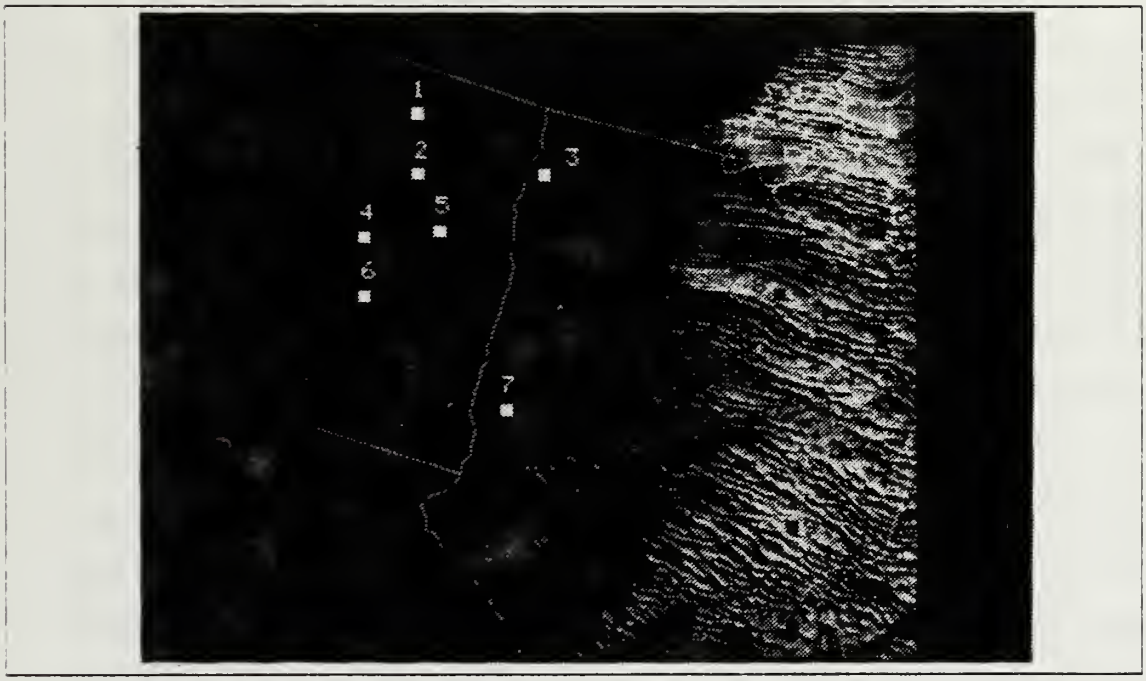

Fig. 3.12 Same as Fig. 3.11 except for derived channel 3 reflectance with data samples.

solar zenith angle categories were reduced from 10 to 7 covering the interval from 45° to 90°, since all of the images analyzed for this study have the solar zenith angle within this interval. With all of these assumptions taken into account, the program chose the anisotropic factor from one table of 343 values rather than six tables of 490 values.

TABLE 3

Observed reflectance for channels 1 and 3 and the channel 3-channel 4 temperature factor (Nov 9).

Surface (Group)	Solar Zenith	Ch 1	Ch 3	Temp Factor	Pct Chg
Ice Cloud (1)	76	0.58 - 0.74	0.04 - 0.06	10.29 - 15.79	-19
Ice Cloud (2)	79	0.57 - 0.66	0.03 - 0.05	17.63 - 27.61	-25
Ice Cloud (3)	68	0.64 - 0.87	0.09 - 0.27	3.78 - 8.88	15
Land (4)	67	0.09 - 0.11	0.03 - 0.04	52.21 - 113.07	-24
Land (5)	71	0.13 - 0.16	0.04 - 0.06	38.36 - 74.00	-29
Land (6)	71	0.12 - 0.14	0.05 - 0.07	40.48 - 60.49	-18
Liquid Cloud (7)	79	0.63 - 0.77	0.14 - 0.20	9.04 - 11.42	0

Accounting for anisotropy is important in the calculations and the degree of importance can be determined by the amount that the factor is different from 1.0. For example, a factor of 0.85 means that if the factor were left out of the calculations the reflectance would be about 15 percent less than what it should be. In general, the anisotropic factor becomes large when the solar zenith angle, the satellite zenith angle and the relative azimuth angle are all large (see Fig. 2.1). NOAA's polar orbiters have both morning and afternoon passes so in all cases the solar zenith angle is large. The satellite zenith and relative azimuth angles are large when the sensor is looking in the direction of the sun, and this occurred with the morning pass when the sensor looked to the east, and for the afternoon pass when the sensor looked to the west. For both passes, when the sensor looked towards the sun the relative azimuth decreased northward, and when the satellite looked away from the sun, the relative azimuth increased northward. There were some instances where the anisotropic factor was

TABLE 4

Observed reflectance for channels 1 and 3 and the channel 3-channel 4 temperature factor (Nov 10).

Surface (Group)	Solar Zenith	Ch 1	Ch 3	Temp Factor	Pct Chg
Liquid Cloud (1)	74	0.39 - 0.60	0.20 - 0.36	1.77 - 10.83	1
Snow (2)	67	0.49 - 0.61	0.02 - 0.03	20.09 - 23.71	10
Snow (3)	70	0.75 - 0.85	0.03 - 0.04	25.36 - 35.08	-24
Snow (4)	65	0.53 - 0.69	0.02 - 0.03	19.61 - 29.87	-0.4
Ice Cloud (5)	70	0.60 - 0.73	0.02 - 0.04	10.53 - 14.98	-26
Liquid Cloud (6)	78	0.48 - 0.67	0.12 - 0.22	3.97 - 20.59	0

TABLE 5

Observed reflectance for channels 1 and 3 and the channel 3-channel 4 temperature factor (Nov 9-subscene 1).

Surface (Group)	Solar Zenith	Ch 1	Ch 3	Temp Factor
Liquid Cloud (1)	73	0.43 - 0.55	0.16 - 0.19	8.58 - 9.50
Liquid Cloud (2)	73	0.41 - 0.53	0.16 - 0.20	8.46 - 9.63
Liquid Cloud (3)	75	0.64 - 0.72	0.17 - 0.21	8.01 - 8.97
Liquid Cloud (4)	74	0.60 - 0.67	0.13 - 0.16	9.09 - 10.01
Land (5)	71	0.14 - 0.17	0.04 - 0.06	39.33 - 65.05
Land (6)	72	0.14 - 0.17	0.04 - 0.06	43.21 - 61.93
Land (7)	72	0.16 - 0.18	0.05 - 0.07	34.31 - 46.74
Land (8)	71	0.13 - 0.15	0.04 - 0.05	52.71 - 63.93
Land (9)	71	0.16 - 0.17	0.05 - 0.07	38.75 - 46.92
Land (10)	70	0.15 - 0.18	0.03 - 0.10	38.07 - 58.79

TABLE 6

Observed reflectance for channels 1 and 3 and the channel 3-channel 4 temperature factor (Nov 9-subscene 2).

Surface (Group)	Solar Zenith	Ch 1	Ch 3	Temp Factor
Ice Cloud (1)	65	0.47 - 0.53	0.06 - 0.08	5.23 - 6.05
Ice Cloud (2)	65	0.48 - 0.52	0.06 - 0.08	5.22 - 5.66
Ice Cloud (3)	64	0.57 - 0.63	0.06 - 0.07	5.29 - 6.05
Ice Cloud (4)	67	0.26 - 0.29	0.08 - 0.09	12.38 - 14.02
Ice Cloud (5)	68	0.19 - 0.21	0.06 - 0.07	21.92 - 24.64
Ice Cloud (6)	67	0.15 - 0.17	0.04 - 0.06	30.59 - 39.37

TABLE 7

Observed reflectance for channels 1 and 3 and the channel 3-channel 4 temperature factor (Nov 10-subscene 1).

Surface (Group)	Solar Zenith	Ch 1	Ch 3	Temp Factor
Ice Cloud (1)	76	0.34 - 0.44	0.03 - 0.05	25.86 - 34.82
Ice Cloud (2)	76	0.34 - 0.45	0.02 - 0.04	24.79 - 35.22
Ice Cloud (3)	74	0.53 - 0.56	0.02 - 0.03	23.72 - 30.25
Ice Cloud (4)	75	0.61 - 0.68	0.05 - 0.06	9.06 - 11.10
Ice Cloud (5)	75	0.53 - 0.62	0.05 - 0.06	9.06 - 11.00
Liquid Cloud (6)	76	0.55 - 0.58	0.08 - 0.09	18.22 - 19.46
Liquid Cloud (7)	76	0.50 - 0.62	0.09 - 0.13	13.75 - 17.45
Liquid Cloud (8)	76	0.47 - 0.62	0.10 - 0.16	12.33 - 15.84
Ice Cloud (9)	75	0.44 - 0.61	0.09 - 0.18	5.56 - 7.44

TABLE 8

Observed reflectance for channels 1 and 3 and the channel 3-channel 4 temperature factor (Nov 10-subscene 2).

Surface (Group)	Solar Zenith	Ch 1	Ch 3	Temp Factor
Snow (1)	71	0.68 - 0.76	0.03 - 0.04	22.98 - 28.53
Snow (2)	71	0.77 - 0.82	0.03 - 0.04	23.87 - 33.15
Snow (3)	71	0.75 - 0.81	0.03 - 0.04	24.92 - 32.00
Snow (4)	70	0.82 - 0.85	0.02 - 0.03	23.14 - 28.89
Snow (5)	71	0.81 - 0.85	0.02 - 0.03	26.84 - 34.64
Snow (6)	70	0.76 - 0.81	0.03 - 0.04	23.14 - 28.89
Snow (7)	70	0.57 - 0.69	0.02 - 0.03	32.57 - 41.51
Liquid Cloud (8)	72	0.42 - 0.56	0.21 - 0.30	4.51 - 8.18
Liquid Cloud (9)	71	0.43 - 0.62	0.23 - 0.34	5.03 - 7.85
Liquid Cloud (10)	71	0.42 - 0.63	0.19 - 0.33	3.76 - 12.63

significantly less than 1.0. This occurred at various combinations of sun-satellite geometry when the satellite sensor was not looking towards the sun.

Tables 3 and 4 show the change in the channel 3 calculated reflectance, as a percentage of the channel 3 reflectance, neglecting the anisotropic reflectance factor. A negative change means that the reflectance is less when the factor is neglected. Referring to Eq. 2.12, a negative change occurs when the factor is less than 1.0. so the denominator of Eq. 2.12 is larger when the factor is neglected. As discussed in Chapter II. when the factor is less than 1.0 the calculated reflectance would yield an underestimate of the radiant exitance if anisotropy were neglected, and the calculated reflectance would yield an overestimate when the factor is greater than 1.0.

A closer analysis reveals that the anisotropic factors ranged from a minimum of 0.59 to a maximum of 3.41, meaning that there was as much as a four-fold variability in reflectance due to anisotropy alone, clearly indicating that this effect cannot be neglected. The factors for these surfaces in the tables of Taylor and Stowe show values as high as 5.98 but the values applicable to this study were restricted to this range

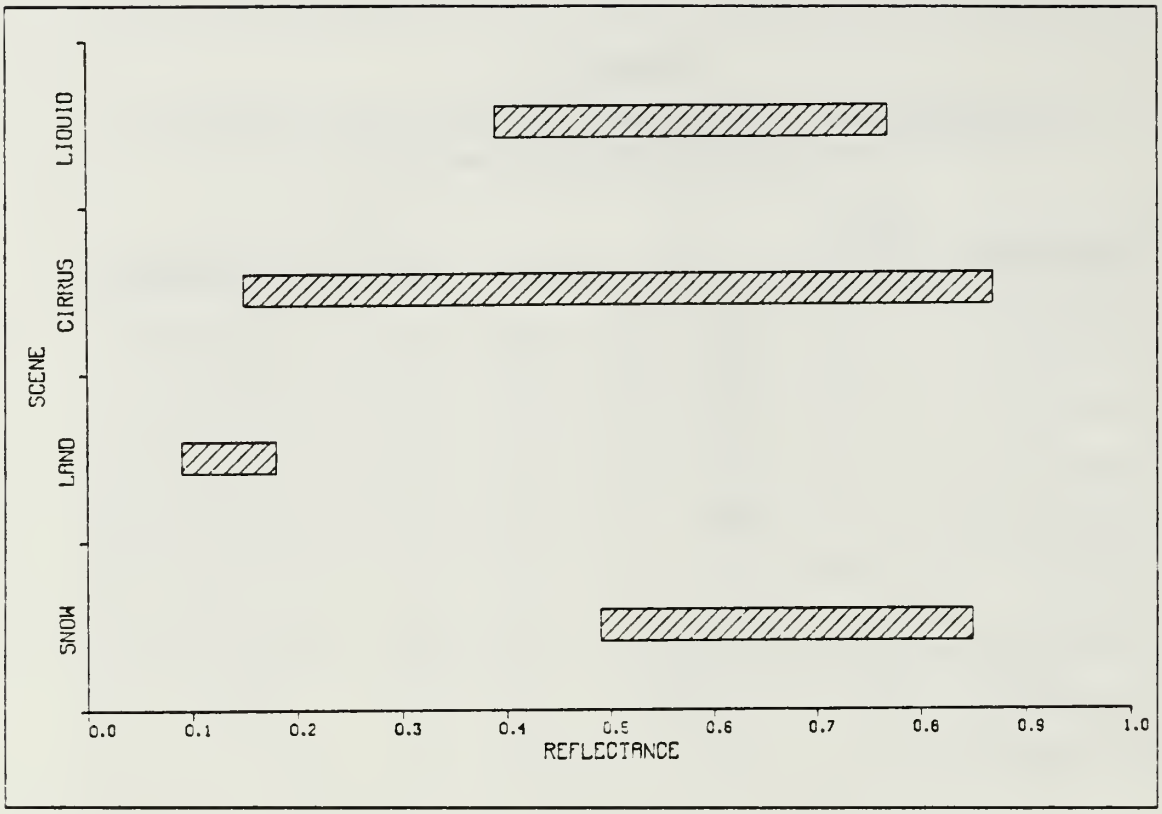

Fig. 3.13 Summary of NOAA-9 AVHRR observed channel 1 reflectance for 900 land pixels, 1600 ice cloud pixels, 1300 liquid cloud pixels, and 1000 snow pixels.

because the satellite zenith angle at the edge of these passes was approximately 69°. Thus the angular bins were restricted to between 1 and 41. This fact can be used to effect a slight improvement in computer processing. Fewer data values to be stored means the program will run slightly faster and that is important with this computationally-intensive routine that chooses a factor for a total of 262,144 pixels in a single image. There are some instances where the factors for the various scenes vary widely within a particular bin and solar zenith angle category. In these cases the average is not a very good estimate for the program to use and it may be better to sacrifice an improvement in speed to gain more in accuracy of the anisotropic factor. Now that fewer values need to be stored, instead of using an average for all scenes, a table of values for each individual type of classification could be used in the program. A preliminary guess of the scene classification could be made and then an iterative process used to arrive at the correct factor for that particular classification.

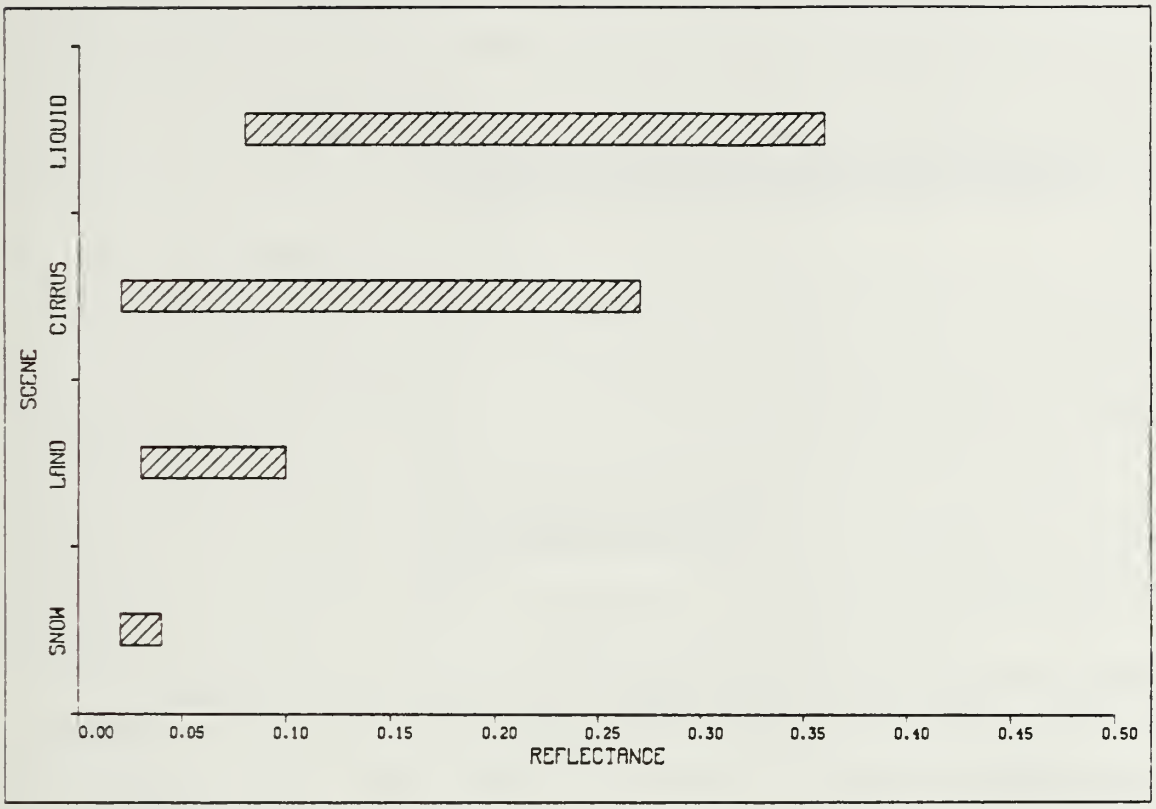

Fig. 3.14 Same as Fig. 3.13 except for derived channel 3 reflectance.

The following are important points from both overviews concerning the anisotropic factor:

1. November 9 (Table 3): For Group 7 the satellite was looking away from the sun so neglecting anisotropy had a very small effect on the calculated reflectance. Contrast this with Group 3 where the satellite was looking towards the sun. In this case neglecting anisotropy had a significant effect. For Group 7 the relative azimuth was about 25-26° and the anisotropic factor was constant at 1.0. For Group 3, the relative azimuth was about 134-136° and the anisotropic factor varied between 0.96 and 1.22, making a positive change in reflectance when anisotropy was neglected. It is interesting to note that the change for land was very significant. Groups 4, 5 and 6 are relatively close to the satellite subpoint but the anisotropic factors all came out to be between 0.75 and 0.85 and this translated into a large percentage change. This may be due to the fact that there was a large difference between the average factor used in the program and the factors for land reported by Taylor and Stowe.
2. November 10 (Table 4): In this image, both Groups 1 and 6 had a small change. For Group 6 the relative azimuth was very small. For Group 1 the relative azimuth was larger than for Group 6, but the solar zenith and satellite zenith did not work together to make the factor very much different from 1.0.

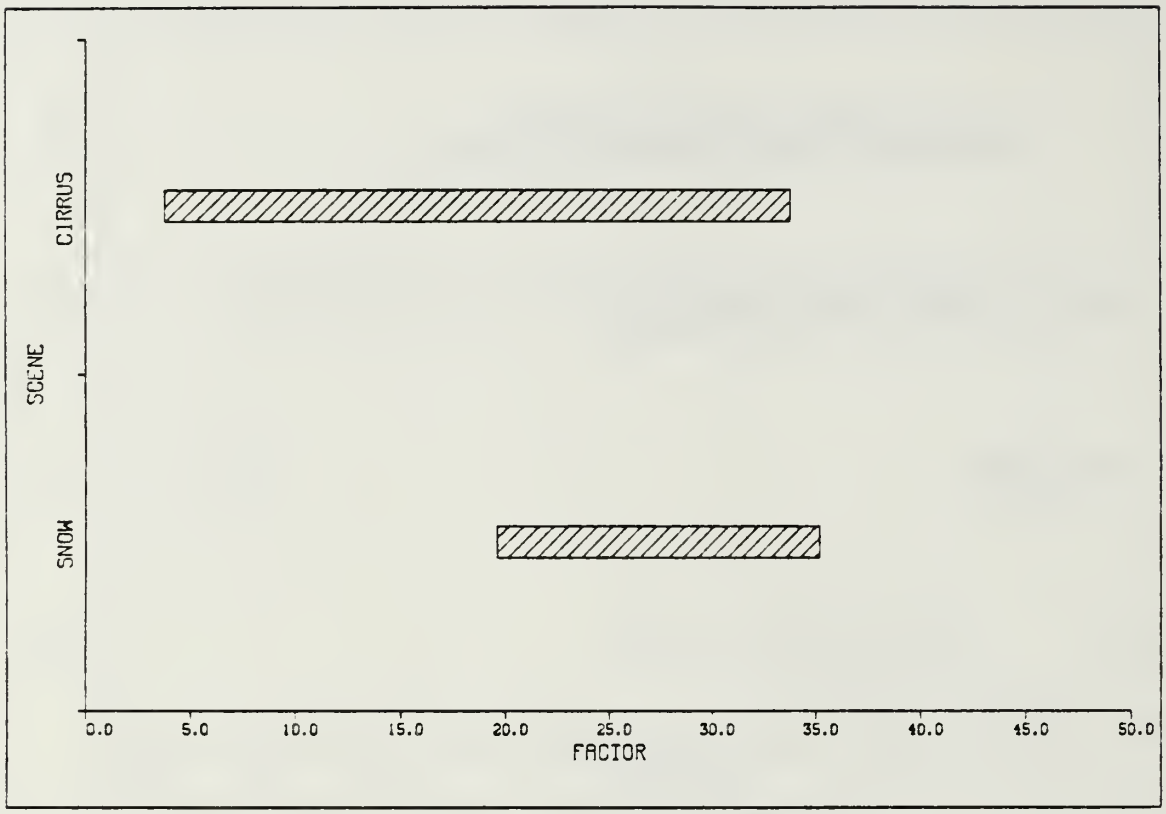

Fig. 3.15 Same as Fig. 3.13 except for channel 3-channel 4 temperature factor, 1000 snow pixels and 1600 ice cloud pixels.

Group 5 is near the satellite subpoint and the factor here was constant at 0.74, giving a large percentage change when anisotropy is neglected. The most interesting values for this image are for the snow cover of Groups 2, 3 and 4. These groups are fairly close together and the sun-satellite geometry was similar for them all, however it was different enough to cause a quite variable change in reflectance among the 3 groups when anisotropy is neglected.

To summarize, accounting for anisotropy is important when calculating reflectance. The change in reflectance becomes important (greater than 10 percent) when the factor is greater than approximately 1.10 or less than approximately 0.90. It seems as though the greatest effect of neglecting anisotropy should be when the satellite is looking towards the sun, but it was shown here that for these images it is also important near the satellite subpoint with a large solar zenith angle. With the former the effect is large due to forward scattering, while with the latter the effect is large due to the small degree of backward scattering. The factors used here are admittedly only first-order approximations and in some instances provide only very

crude estimates. Taylor and Stowe state that some of the angular bins were very sparsely populated and subject to large error in the estimate for that bin. The factors could be improved by making the angular resolution of the bins finer and taking more observations for the sparsely populated bins. Measurements should also be taken in smaller spectral intervals to address the possibility of spectral variability of the factors.

D. ALGORITHM DEVELOPMENT

The algorithm was developed in phases, and additional data were gathered as necessary to determine the conditions under which the algorithm failed. Analyses for each phase were evaluated subjectively and compared with visual and infrared imagery along with plotted surface observations for the area. Subscene 2 of November 10 is the only one of these images with snow cover. Since the focus of this study is the problem of snow/low cloud discrimination, this image will be included again in Chapter IV where it will be evaluated against the individual surface observations in the area and its verification statistics included with the other images evaluated there.

In order to satisfy the primary objective of this analysis routine, it was decided that there should be three steps executed in order during the classification process:

1. Separate liquid clouds and as many of the ice clouds as possible from everything else.
2. Separate land from snow and the remaining ice clouds.
3. Finally, separate snow and the remaining ice clouds.

This approach was adopted because the distinction between clouds and everything else is the sharpest. Any ambiguities that arose between low clouds and snow or land were resolved as clouds since, for operational forecasting, it is better to overestimate the low cloud cover than to underestimate it. This logic was employed to correctly separate all snow and low clouds, then any confusion between snow and ice clouds could be resolved later by manual analysis of the infrared imagery.

All images of the analyses presented in this section emphasize the cloud cover analysis. First the pixel classification was made, then land pixels were assigned a grayshade value between 0 and 25 and snow pixels were assigned a grayshade value between 26 and 50. The actual value was assigned based on the channel 1 reflectance. All snow and snow-free land areas appear dark in these images but enough variation is actually present to analyze the surface features in greater detail by using an image enhancement technique. The cloud pixels were assigned a grayshade value from 75 to 255 based on their channel 4 temperature. This provides some texture to the cloud analysis and also shows variability in cloud height.

1. Phase 1

According to Fig. 3.14, liquid clouds and most ice clouds can be separated from land and snow by specifying a threshold with the channel 3 reflectance alone. A reasonable choice for the boundary between liquid clouds and snow/land is somewhere between 7 and 10 percent. Snow should be separated well but there is some overlap between clear land and clouds since the channel 3 reflectance of land was as high as 10 percent. There are very few land pixels with a reflectance this high, so a threshold of 7.7 percent was decided upon for this first attempt. Ice cloud reflectance ranged from 2 to 27 percent so many of the ice clouds will make this separation.

Channel 3 reflectance cannot be used to separate land from snow cover and the remaining ice clouds (see Fig. 3.14). There is adequate distinction in the channel 1 reflectance (Fig. 3.13), and a threshold of 20 percent was decided upon to accomplish this separation. This allows thin snow cover and thin ice clouds to be analyzed correctly if the channel 1 reflectance is at least 20 percent, thus making the pixel approximately 25-30 percent cloud-filled. If snow or ice clouds have a channel 1 reflectance lower than 20 percent and are thus incorrectly analyzed as land, then the clouds are probably so thin that it will not greatly affect the accuracy of the analysis.

The final separation is between snow and the remaining ice clouds. Neither the channel 1 nor channel 3 reflectance can be used to distinguish them, so this is where the channel 3-channel 4 temperature factor was used (Eq. 2.7). This factor was generally greater than 20 for snow cover, although there was some overlap with ice clouds (Fig. 3.15). For phase 1 the threshold for this factor was set at 20.

Summarizing the logic for the analysis routine at this phase of development:

1. Pixels with a channel 3 reflectance greater than or equal to 7.7 percent were analyzed as cloud. Land and snow/ice clouds were passed on.
2. Pixels with a channel 1 reflectance less than 20 percent were analyzed as land. Snow/ice cloud pixels were passed on.
3. Pixels with a channel 3-channel 4 temperature factor of greater than or equal to 20 were analyzed as snow and the remaining pixels were analyzed as cloud.

2. Results of Phase 1 Test

Figs. 3.16 and 3.17 show the results of applying the algorithm to the November 9 subscenes. For subscene 1, many of the clear land pixels in Wisconsin and northern Illinois were analyzed as cloud. According to the additional data samples that were taken from this area, the misanalysis occurred because the channel 3

reflectance of some land pixels was as high as 10 percent. The liquid clouds were handled very well but much of the cirrus north of Lake Michigan was analyzed as snow because it did not meet the criteria for the first separation, and then in the final separation the temperature factor was between 30 and 40, well within the range for snow. For subscene 2, practically all of the cirrus was handled correctly, including much of the thin cirrus. Some of this was due to the clouds making the reflectance threshold, but much was due to the temperature factor. As noted in Table 6, only a few of these pixels had a channel 3 reflectance greater than 7.7 percent, but many had a temperature factor less than 20. When the channel 1 reflectance of the thin cirrus went below 20 percent it was analyzed as land, as expected. The remaining cirrus that was missed was due to its being greater than the threshold for the temperature factor.

Figs. 3.18 and 3.19 show the results of applying the algorithm to the November 10 subscenes. On subscene 1, the difficulty with cirrus is evidenced by the gaps in the cirrus band between Lakes Michigan and Superior. The routine handled the low clouds over Lake Huron well, but there are some gaps indicating a channel 3 reflectance that is lower than 7.7 percent. Land was analyzed correctly in this image. For subscene 2, it did an outstanding job in separating the snow and low clouds. Most of the convective clouds in this image can be picked out on the visual image (Fig. 3.11) due to their texture difference with the smooth snow cover. This analysis maintained the texture and structure of these cloud streets, and it is easy to see where the snow depth increases. Snow pixel grayshades range from 26 to 50 according to their channel 1 reflectance, thus the deeper snow (greater reflectance) is displayed on the higher end of this range. Additional data were taken from eastern North Dakota to further verify the channel 3 reflectance threshold of 7.7 percent. The highest measured channel 3 reflectance of the snow in this area was 5.4 percent.

3. **Phase 2**

In the first separation, too many land pixels were mistakenly analyzed as clouds because the channel 3 reflectance was higher than 7.7 percent. Also, many of the ice clouds were incorrectly analyzed as snow. The problem with the land pixels was handled by adding a threshold for the channel 1 reflectance of 20 percent. At the same time there was plenty of room to adjust the channel 3 reflectance threshold downward. It was adjusted to 6.5 percent to allow more ice cloud pixels to be analyzed correctly and not interfere with the excellent results in the snow area obtained on subscene 2 of November 10. An adjustment was also made in the temperature factor. The

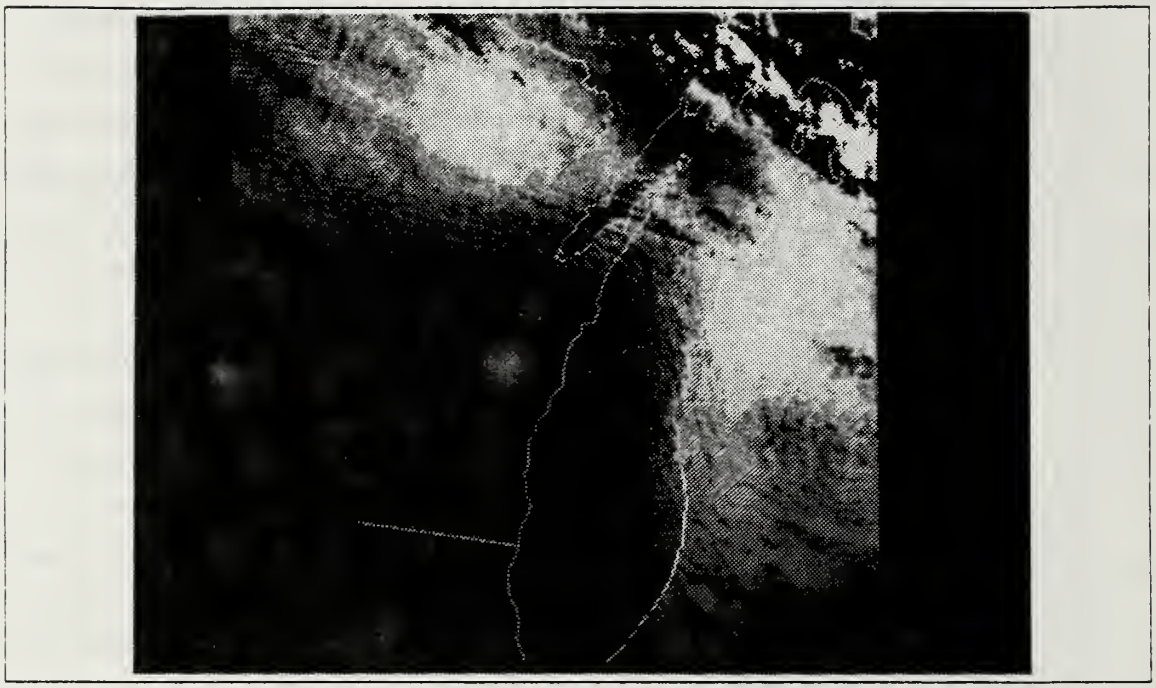

Fig. 3.16 9 Nov 86 subscene 1 - phase 1 cloud cover analysis results.

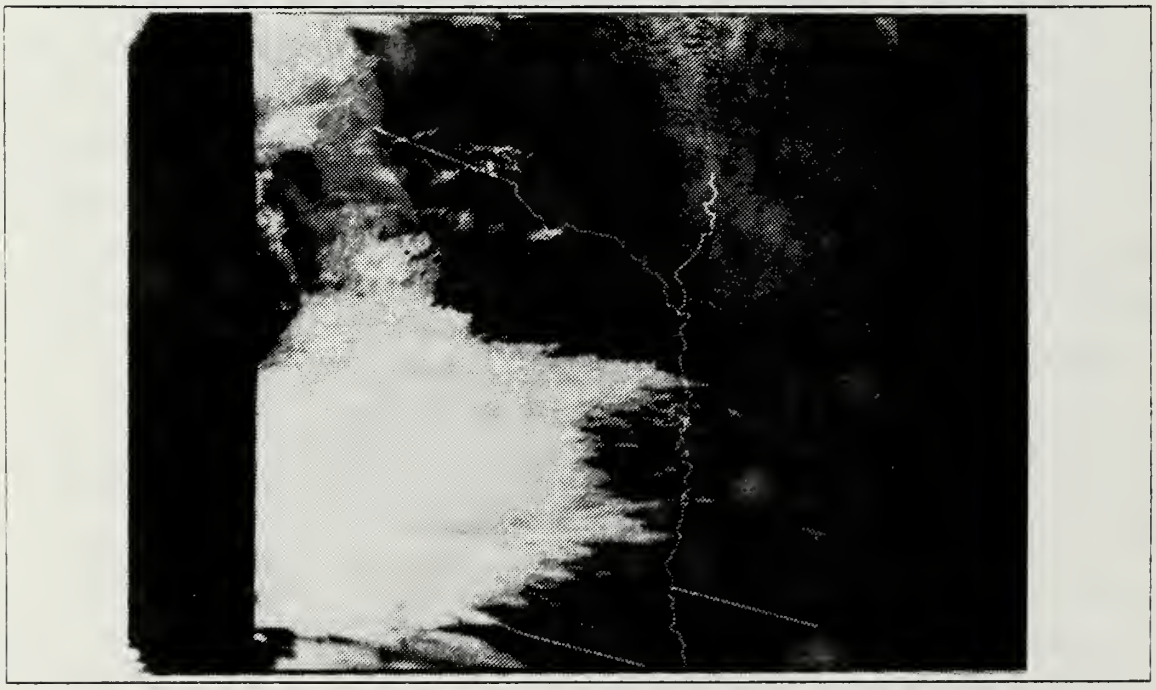

Fig. 3.17 Same as Fig. 3.16 for 9 Nov 86 subscene 2.

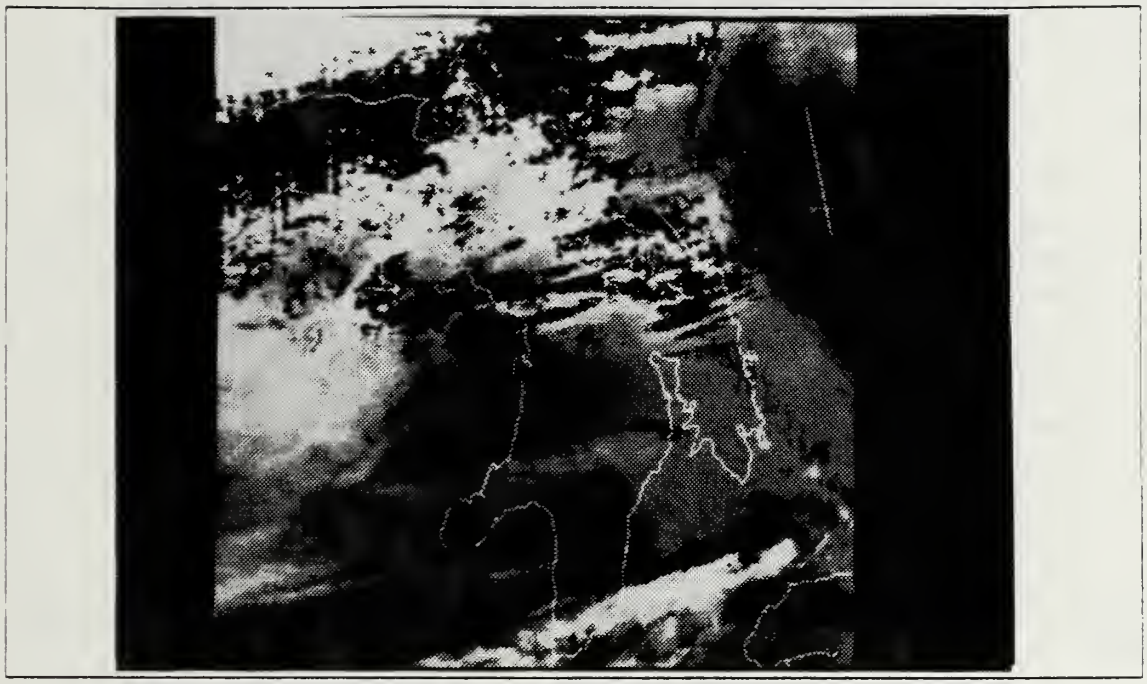

Fig. 3.18 Same as Fig. 3.16 for 10 Nov 86 subscene 1.

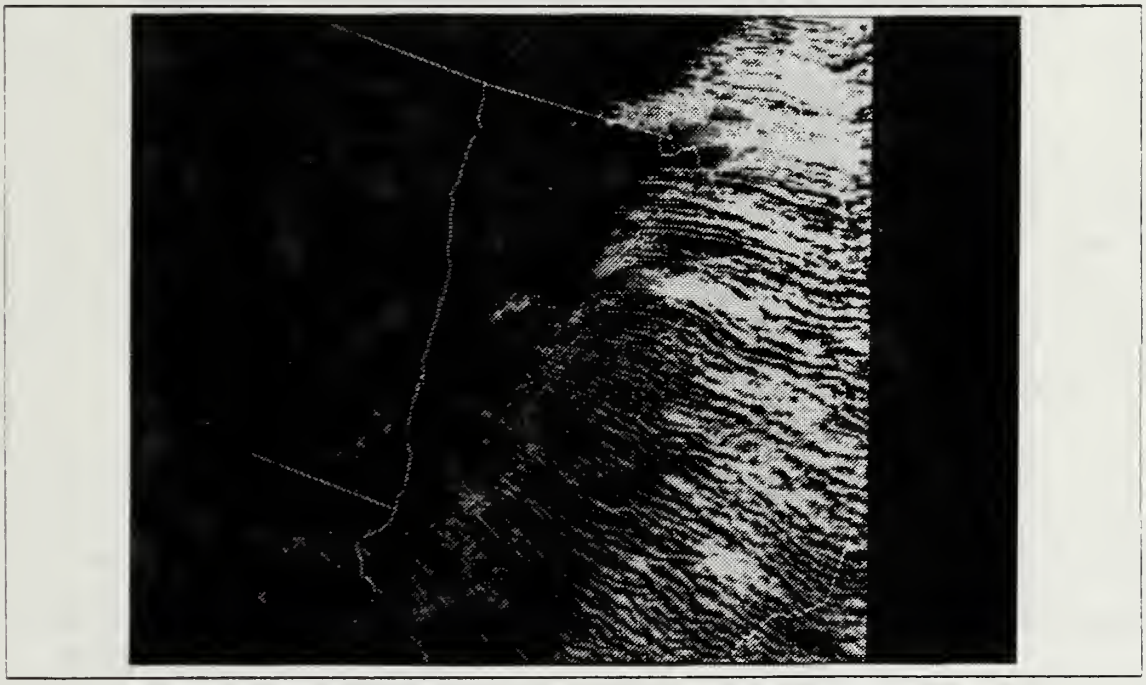

Fig. 3.19 Same as Fig. 3.16 for 10 Nov 86 subscene 2.

additional data taken from the snow cover of eastern North Dakota showed that the temperature factor was as low as 15.7. It was understood that adjusting this threshold downward would worsen the analysis of cirrus but it was lowered to 15.0 to ensure that all the snow cover was analyzed correctly.

Summarizing the logic for the analysis routine at this phase of development:

1. Pixels with a channel 3 reflectance of greater than or equal to 6.5 percent AND channel 1 reflectance of greater than or equal to 20 percent were analyzed as cloud. Land and snow/ice cloud pixels were passed on.
2. Pixels with a channel 1 reflectance of less than 20 percent were analyzed as land. Snow/ice cloud pixels were passed on.
3. Pixels with a channel 3-channel 4 temperature factor of greater than or equal to 15 were analyzed as snow and the remaining pixels were analyzed as cloud.

4. **Results of Phase 2 Test**

Figs. 3.20 and 3.21 show the results of application to the subscenes of November 9. These adjustments completely solved the problem of land pixels being analyzed as cloud but the analysis of ice clouds was worse than in phase 1. Apparently lowering the temperature factor to 15 sacrificed more of the ice cloud pixels than lowering the channel 3 reflectance added. On subscene 2, the low clouds in Iowa, South Dakota and Minnesota were handled worse than in phase 1. The additional samples taken from this area showed that the clouds that were missed met neither the channel 1 nor the channel 3 thresholds and were so thin that they were analyzed as land.

Figs. 3.22 and 3.23 show the results of application to the subscenes of November 10. On subscene 1 it seems again as though the adjustment in the temperature factor overwhelmed what should have been an improvement in the ice cloud analysis due to lowering the channel 3 reflectance threshold, while on subscene 2 the excellence of the snow/cloud analysis was maintained.

5. **Phase 3**

In order to improve the low cloud analysis in Iowa, South Dakota and Minnesota on subscene 2 of November 9, the channel 1 reflectance threshold was lowered to 19 percent. Overall, more ice clouds should also be analyzed correctly as a result of this change. The highest observed reflectance for land was 20.3 percent. This value was observed in one pixel on subscene 1 of November 9, and out of 900 pixels from the original sample, only 3 had a channel 1 reflectance between 19 and 20.3

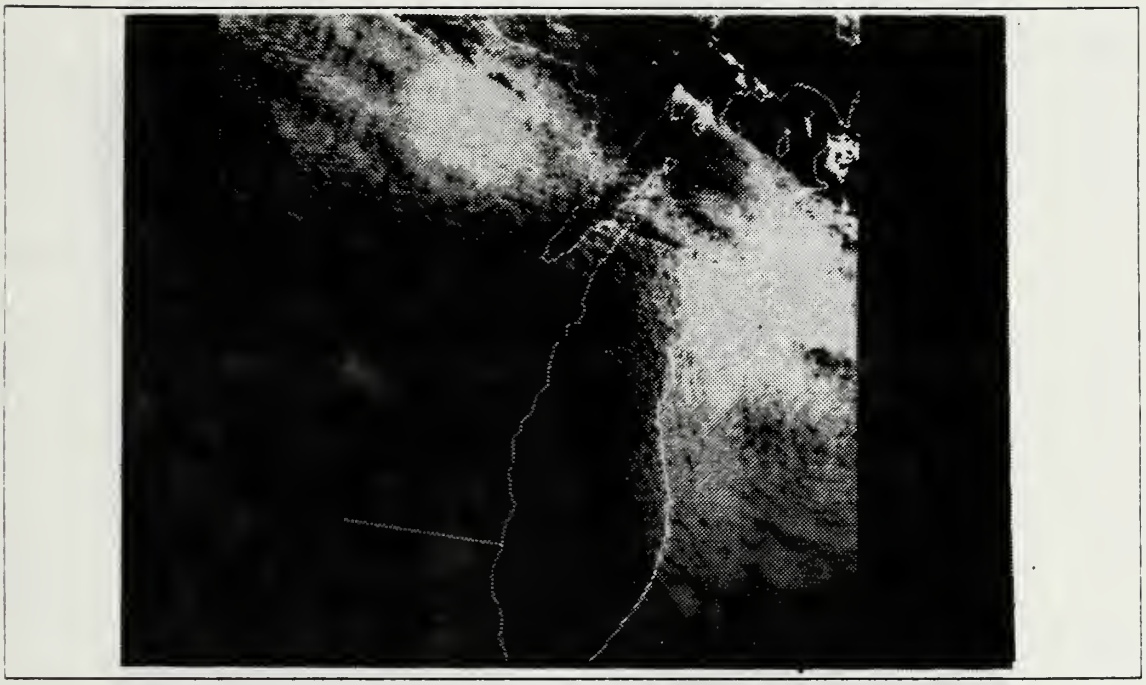

Fig. 3.20 9 Nov 86 subscene 1 - phase 2 cloud cover analysis results.

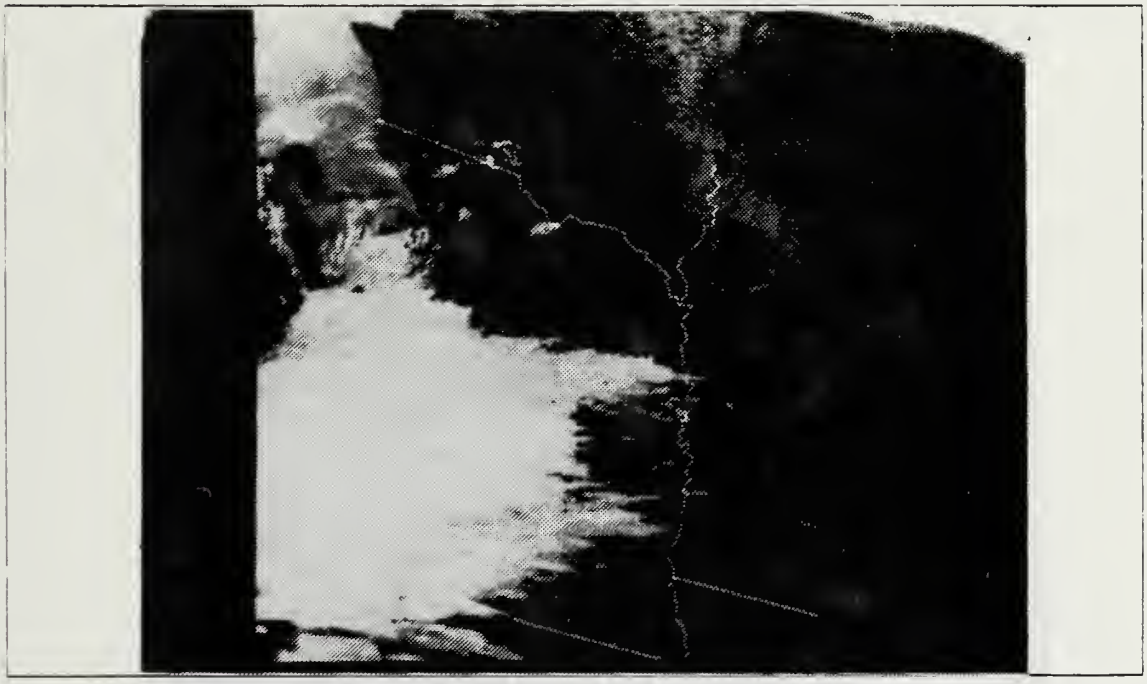

Fig. 3.21 Same as Fig. 3.20 for 9 Nov 86 subscene 2.

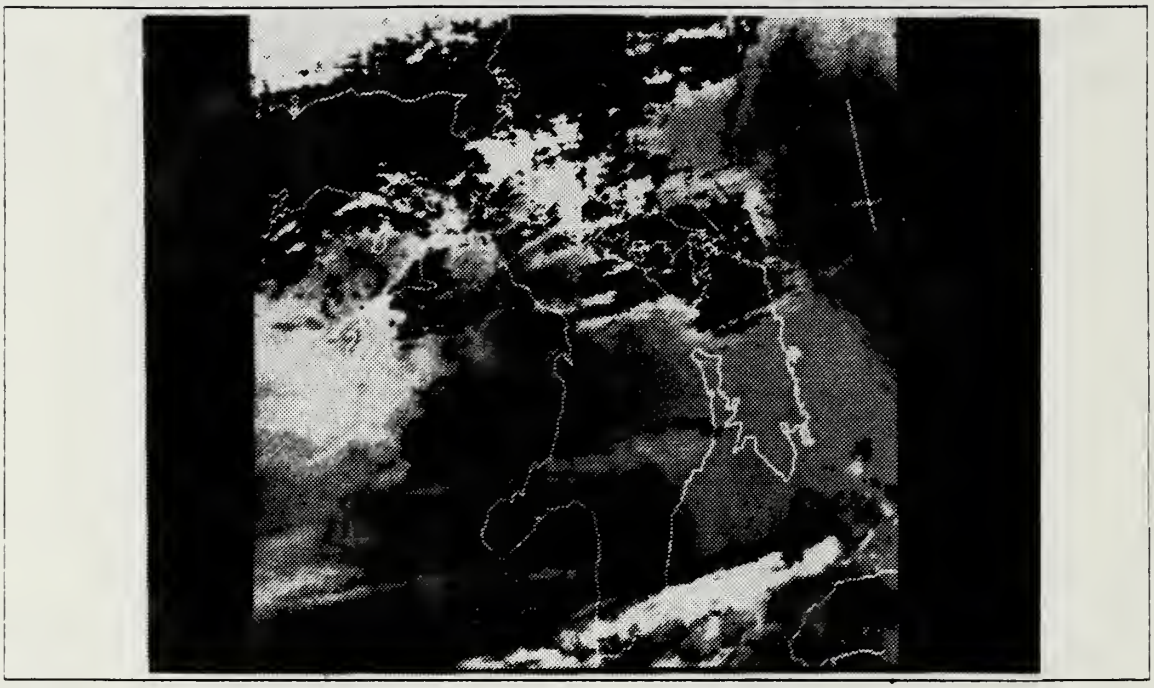

Fig. 3.22 Same as Fig. 3.20 for 10 Nov 86 subscene 1.

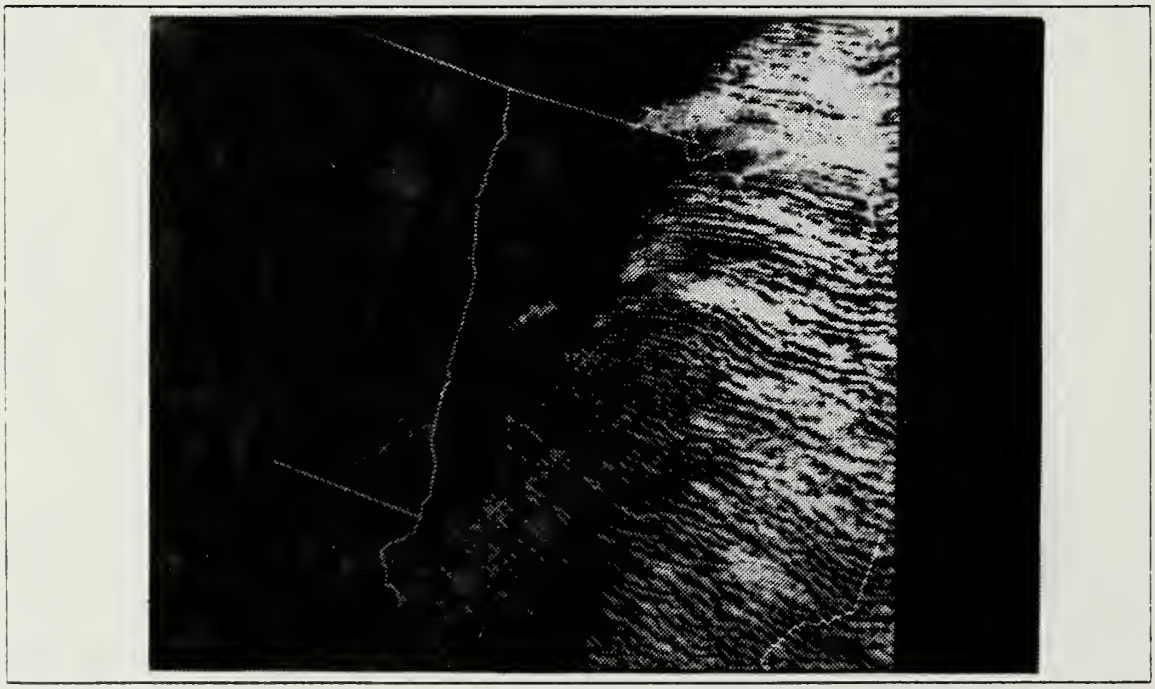

Fig. 3.23 Same as Fig. 3.20 for 10 Nov 86 subscene 2.

percent. Lowering the threshold will cause these pixels to be analyzed as cloud since their channel 3 reflectance also meets the threshold for cloud, but in this particular subscene, the low cloud will be overestimated by much less than 1 percent of the total land pixels. The tradeoff was an overall improvement in the cloud analysis by correctly analyzing more low clouds and ice clouds.

The highest measured channel 3 reflectance for snow was 5.4 percent. This is approximately 1.5 percent higher than theory suggests the maximum ought to be so it was assumed that the channel 3 reflectance would be no higher than this. The channel 3 reflectance was lowered in this phase to 5.7 percent in a final effort to get more ice clouds analyzed correctly without interfering with the accuracy of the snow cover analysis. The temperature factor was not adjusted further. Summarizing the logic for the analysis routine at this phase of development:

1. Pixels with a channel 3 reflectance of greater than or equal to 5.7 percent AND channel 1 reflectance of greater than or equal to 19 percent were analyzed as cloud. Land and snow/ice cloud pixels were passed on.
2. Pixels with a channel 1 reflectance of less than 19 percent were analyzed as land. Snow/ice cloud pixels were passed on.
3. Pixels with a channel 3-channel 4 temperature factor of greater than or equal to 15 were analyzed as snow and the remaining pixels were analyzed as cloud.

6. **Results of Phase 3 Test**

Figs. 3.24 and 3.25 show the results of applying the algorithm to the November 9 subscenes. All clouds were handled better as a result of the changes made in this phase. As expected, a very few of the land pixels were analyzed as cloud, primarily in Michigan and Indiana, but this did not significantly affect the accuracy of the analysis. There was an improvement in the ice cloud analysis but still there was a significant portion incorrectly analyzed as snow. This was evident particularly in subscene 1. In this image it is possible to claim only about a 40 percent accuracy in the analysis of the ice clouds, however for subscene 2 an accuracy of about 70 percent can be claimed. With subscene 2, a particularly good analysis was obtained with the thick cirrus in Nebraska because with these clouds the temperature factor is between 5 and 10. Even as this cirrus thins out over Iowa the analysis remained good until finally the channel 1 reflectance dropped below 19 percent and it was analyzed as land. This deficiency in the analysis routine can be resolved by manual analysis of the coincident visual and infrared imagery.

Figs. 3.26 and 3.27 show the results of applying the algorithm to the November 10 subscenes. The changes made in this phase did improve the cloud analysis overall for subscene 1. About 50 percent of the ice clouds were analyzed correctly while nearly all the low clouds were handled correctly. On subscene 2, the analysis of the low clouds and snow cover was not affected by these changes.

E. SUMMARY

Fig. 3.28 summarizes in graphical form the reflectance thresholds that were decided upon from the experiments just discussed. The dotted line at a channel 3 reflectance of 15 percent for land indicates the maximum expected channel 3 reflectance although the algorithm actually allows the value to be higher. Ice clouds were separated from snow cover using the channel 3-channel 4 temperature factor threshold of less than 15.0. As suspected, this did not add much to the analysis of cirrus because solar reflection added too much variability when trying to make a distinction between cirrus and snow cover. About 50 percent of the cirrus clouds were handled correctly with the channel 3 reflectance threshold of 5.7 percent, and this factor added approximately 2 to 5 percent to that. The variability of reflectance for both surfaces below 5.7 percent was enough to make unambiguous separation of them possible for only a very small range of optical depths. Very few of the remaining ice clouds after the first separation were within this range.

Assuming the data samples are representative of the surfaces being analyzed, enough data were taken from the images so that these thresholds should be applicable in general. Reflectance is a conservative property of these surfaces so the only significant restriction on use of this routine is the presence of daylight. This effectively eliminates polar regions during winter, but where there is sunlight this routine should work well in general. This will be tested in the next chapter, where the routine will be applied to another group of images with different solar illumination and under varying conditions of cloud cover and land/snow cover.

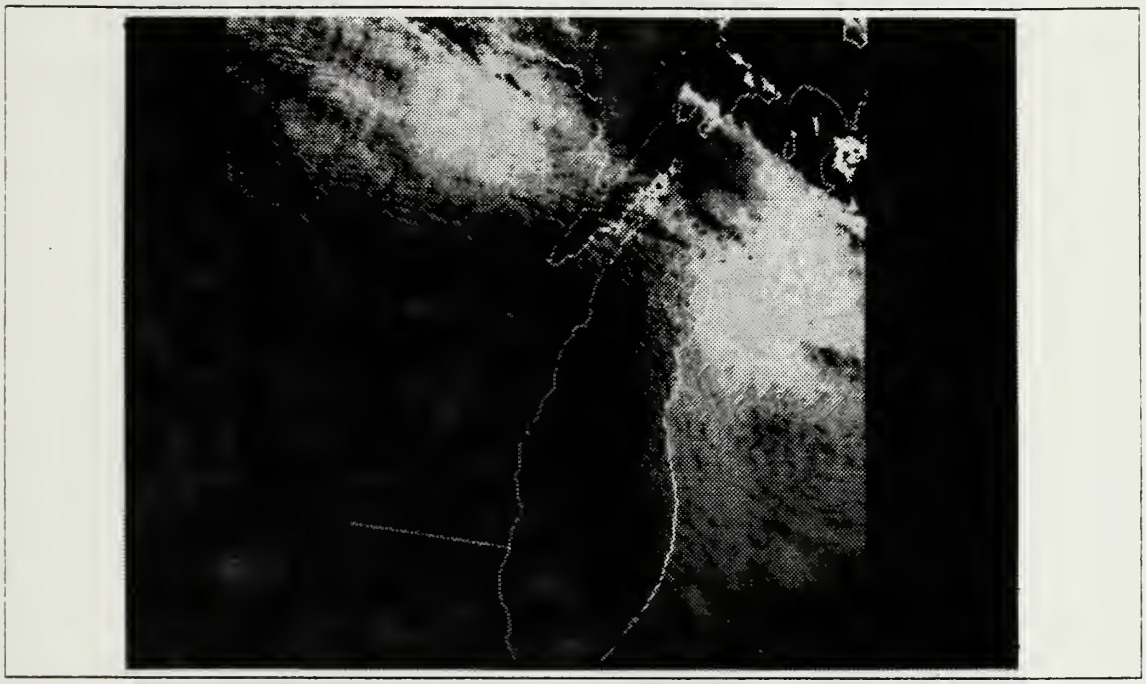

Fig. 3.24 9 Nov 86 subscene 1 - phase 3 cloud cover analysis results.

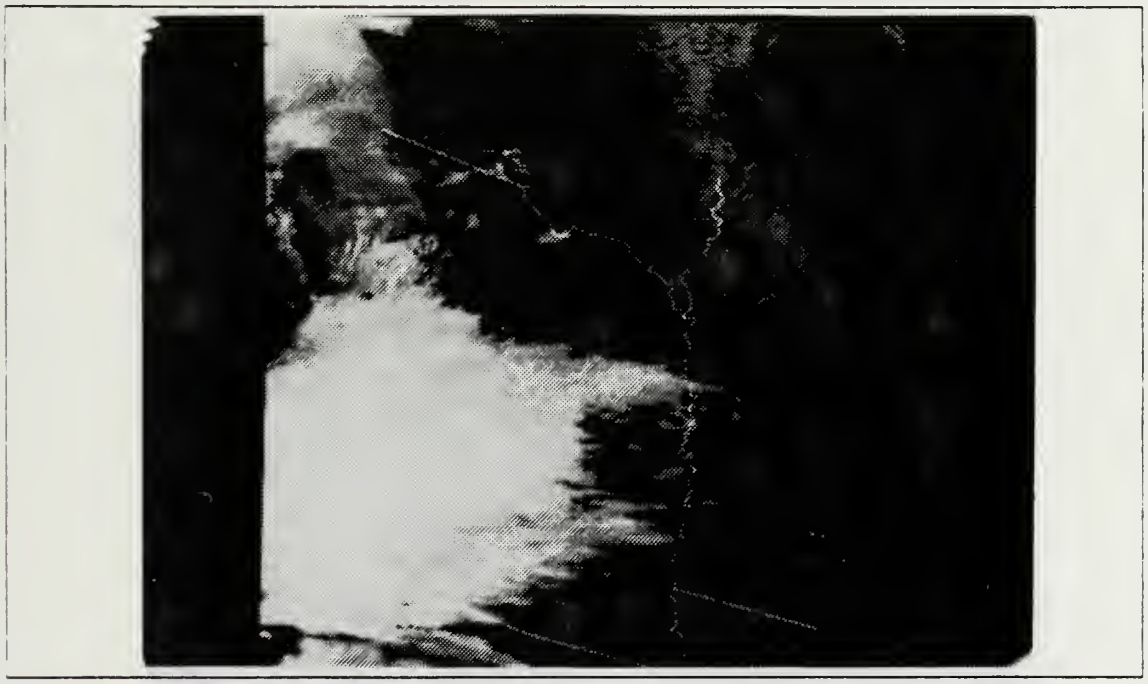

Fig. 3.25 Same as Fig. 3.24 for 9 Nov 86 subscene 2.

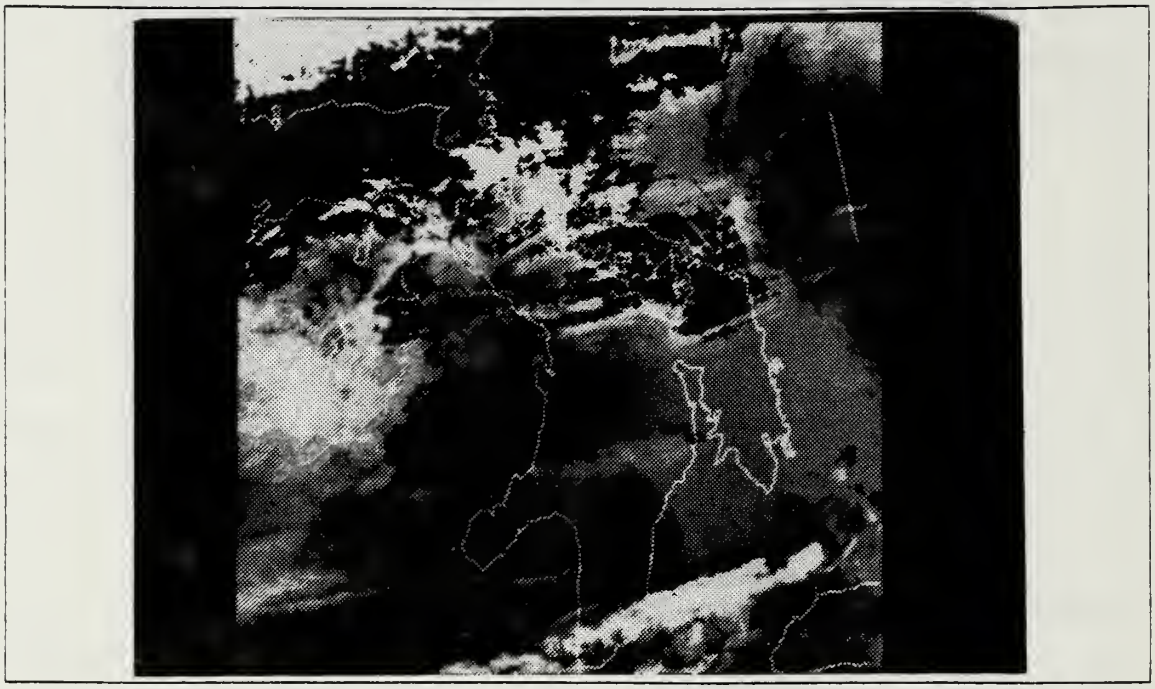

Fig. 3.26 Same as Fig. 3.24 for 10 Nov 86 subscene 1.

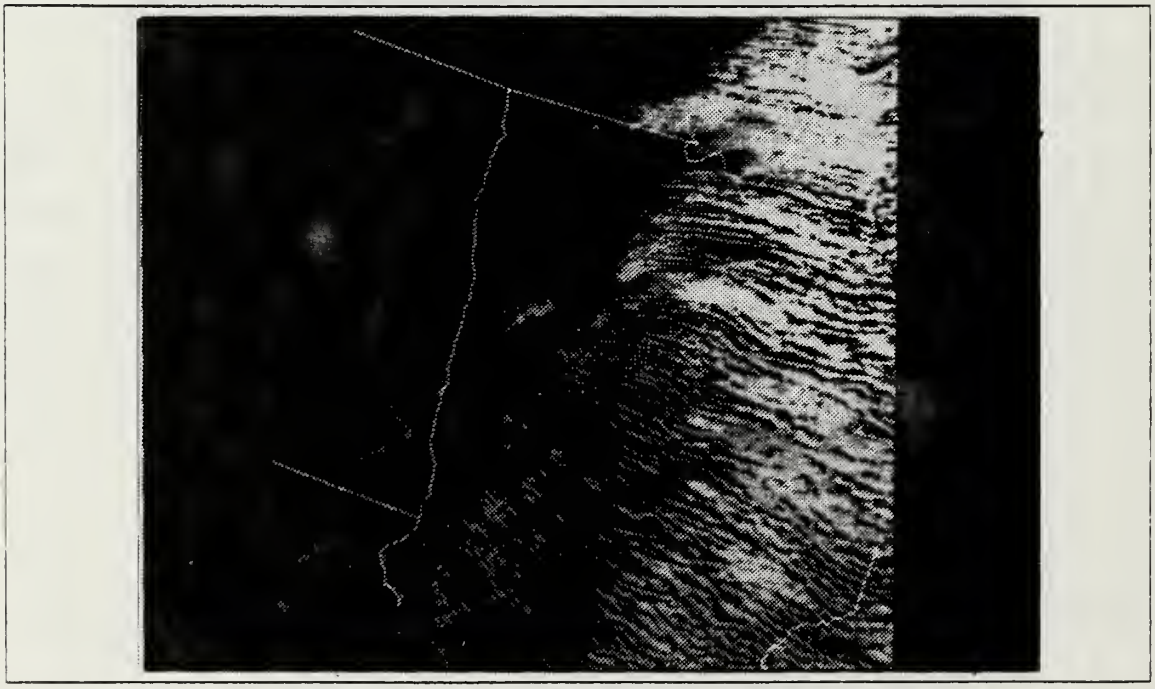

Fig. 3.27 Same as Fig. 3.24 for 10 Nov 86 subscene 2.

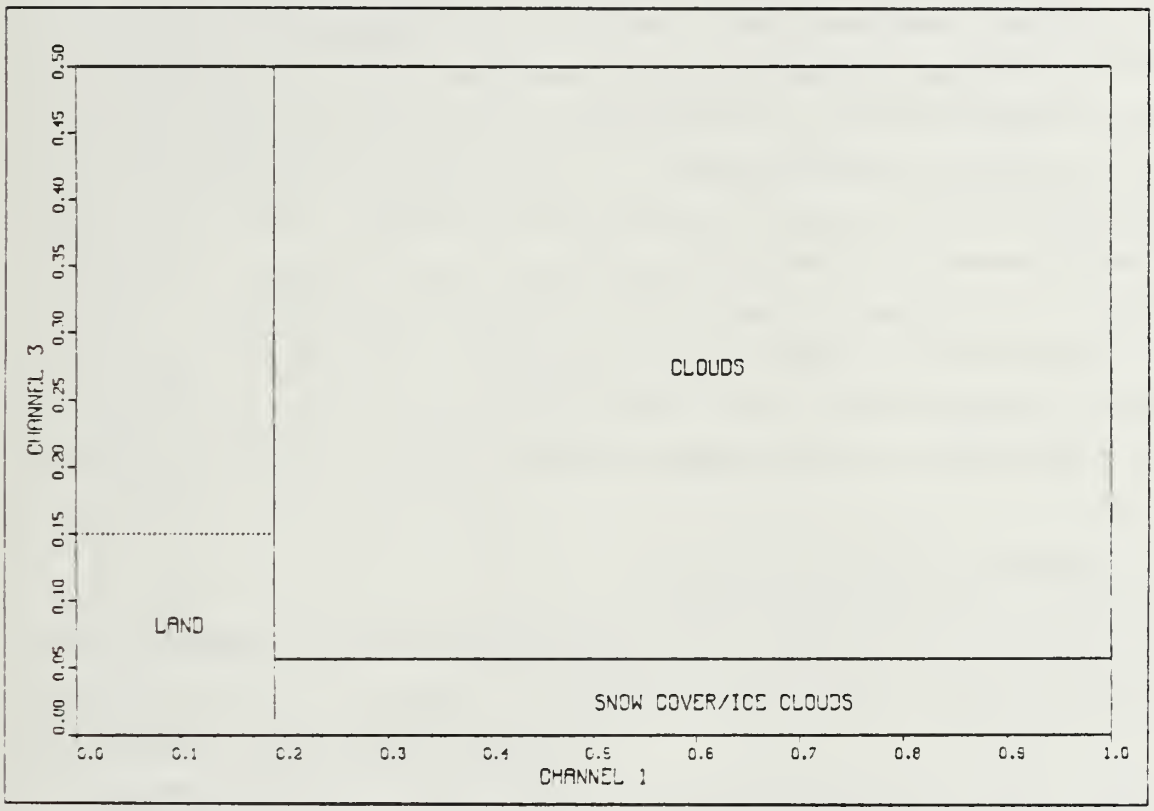

Fig. 3.28 Reflectance thresholds for the automated analysis routine.

IV. APPLICATION OF THE ANALYSIS ROUTINE

A. OVERVIEW

The performance of the analysis technique developed for this study is evaluated in this chapter. Data from two different NOAA satellites, NOAA-9 and NOAA-10, were analyzed to add independence to the statistical results. A total of 6 images are presented, all of which are independent of each other in terms of areal coverage or different satellite. Three of these images were taken from NOAA-9 and three from NOAA-10. Two images were analyzed from the November 10, 1986, pass discussed in Chapter III, including subscene 2 of November 10. Four additional images were taken from a data set from the period January 17-23, 1987. A series of winter storms had recently passed through the central United States leaving significant snow cover from Oklahoma and Kansas northeastward through Missouri, Iowa, and Illinois. The data were processed as described in Chapter III, but only the subscenes are presented. Each of the analyses were evaluated subjectively and then a statistical evaluation accomplished with the available surface observations. Finally, the statistical results from these images were totalled to assess the general performance of the analysis routine.

B. STATISTICAL EVALUATION PLAN

It was assumed that the ground observer can see approximately 30 kilometers, so the reporting stations were located on each image and each pixel within about 30 kilometers was sampled for cloud cover. The number of pixels sampled was either 709 or 1257 depending on the resolution for the particular image. The sampled area was drawn around each of the reporting stations in the images shown here. Two of the images were taken close to the edge of the pass so a 15-pixel radius was sampled for these. The other four were taken closer to the satellite subpoint where the resolution is better and for these a 20-pixel radius was sampled. All the cloud pixels from these samples were then tallied for each station and the cloud cover was determined by the ratio of the number of cloud pixels to the total number of pixels sampled. The percent coverage was then converted to four categories as follows:

1. Clear - less than 2 percent coverage.
2. Scattered - 2 to 50 percent coverage.
3. Broken - 50 to 98 percent coverage.

4. Overcast - greater than 98 percent coverage.

The total sky cover from the surface observation was compared with that calculated from the satellite analysis.

The statistics for each image are presented in three different groups. The first group of statistics reported for each image is those for which both observations either side of the analysis were the same. Included in this group are those stations where only one observation was available, whether or not it was the closest observation to the time of the analysis. Included in the second group of statistics is those stations for which there was a one-category difference in the two surface observations. The analysis was considered to have matched the observation if there was a match between the analysis and either of the observations. If there was no match then the difference was evaluated based on the closest available observation. Finally, the third group is those stations for which there was a two- or three-category difference in the two surface observations. In this group, the analysis was considered to have matched the observation if it matched either observation or was any category in between the two observations. This happened infrequently but occurred when the sky cover changed rapidly during the hour. It can be argued that since the analysis took place in between the observations, the analysis is accurate if it is any category in between or if it matches either observation. The analysis was scored as incorrect if, for example, the observations were broken and clear with the analysis showing overcast for that station. As with the second group, if the analysis was incorrect the difference was based on the closest available observation. For all groups, the reported percentages include the stations where the analysis and observation matched exactly, and those stations for which there was a one-category, a two-category, and a three-category difference between the observation and the analysis.

This approach was taken because it was not possible to verify the satellite analysis with a surface observation taken at the exact same time. Surface observations are available on the hour and there was a time difference of 10 to 50 minutes between these observations and the time of the satellite image. Most of the observations for the hours either side of the satellite pass were the same, leaving little doubt the same sky cover was also present at the analysis time. There were many cases, however, where the observations either side of the analysis were different, making it impossible to know the exact sky cover at analysis time.

C. RESULTS OF THE ANALYSES

Two images on each of three different days were analyzed and evaluated. For each day, each image was independent of the other based on either different areal coverage or different satellite. These cases are described in this section along with the results of the analyses. The images shown in this section are the analyses with the location of the reporting stations shown. Refer to Appendix C for comparison of these analyses with the coincident visible and infrared images.

1. November 10, 1986

These first two cases to be evaluated came from NOAA-9, 2035 GMT, passes of the upper midwestern portion of the United States. The first major storm and snowfall of the 1986-87 season had occurred in this section of the country, leaving 6-10 inches of snow on the ground. The cloud pattern was typical, with a well defined band of jet stream cirrus and a large area of enhanced low-level cumulus streaming into this area as the storm progressed eastward. A complete sequence of channels 1, 3 and 4 images along with the analyses of these cases is shown in Appendix C, Figs. C.13-C.16 (Case 1) and Figs. C.17-C.20 (Case 2).

Case 1 shows eastern North and South Dakota, western Minnesota and the extreme southern portion of Quebec, Canada. The results of this analysis are shown in Fig. 4.1. The deepest snow cover is in northern North Dakota and Minnesota and the depth decreases southward. The clouds in this image are all low-level enhanced cumulus with bases at about 1500 meters and are approximately 100 to 500 meters thick. Table 9 lists the observed sky cover for 2000 GMT and 2100 GMT, along with the analyzed sky cover. The results of the statistical analysis are summarized in Table 10. Case 2 is southwestward of the area shown in Case 1 and shows southeastern South Dakota, southwestern Minnesota, eastern Nebraska and western Iowa. The results of this analysis are shown in Fig. 4.2. The snow cover in this image is rather thin for the most part, but increases in depth in western Nebraska and South Dakota. The cloud cover is a portion of the frontal band and jet stream cirrus, with a small portion of low-level cumulus in central South Dakota and southwestern Minnesota. Table 11 lists the observed sky cover for 2000 GMT and 2100 GMT, along with the analyzed sky cover. The results of the statistical analysis are summarized in Table 12.

The routine produced excellent results with these cases. For Case 1 there is a definite separation between the low clouds on the right hand side of the image and the snow cover on the left hand side, and there is some low cloud over snow in the center

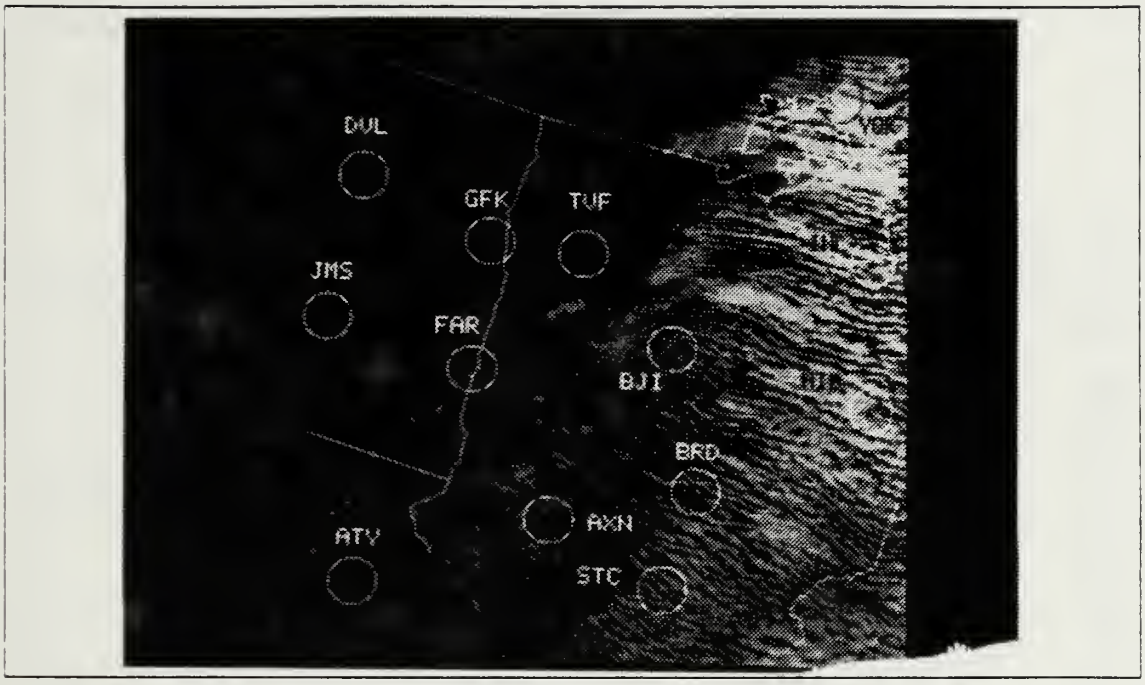

Fig. 4.1 Case 1 cloud cover analysis results. The location of the surface reporting stations is at the center of the labeled circles.

(see Appendix C, Figs. C.13-C.15). The general pattern evident from the visible and infrared images is apparent in the analysis. In both cases, the section of clouds over snow cover in Minnesota and South Dakota can be seen from the texture differences in the visible image and this, along with the entire snow covered area, was handled very well. The cirrus shield in Case 2 was handled generally well but, as expected, the analysis had difficulty with the thinner cirrus in central Iowa.

At FAR (Fargo, ND) on Case 1, there are some snow pixels that had a channel 3 reflectance above the 0.057 threshold, but there also appear to be some genuine cloud pixels within the area sampled. However these cloud pixels are so few that they were possibly not seen by the observer. In Case 2, three stations were affected by the routine's difficulty with cirrus: DSM (Des Moines, IA), FRM (Fairmont, MN), and OTG (Worthington, MN). In this area, the channel 3 reflectance of the cirrus was below threshold and the channel 3-channel 4 temperature factor did not help appreciably. The factor did, however, add to the cirrus analysis in southwestern Iowa.

TABLE 9

Analyzed versus reported sky cover for Case 1.

Station	Reported Coverage-20Z	Analyzed Coverage	Reported Coverage-21Z
ATY	Clear	Clear	Clear
AXN	Overcast	Scattered	Overcast
BJI	Scattered	Scattered	Scattered
BRD	Scattered	Scattered	Not available
DVL	Overcast	Scattered	Not available
FAR	Clear	Scattered	Not available
GFK	Clear	Clear	Clear
HIB	Scattered	Broken	Scattered
INL	Scattered	Broken	Not available
JMS	Clear	Clear	Clear
STC	Scattered	Broken	Scattered
TVF	Clear	Clear	Overcast
YQK	Scattered	Broken	Scattered

There are some discrepancies between the analysis and the observations due perhaps to differences in perspectives of the satellite and observer. Two particularly close calls in Case 1 are STC (St. Cloud, MN) and INL (International Falls, MN). The sky cover for both stations was composed of individual cumulus elements scattered around the sky and it is difficult for the observer to evaluate the total sky cover under these conditions. The analyzed sky cover was 70 percent for INL and 62 percent for STC which is close enough to the observed scattered condition to make this a possible explanation. In Case 2, PIR (Pierre, SD) and RWF (Redwood Falls, MN) had an analyzed sky cover that was much less than observed. This also occurred at DVL (Devils Lake, ND) on Case 1. At all three of these stations the cloud cover appears to be directly over the airfield, perhaps leading the observer to evaluate it as overcast even though the horizontal extent of the cloud was not great. The remaining discrepancies for Case 1 were at AXN (Alexandria, MN), HIB (Hibbing, MN), and YQK (Kenora,

TABLE 10

Verification of Case 1 cloud cover analysis results.

	Category	Count	Percentage
Group 1	Correct	5/12	42
	1-category difference	5/12	42
	2-category difference	2/12	16
	3-category difference	0/12	0
Group 2	Correct	0/0	0
	1-category difference	0/0	0
	2-category difference	0/0	0
	3-category difference	0/0	0
Group 3	Correct	1/1	100
	1-category difference	0/1	0
	2-category difference	0/1	0
	3-category difference	0/1	0
Totals	Correct	6/13	46
	1-category difference	5/13	38
	2-category difference	2/13	16
	3-category difference	0/13	0

Quebec, Canada). It is difficult to attribute these to a weak spot in the analysis algorithm; they may be due to a difference in perspectives of the observer and the satellite. For Case 2 the remaining discrepancies were at FSD (Sioux Falls, SD), OFK (Norfolk, NE), and OLU (Columbus, NE). At both OLU and OFK the problem with cirrus again was the culprit and the temperature factor did not add very much to the cirrus analysis. At OLU the analyzed sky cover was 95 percent, which is within 3 percent of the observed sky cover. At FSD, all analyzed brightness temperatures were within 3 degrees of the observed shelter temperature, so any of the scattered clouds that were reported are either below the resolution of the satellite or too thin to be analyzed correctly.

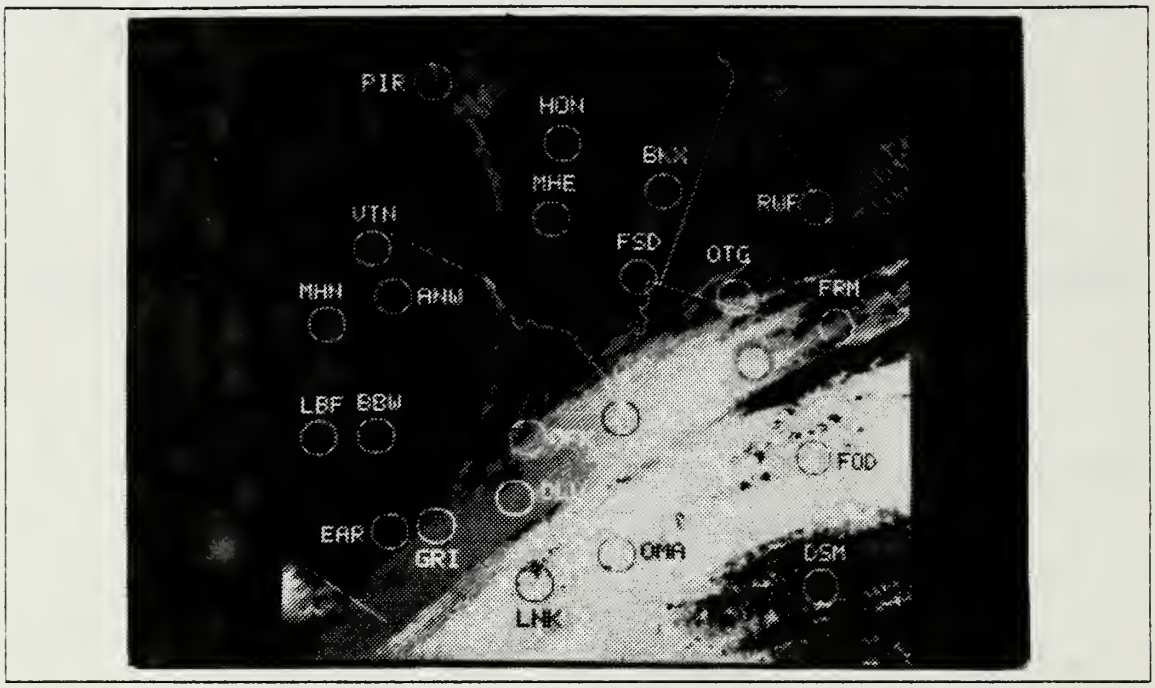

Fig. 4.2 Same as Fig. 4.1 for Case 2.

2. **January 17, 1987**

The next two cases to be evaluated were from the same area but from different satellites and were separated by about 6-7 hours. Major storms the previous week deposited a very deep layer of snow and the snow depth is about 10-16 inches in eastern Colorado, thinning out in western Kansas. There is a frontal cloud band and cirrus shield in these images and some low-level clouds in the cold air to the north. A complete sequence of channels 1, 3, and 4 images along with analyses for these cases is shown in Appendix C, Figs. C.21-C.24 (Case 3) and Figs. C.25-C.28 (Case 4).

Case 3 shows eastern Colorado, southwestern Nebraska, western Kansas and the Oklahoma panhandle. The deep snow in eastern Colorado thins out and seems to merge with an area of low clouds in southwestern Nebraska. The frontal band and cirrus shield extend northeastward from northern New Mexico into south-central Nebraska. This image was taken from the NOAA-9 pass of 2135 GMT and the results of the analysis are shown in Fig. 4.3. Table 13 lists the observed sky cover for 2100 GMT and 2200 GMT, along with the analyzed sky cover, and the results of the analysis are summarized in Table 14. Case 4 shows generally the same area as Case 3 but a little farther to the south. This image shows more of the frontal band and cirrus

TABLE 11

Analyzed versus reported sky cover for Case 2.

Station	Reported Coverage-20Z	Analyzed Coverage	Reported Coverage-21Z
3SE	Overcast	Overcast	Overcast
ANW	Clear	Clear	Clear
BBW	Clear	Clear	Clear
BKX	Not Available	Clear	Clear
DSM	Broken	Scattered	Not available
EAR	Overcast	Clear	Clear
FOD	Overcast	Overcast	Broken
FRM	Overcast	Broken	Not available
FSD	Scattered	Clear	Not available
GRI	Broken	Broken	Overcast
HON	Clear	Clear	Clear
LBF	Clear	Clear	Clear
LNK	Broken	Broken	Broken
MHE	Clear	Clear	Clear
MHN	Clear	Clear	Clear
OFK	Overcast	Broken	Not available
OLU	Overcast	Broken	Overcast
OMA	Overcast	Overcast	Overcast
OTG	Not available	Broken	Overcast
PIR	Overcast	Scattered	Overcast
RWF	Overcast	Scattered	Not available
SUX	Overcast	Overcast	Broken
VTN	Clear	Clear	Clear

TABLE 12

Verification of Case 2 cloud cover analysis results.

	Category	Count	Percentage
Group 1	Correct	11/19	58
	1-category difference	6/18	32
	2-category difference	2/19	10
	3-category difference	0/19	0
Group 2	Correct	3/3	100
	1-category difference	0/3	0
	2-category difference	0/3	0
	3-category difference	0/3	0
Group 3	Correct	1/1	100
	1-category difference	0/1	0
	2-category difference	0/1	0
	3-category difference	0/1	0
Totals	Correct	15/23	65
	1-category difference	6/23	26
	2-category difference	2/23	9
	3-category difference	0/23	0

shield and there are low clouds present over the snow cover in eastern Colorado and western Kansas. Additionally, there is a widespread area of low- to mid-level clouds in the Texas panhandle. The results of the analysis are shown in Fig. 4.4. Table 15 lists the observed sky cover for 1500 GMT and 1600 GMT, along with the analyzed sky cover. This image came from the NOAA-10 pass of 1513 GMT and the results are summarized in Table 16.

In spite of the fact that there is a great deal of cirrus in these images, the analysis routine worked quite well. Particularly encouraging is the analysis of the low clouds and snow, which was virtually all correct. The most interesting point about these analyses is the role of shadows cast due to the large solar zenith angle. This was not considered at the beginning as a possible source of error but these analyses

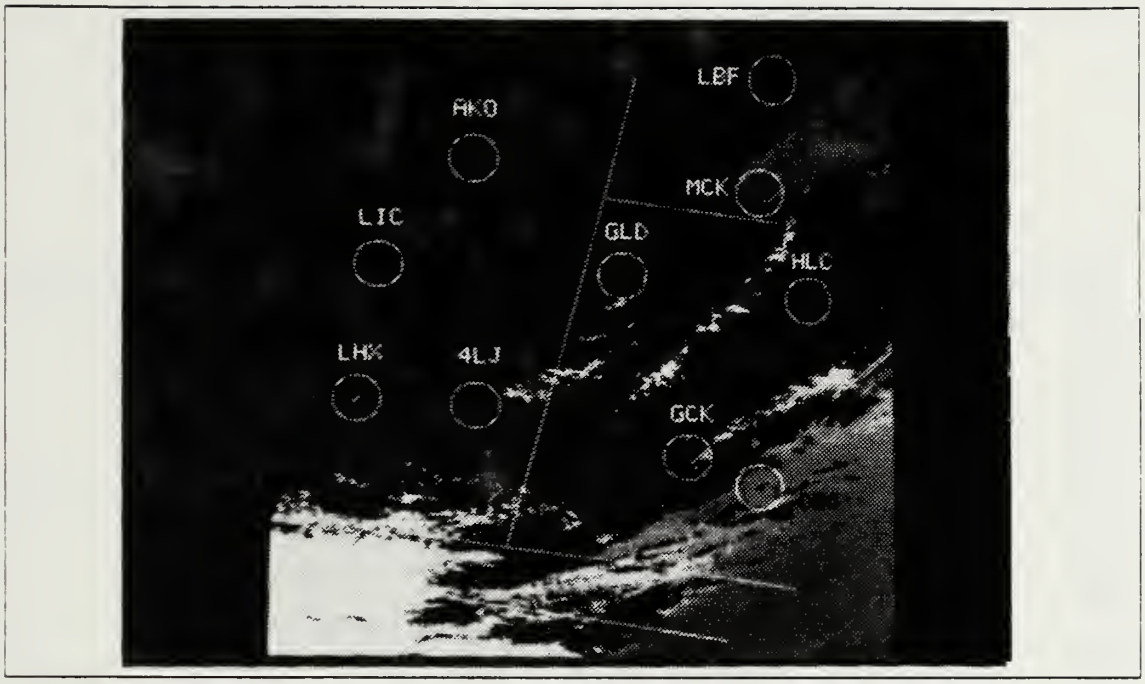

Fig. 4.3 Same as Fig. 4.1 for Case 3.

illustrate the effect quite graphically. Case 3 was an afternoon pass and the sun was to the southwest casting shadows on the snow cover in Colorado and Kansas. Case 4 was a morning pass and the sun was to the southeast casting shadows on the snow cover in Colorado and there seem to be high-level clouds in the cirrus shield and frontal band casting shadows on the low-level clouds. When this happened, both the channel 1 and channel 3 reflectances were reduced considerably and the surface on which the shadow is cast was analyzed as land. This had a very noticeable effect on the quality of both of these analyses.

The major problem with Case 3 was the analysis of cirrus. Three of the stations that were different from the surface observation were 4LJ (Lamar, CO), GCK (Garden City, KS), and HLC (Hill City, KS), all due to the problem with cirrus. The discrepancy at LBF (North Platte, NE) appears to be a problem with the observation, perhaps an error in transmission. The clouds in this area were handled very well by the analysis and are to the southeast and west of LBF. Case 4 had discrepancies at 7 stations all due to shadows on low clouds being cast by high clouds. Those stations are 4LJ (Lamar, CO), PUB (Pueblo, CO), TAD (Trinidad, CO), TCC (Tucumcari, NM), DHT (Dalhart, TX), GLD (Goodland, KS), and GCK (Garden City, KS). The

TABLE 13

Analyzed versus reported sky cover for Case 3.

Station	Reported Coverage-21Z	Analyzed Coverage	Reported Coverage-22Z
4LJ	Scattered	Clear	Not available
AKO	Clear	Clear	Clear
DDC	Broken	Broken	Not available
GCK	Not Available	Scattered	Overcast
GLD	Scattered	Scattered	Scattered
HLC	Broken	Clear	Scattered
LBF	Scattered	Clear	Overcast
LHX	Overcast	Scattered	Scattered
LIC	Clear	Clear	Clear
MCK	Overcast	Broken	Scattered

shadows were quite prominent in the visible image (see Appendix C, Fig. C.25) and also in the analysis shown here. The shadows were so prominent that the darker area in the analysis of snow cover between PUB and COS (Colorado Springs, CO) had the exact shape of the cloud element between PUB and LHX (La Junta, CO). Two other stations on Case 4 had discrepancies: COS and APA (Arapahoe, CO). For COS, low-level overcast was reported and the analysis was clear. The channel 4 brightness temperatures were mostly within 3 to 4 degrees of the reported surface temperature. There were some temperatures that were 10 degrees colder but these were in the higher elevations and the channel 3 reflectance associated with these pixels was 0.01. These characteristics are very indicative of snow cover. It is possible that there was a transmission or a data storage problem associated with this observation. The observed sky cover for APA was clear and the analysis was broken. The probability of an error in the observation is more likely here because there are quite obviously clouds in the visible and infrared images (see Appendix C, Figs. C.21 and C.23). The clouds that are present are even casting shadows so there may even be an overcast sky condition present at this station. Another explanation may lie in the fact that the 1500 GMT

TABLE 14

Verification Case 3 cloud cover analysis results.

	Category	Count	Percentage
Group 1	Correct	4/6	67
	1-category difference	1/6	17
	2-category difference	1/6	16
	3-category difference	0/6	0
Group 2	Correct	0/1	0
	1-category difference	1/1	100
	2-category difference	0/1	0
	3-category difference	0/1	0
Group 3	Correct	2/3	67
	1-category difference	0/3	0
	2-category difference	0/3	0
	3-category difference	1/3	33
Totals	Correct	6/10	60
	1-category difference	2/10	20
	2-category difference	1/10	10
	3-category difference	1/10	10

observation was not available for APA. This could be a case of clearing skies within the hour with the analysis being in between the changes.

3. **January 23, 1987**

The final two cases to be evaluated both came from NOAA-10 at 1443 GMT. A series of winter storms left a long swath of snow cover from New Mexico and Texas northeastward to the Great Lakes. Both images have snow-free land along with snow cover ranging from less than an inch in Iowa and Kansas to 11 inches in Indiana. The cloud cover in these images is only low- to mid-level clouds, with lake-effect clouds and snow showers in Michigan and Indiana. A complete sequence of channels 1, 3, and 4 images for these cases along with the analyses is shown in Appendix C, Figs. C.29-C.32 (Case 5) and C.33-C.36 (Case 6).

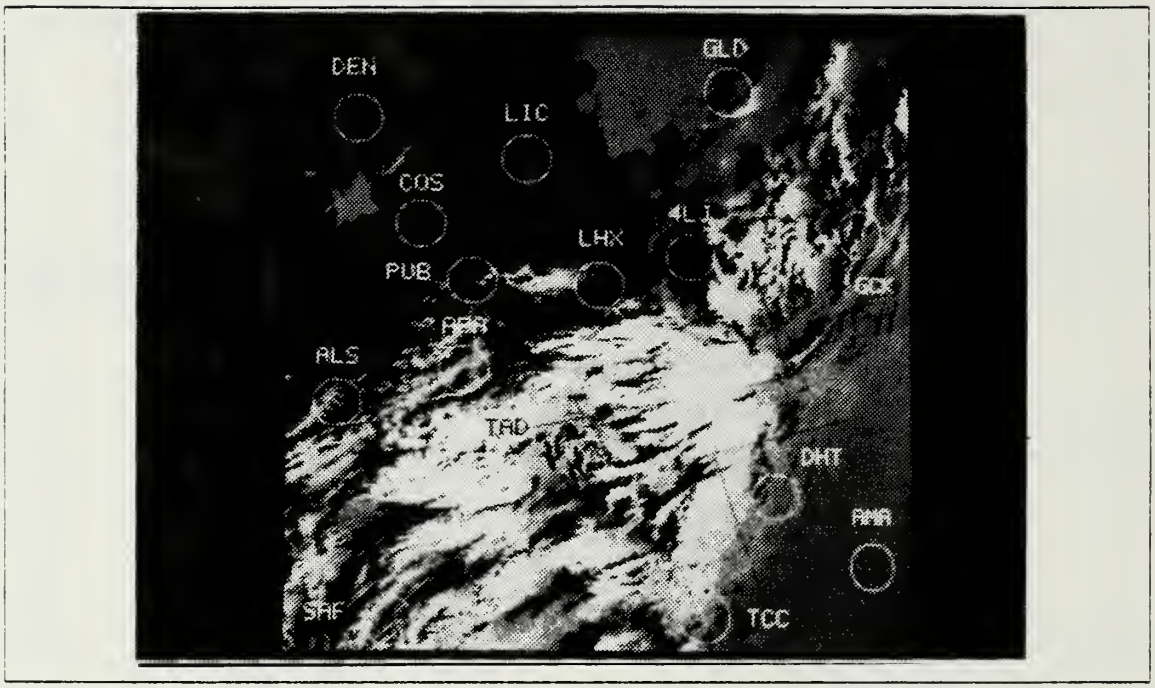

Fig. 4.4 Same as Fig. 4.1 for Case 4.

Case 5 shows nearly all of Kansas, the northern half of Oklahoma and northwestern Missouri. Of particular interest in this image is the low clouds directly over the snow cover in Kansas. Table 17 lists the observed sky cover for 1400 GMT and 1500 GMT, along with the analyzed sky cover. The results of the analysis are shown in Fig. 4.5 and the results of the verification are summarized in Table 18. Case 6 covers eastern Iowa, southern Wisconsin and nearly all of Illinois, Indiana, Michigan and Lake Michigan. This image is from near the edge of the pass and has negligible snow cover except in Illinois and Indiana. This was a very cold airmass and the clouds in the image were generated by this very cold air flowing over the warmer Lake Michigan. Table 19 lists the observed sky cover for 1400 GMT and 1500 GMT, along with the analyzed sky cover. The analysis is shown in Fig. 4.6 and the verification results are summarized in Table 20.

Case 5 is perhaps the best of these 6 cases for illustrating the strength of this routine in handling low clouds over snow. The clouds in southern and western Kansas are apparent on the visible image only because of shadows around the edge of the cloud (Appendix C, Fig. C.29). They are virtually invisible on the infrared image (Appendix C, Fig. C.31), except that they appear to be slightly darker than the cloud-

TABLE 15

Analyzed versus reported sky cover for Case 4.

Station	Reported Coverage-15Z	Analyzed Coverage	Reported Coverage-16Z
4LJ	Broken	Scattered	Not available
ALS	Overcast	Scattered	Scattered
AMA	Broken	Overcast	Overcast
APA	Not available	Broken	Clear
COS	Overcast	Clear	Overcast
DEN	Overcast	Clear	Clear
DHT	Overcast	Broken	Overcast
GCK	Overcast	Broken	Overcast
GLD	Broken	Scattered	Overcast
LHX	Overcast	Scattered	Scattered
LIC	Not available	Clear	Clear
PUB	Overcast	Scattered	Overcast
SAF	Scattered	Broken	Broken
TAD	Overcast	Broken	Overcast
TCC	Overcast	Broken	Overcast

free areas indicating the presence of a temperature inversion. The objective analysis cleared up the confusion quite dramatically and it even picked up a thin strip of cirrus cloud in Oklahoma that is evident on the infrared image but not on the visible image.

Case 6 brought out the fact that the anisotropic factor is very critical when analyzing an image close to the edge of the pass. The only clouds in this image are directly over Lake Michigan with some cloud lines extending into Michigan and Indiana. These clouds can be seen fairly well in the images of Channels 1, 3, and 4 in Appendix C, Figs. C.33 through C.35. The analysis overestimated the cloud cover, and it appears that this occurred over either clear land or land with very little snow cover. This is a morning pass so at the right hand side of this image, the satellite zenith angle is large and the relative azimuth angle is large, along with a large solar zenith angle.

TABLE 16

Verification of Case 4 cloud cover analysis results.

	Category	Count	Percentage
Group 1	Correct	1/9	11
	1-category difference	5/9	56
	2-category difference	2/9	22
	3-category difference	1/9	11
Group 2	Correct	2/3	67
	1-category difference	1/3	33
	2-category difference	0/3	0
	3-category difference	0/3	0
Group 3	Correct	3/3	100
	1-category difference	0/3	0
	2-category difference	0/3	0
	3-category difference	0/3	0
Totals	Correct	6/15	40
	1-category difference	6/15	40
	2-category difference	2/15	13
	3-category difference	1/15	7

At IND (Indianapolis, IN) the skies were reported clear and there was 1 inch of snow on the ground. The solar zenith, satellite zenith, and relative azimuth angles were about 74°, 60°, and 140° degrees respectively making the anisotropic factor 1.09. This factor is the average for bin 31 of snow and low cloud from the tables of Taylor and Stowe (1984) since land values were not reported for a solar zenith angle of greater than 72°. However, for a solar zenith angle ranging from 66° to 72°, the factor for land in this bin is 1.44. This value from the tables is based on only 6 observations, but is still much greater than the average that is used in the analysis routine. What has happened is that the anisotropic factor used in the program was not as large as it should have been for this configuration of sun-satellite geometry. This caused the reflectance to be *above* the established threshold for land and resulted in many of these

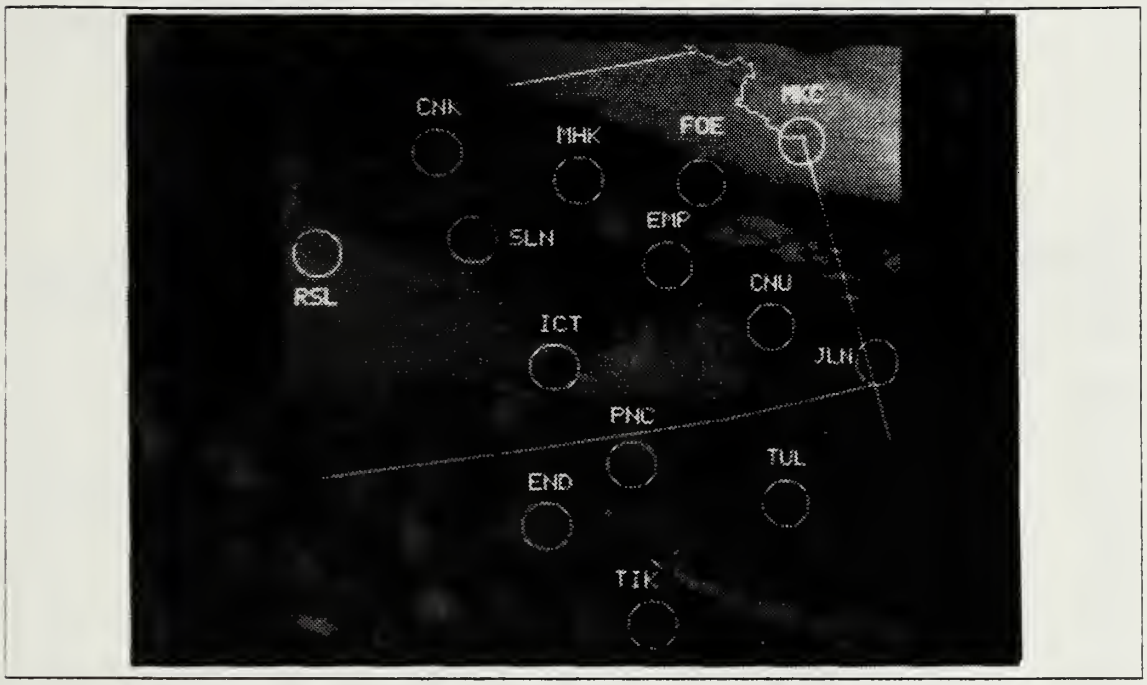

Fig. 4.5 Same as Fig. 4.1 for Case 5.

pixels being analyzed as cloud (see Eq. 2.12). Table 2.1 of Taylor and Stowe shows that land is more variable in terms of anisotropy than is snow, and values for land are not reported at a solar zenith of greater than 72°. It would have been better to have assumed that the values valid for the solar zenith angle range from 66° to 72° were also valid for the higher ranges for which values were not reported, rather than to just average the values in these ranges for snow and cloud. This would have produced a higher average value to be used by the program and may have avoided some of this problem.

The verification of Case 5 was disappointing because the analysis appeared to produce excellent results. There was a discrepancy with all the stations in Oklahoma: TUL (Tulsa), TIK (Tinker AFB), END (Vance AFB), and PNC (Ponca City). The visible image shows surface features in the snow cover for END and PNC, and clear land is present for TIK and TUL (Appendix C, Fig. C.29). Channel 4 temperatures for all of these stations were within 3 to 5 degrees of the reported temperature, indicating no cloud cover at the height it was reported. This also appears to be the case at FOE (Forbes AFB, KS), where surface features are present in the snow cover on the visible image and were captured well by the analysis. At SLN (Salina, KS) and MKC (Kansas

TABLE 17

Analyzed versus reported sky cover for Case 5.

Station	Reported Coverage-14Z	Analyzed Coverage	Reported Coverage-15Z
CNK	Clear	Clear	Clear
CNU	Scattered	Clear	Clear
EMP	Not available	Clear	Clear
END	Overcast	Clear	Overcast
FOE	Overcast	Clear	Overcast
ICT	Overcast	Scattered	Scattered
JLN	Overcast	Clear	Clear
MHK	Clear	Clear	Clear
MKC	Broken	Overcast	Broken
PNC	Scattered	Clear	Scattered
RSL	Broken	Broken	Broken
SLN	Clear	Scattered	Clear
TIK	Overcast	Clear	Scattered
TUL	Scattered	Clear	Scattered

City, MO) the discrepancy is probably due to the different perspectives of the observer and satellite. At SLN the analysis had clouds only at the outer limit of the sampled area making it very reasonable to assume the observer could not see them. At MKC it is reasonable to assume that the observer reported broken low-level clouds and was unable to see anything above these breaks. This overcast layer is evident in all images (see Appendix C, Fig. C.29-C.31) and was analyzed nearly perfectly by the routine. On Case 6, of the 15 stations with a discrepancy between the analysis and observation, 11 can be attributed to the problem with the anisotropic reflectance factor. The other 4 stations are GRR (Grand Rapids, MI), JXN (Jackson, MI), MKG (Muskegon, MI), and SBN (South Bend, IN). These stations reported greater cloud cover that was analyzed, possibly due to clouds being directly over the station and the sampled area for each station including some clear areas. A 15-pixel radius was sampled in this

TABLE 18

Verification of Case 5 cloud cover analysis results.

	Category	Count	Percentage
Group 1	Correct	4/10	40
	1-category difference	4/10	40
	2-category difference	0/10	0
	3-category difference	2/10	20
Group 2	Correct	1/1	100
	1-category difference	0/1	0
	2-category difference	0/1	0
	3-category difference	0/1	0
Group 3	Correct	2/3	67
	1-category difference	1/3	33
	2-category difference	0/3	0
	3-category difference	0/3	0
Totals	Correct	7/14	50
	1-category difference	5/14	36
	2-category difference	0/14	0
	3-category difference	2/14	14

image and close to the right hand side, where all these stations are located, the resolution degrades to the point where this may be too large an area to be sampled. The discrepancy at MKE (Milwaukee, WI) can be attributed somewhat to the error in estimating the anisotropic factor as discussed above, but this is more likely due to most of the analyzed clouds being over Lake Michigan while directly over the station it was clear.

4. **Evaluation of the Analysis Routine**

The combined results of all six analyses are summarized in Table 21. It is especially encouraging that the results are heavily weighted on the positive side, that is, there were very few stations that had an analyzed sky cover two or three categories different from the analysis.

The significant problems noted are as follows:

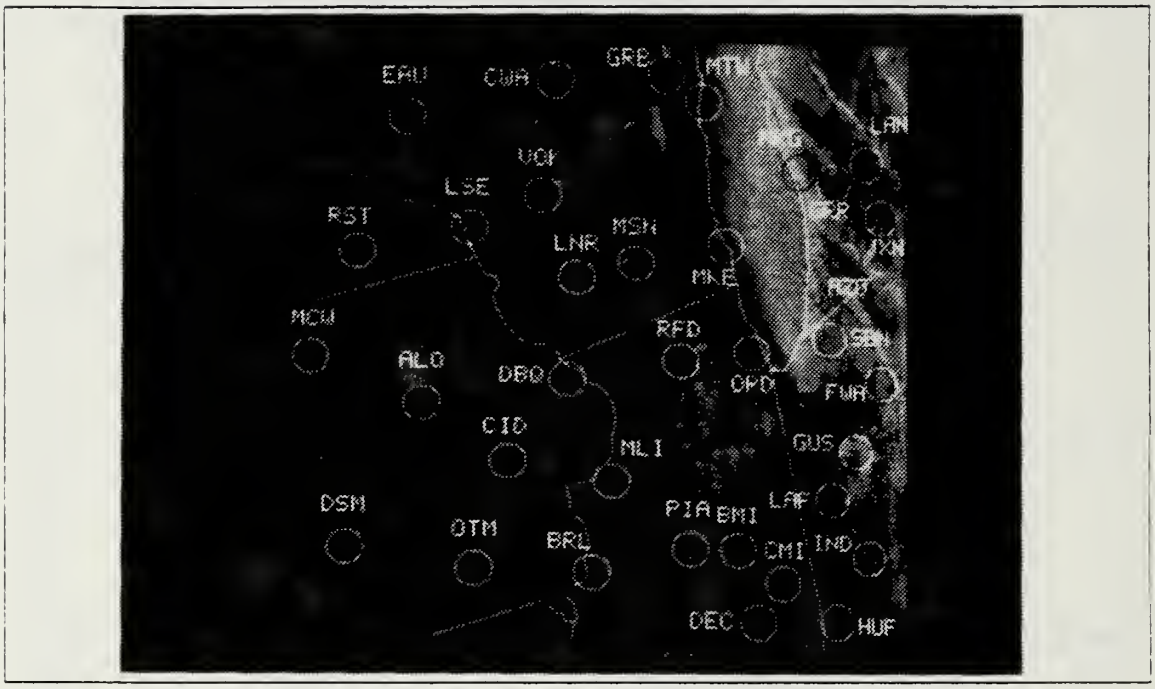

Fig. 4.6 Same as Fig. 4.1 for Case 6.

1. Snow cover and cirrus have very similar reflective properties in channels 1 and 3 so their correct analysis cannot be based on reflectance. There is a difference in the transmissive properties of cirrus between channels 3 and 4 that can be used to aid in the analysis of cirrus, but there are still significant problems in that regard. It is estimated that about 50 percent of the cirrus on all of the images analyzed here was handled correctly based strictly on the channel 3 reflectance, with less than 5 percent added to this based on the channel 3-channel 4 temperature factor. About 55 percent of all cirrus was analyzed correctly. The temperature factor did not add very much to the analysis because solar reflection is included in the brightness temperature difference between channels 3 and 4. The attempt was to analyze cirrus based on a brightness temperature difference due the the different transmissive properties of cirrus between channels 3 and 4, but the effects of solar reflection nearly completely wiped out any detectable differences in thermal emission. Cirrus clouds only within a narrow range of optical depths could be unambiguously separated from snow cover.

2. Channel 1 reflectance was used in the analysis of land. There were instances where there was some overlap with liquid clouds and the threshold setting was such that some land was analyzed as cloud. Much more significant in the analysis of land was the fact that anisotropic factors are not available for land when the solar zenith angle is greater than 72°. This was critical because according to the values of Taylor and Stowe (1984), land is more variable in terms of anisotropy than is snow or cloud. In Case 6, clouds were incorrectly

TABLE 19

Analyzed versus reported sky cover for Case 6.

Station	Reported Coverage-14Z	Analyzed Coverage	Reported Coverage-15Z
ALO	Clear	Clear	Clear
AZO	Scattered	Broken	Scattered
BMI	Clear	Clear	Clear
BRL	Clear	Clear	Not available
CID	Clear	Clear	Not available
CMI	Clear	Clear	Not available
CWA	Clear	Clear	Not available
DBQ	Clear	Clear	Clear
DEC	Clear	Clear	Clear
DSM	Clear	Clear	Clear
EAU	Clear	Clear	Clear
FWA	Scattered	Broken	Not available
GRB	Clear	Scattered	Clear
GRR	Overcast	Scattered	Overcast
GUS	Overcast	Broken	Clear
HUF	Clear	Clear	Clear
IND	Clear	Scattered	Clear
JXN	Overcast	Scattered	Overcast
LAF	Clear	Scattered	Clear
LAN	Overcast	Scattered	Clear
LNR	Clear	Clear	Not available
LSE	Clear	Scattered	Clear
MCW	Clear	Clear	Clear
MKE	Clear	Broken	Clear
MKG	Overcast	Broken	Overcast
MLI	Clear	Clear	Clear
MSN	Clear	Scattered	Clear

TABLE 19

Analyzed versus reported sky cover for Case 6. (cont'd.)

MTW	Not available	Broken	Overcast
ORD	Clear	Scattered	Clear
OTM	Clear	Clear	Clear
PIA	Clear	Clear	Clear
RFD	Clear	Scattered	Clear
RST	Clear	Clear	Clear
SBN	Overcast	Broken	Overcast
VOK	Not available	Clear	Clear

analyzed over clear land close to the edge of the image because the anisotropic factor used was less than what it should have been.

3. An unexpected problem was with shadows. The cloud analysis was affected by this when high-level clouds cast shadows on low-level clouds. For the reader who is more interested in a correct analysis of land versus snow, this problem affected the analysis of snow cover. The shadows caused the reflectance in both channels 1 and 3 to be reduced and the affected pixels were analyzed as land. This problem was particularly noticeable in the winter images when the solar zenith angle was the largest. Unlike the other problems, nothing can be objectively done about this.

There are also some reasons for discrepancies between the analyzed and observed sky cover that are beyond the control of the routine:

1. The time difference between the surface observation and the satellite pass was great enough in some cases to lead to a significant difference in sky cover. This occurred when the weather system was very dynamic and there were rapid changes in cloud cover. It is for this reason that the analyses were compared with the hourly observations on either side.

2. The perspectives of a ground observer and a satellite are very different, the ground observer viewing the clouds from below and the satellite viewing the clouds from above. The ground observer does not spend hours meticulously evaluating the exact coverage of each individual cloud element and then add these together to arrive at a total cloud coverage. A computer can take the time to do this but the observer makes a subjective determination of both height and sky cover and no two observers will make the same determination at any given time. In a convective situation much of the reported sky cover is due to the sides of the clouds, especially those viewed at a large zenith angle.

TABLE 20

Verification of Case 6 cloud cover analysis results.

	Category	Count	Percentage
Group 1	Correct	18/33	55
	1-category difference	12/33	36
	2-category difference	3/33	9
	3-category difference	0/33	0
Group 2	Correct	0/0	0
	1-category difference	0/0	0
	2-category difference	0/0	0
	3-category difference	0/0	0
Group 3	Correct	2/2	100
	1-category difference	0/2	0
	2-category difference	0/2	0
	3-category difference	0/2	0
Totals	Correct	20/35	57
	1-category difference	12/35	34
	2-category difference	3/35	9
	3-category difference	0/35	0

Because of this, gaps between the cloud elements become smaller and disappear as the zenith angle increases. The resulting sky cover will be greater than what a satellite would see for that station since all the clouds within the sampled radius can be viewed within just a few degrees of scan angle. An observer may be limited to the portions of the sky that can be evaluated due to obstructions around the airfield and, in addition, an observer may intentionally limit the distance from the airfield at which cloud cover will be evaluated, concentrating only on what is in the immediate vicinity of the airfield.

3. Characteristic to all polar-orbiting satellites is errors in navigation. Error in location of the individual stations on the images was about 3 to 5 kilometers. The geographical boundaries were corrected on images where landmarks were visible for assistance, but no attempt was made to correct the location of the individual stations.

TABLE 21

Combined statistics for all analyses.

Category	Count	Percentage
Correct	60/110	55
1-category difference	36/110	33
2-category difference	10/110	9
3-category difference	4/110	3

4. Errors in the surface observations arose due to problems with storage in the data base or errors in transmission. Sky cover in the observations used in this study is stored in a single character, making the probability of an error greater than if it were stored as the standard three-character abbreviation. Many stations had to be discarded as potential candidates for verifying the analyses because meaningless characters for sky cover had crept into the data base.

It is unfortunate that so many of the discrepancies between the analysis and observations were attributed to problems beyond the control of the routine. It would have been much more tedious to get copies of actual coded observations from the archives, but that most certainly would have yielded improved verification results. In spite of these problems, however, the statistics indicate that the analysis routine was very successful under a wide variety of circumstances.

V. SUMMARY AND RECOMMENDATIONS

This thesis reported values of solar reflectance of snow, clouds and land at 3.7μm using data from channel 3 of the AVHRR. The reflectance was derived using a method of removing the thermal emission portion of the channel 3 radiance measurement. These values were calculated using a rough estimation of anisotropic reflectance and values agree quite well with those determined from various theoretical studies. The reason is that for most clouds, thermal emission is a much smaller part of the channel 3 radiance measurement than is solar reflection (see Fig. 2.3), so any errors in the technique that removes thermal emission introduce little error into the derived reflectance. The greatest error was noted for the reflectance of snow cover. Its reflectance is typically less than 5 percent and in this situation solar reflection and thermal emission are nearly equal contributors to the channel 3 measured radiance. Thus the error in removing the thermal emission translated into larger error in reflectance.

An automated cloud analysis was then developed to handle the significant problem of snow/cloud discrimination. The routine exploits the fact that snow has a very low reflectance in AVHRR channel 3 while liquid clouds and most ice clouds have a high reflectance. Since the reflective properties of snow cover and many ice clouds are so similar in both channels 1 and 3, the routine attempted analysis of cirrus that did not meet the channel 3 reflectance threshold based on a difference in its transmissive properties between channels 3 and 4. Unfortunately, this technique did not work well because in addition to the difference in transmissive properties, solar reflection contributes to the difference in brightness temperature. The reflectance was variable enough to make unambiguous separation of the two surfaces possible only for cirrus of a limited range of optical depths. The algorithm was very successful and produced excellent results, even at very large solar zenith angles. Its main strength was in separating low clouds from snow cover, while its weakest point was the analysis of cirrus clouds. The analyses were verified against the coincident surface observations and 88 percent of the analyzed stations either matched or were just one category of sky cover different from the observed sky cover.

Although the routine produced generally excellent results, some improvements are recommended:

1. It was suggested in Chapter II that additional theoretical studies be undertaken to improve the available information on the anisotropic reflectance factor. In the interim, what we know can be put to better use. First needed is a very easy near-term solution to the missing values for land at solar zenith angles greater than 72°. The factor currently used is the average for cloud and snow. The land values for the range from 66° to 72° could be used for the higher ranges, thus yielding a higher average for use by the analysis routine. Since the configuration of NOAA satellites limits the range of satellite zenith angle and thus the number of bins that need to be used by the computer program, more accurate values can be used as input to the program. Rather than the averaging technique used in this study, a table of values for each surface should be made available for the program to choose from. A preliminary guess of the scene classification could be made and then an iterative process used to arrive at the correct factor for that particular classification.

2. For the most part, cirrus could be separated successfully by this routine by setting the channel 3 threshold at 0.057. Approximately 50 percent of the cirrus was analyzed correctly with this threshold. An attempt was made to improve the analysis of the cirrus that was too thin to be separated with this threshold by looking at the difference in the transmissive properties between channels 3 and 4. In the presence of cirrus, there is a difference in brightness temperature between these two channels while there is little difference in the clear sky case. This was formulated into a unitless factor and then a threshold was developed from the test data. This factor did not add significantly to the analysis of cirrus because variable solar reflection "contaminated" the difference in brightness temperature due to thermal emission. This characteristic of cirrus in these two channels should be explored further to see if any additional techniques can be developed to improve the analysis. Another possibility is to work out a way to incorporate surface temperature into the analysis routine. A statistical analysis of all the clear sky pixels in the image could be used to determine a dynamic threshold temperature based on conditions present in that particular image. Development of a technique of this kind will require careful evaluation of computer processing time. As it is now written, the routine requires 20 to 30 minutes to generate a single analysis so it is already computationally-intensive. In spite of added quality, the additional time required may lessen the usefulness of the analysis.

3. More work should be done to compile a data base of near-infrared reflectances. The values reported here were based on samples of 4800 pixels from two satellite passes. This may seem to be a large number of pixels but it is not an extensive sampling. The sampling was from only two days of data in one season of the year and with a very limited range of sun-satellite geometry. Building a complete data base should span several future studies and work must continue so that software can be developed to process data from the 1.6μm sensors when they become operational.

This analysis routine is a medium-sized software package written in FORTRAN language and it is adaptable to any computer system. However it is a computationally-intensive routine. Each of the analyses took from 20 to 30 minutes to generate on a Digital Equipment Corporation VAX 11/780 computer system. This compared with 2 to 5 minutes needed to generate an image from any of the individual channels. It should be pointed out that some of this time was due to the program reading the satellite data from tape, but there are many calculations done to derive the channel 3 reflectance. This routine could be put to use directly on a minicomputer system with a graphics capability and would generate analyses in a reasonable time period for operational purposes provided enough disk storage were available for the data, and provided that the scale were reduced from what was presented here. RTNEPH cannot use this routine directly as written because the processing is so much different. RTNEPH processes the visible satellite data and makes a cloud decision based on a comparison of reflectance at an analysis point with a climatological background reflectance for that point. If the analysis has a greater reflectance than the background value, a positive decision is made. Of course this procedure fails when the background is snow because there is no difference in reflectance. Adding a component that is called only for points that are snow-covered could be the solution to this problem. This component would process near-infrared reflectance from the satellite data and compare this with a background near-infrared reflectance. This study confirms the very low near-infrared reflectance of snow compared with the relatively high near-infrared reflectance of clouds so this approach could be used with a great deal of success, however, implementation of this depends on the availability of a data base of near-infrared reflectances as discussed above.

APPENDIX A
SYMBOLS AND CONSTANTS

1. SYMBOLS

θ_o ..... solar zenith angle
θ ..... satellite zenith angle
φ ..... relative azimuth angle
L ..... observed radiance
B(T) ..... Planck function
I ..... incident solar radiance
E ..... solar spectral irradiance
ε ..... emissivity
r ..... reflectance
$r(\theta_o,\theta,\varphi)$ ..... directional reflectance
τ ..... transmissivity
f ..... anisotropic reflectance factor
ρ_l ..... percentage of a pixel covered by clear land
ρ_c ..... percentage of a pixel covered by liquid clouds
ρ_i ..... percentage of a pixel covered by ice clouds
ρ_s ..... percentage of a pixel covered by snow
λ ..... wavelength
ν ..... wavenumber
T ..... brightness temperature
F_T ..... channel 3/channel 4 brightness temperature factor

2. CONSTANTS

h = Planck's constant ..... 6.6262×10^{-34} Joule sec
K = Boltzmann's constant ..... 1.3806×10^{-23} Joule/deg
c = velocity of light ..... 2.99793×10^{8} meter/sec

APPENDIX B
CALCULATION OF AVHRR CHANNEL 3 RADIANCE

Fig. B.1 shows the solar spectral irradiance for the channel 3 spectral band, from measurements taken by Thekaekara *et al.* (1969) at an altitude of 11.58 kilometers. Irradiance values were converted to wavenumber units since channel 3 AVHRR data are calibrated in those units. Since there is no significant absorption below that altitude, these values were assumed to be the incident solar irradiance at the earth's surface. Linear interpolation was used to give values at wavenumbers for which response functions are reported.

The following equation was used to calculate the normalized irradiance for channel 3:

$$E_3(\nu) = \sum_{i=1}^{N} E(\nu_i)\varphi(\nu_i)\Delta\nu_i / \sum_{i=1}^{N} \varphi(\nu_i)\Delta\nu_i \qquad \text{(B.1)}$$

where $\varphi(\nu_i)$ is the spectral response for each interval in the band. Figs. B.2 and B.3 show the normalized spectral response for NOAA-9 and NOAA-10 channel 3 taken from Lauritson *et al.* (1979). Assuming isotropic radiation, the solar radiance was found by:

$$I_3(\nu) = E_3(\nu)/\pi \qquad \text{(B.2)}$$

Using these equations the normalized radiance for NOAA-9 is 5.31085 $mW/m^2 \cdot cm^{-1} \cdot sr$, and for NOAA-10 the normalized radiance is 5.26415 $mW/m^2 \cdot cm^{-1} \cdot sr$.

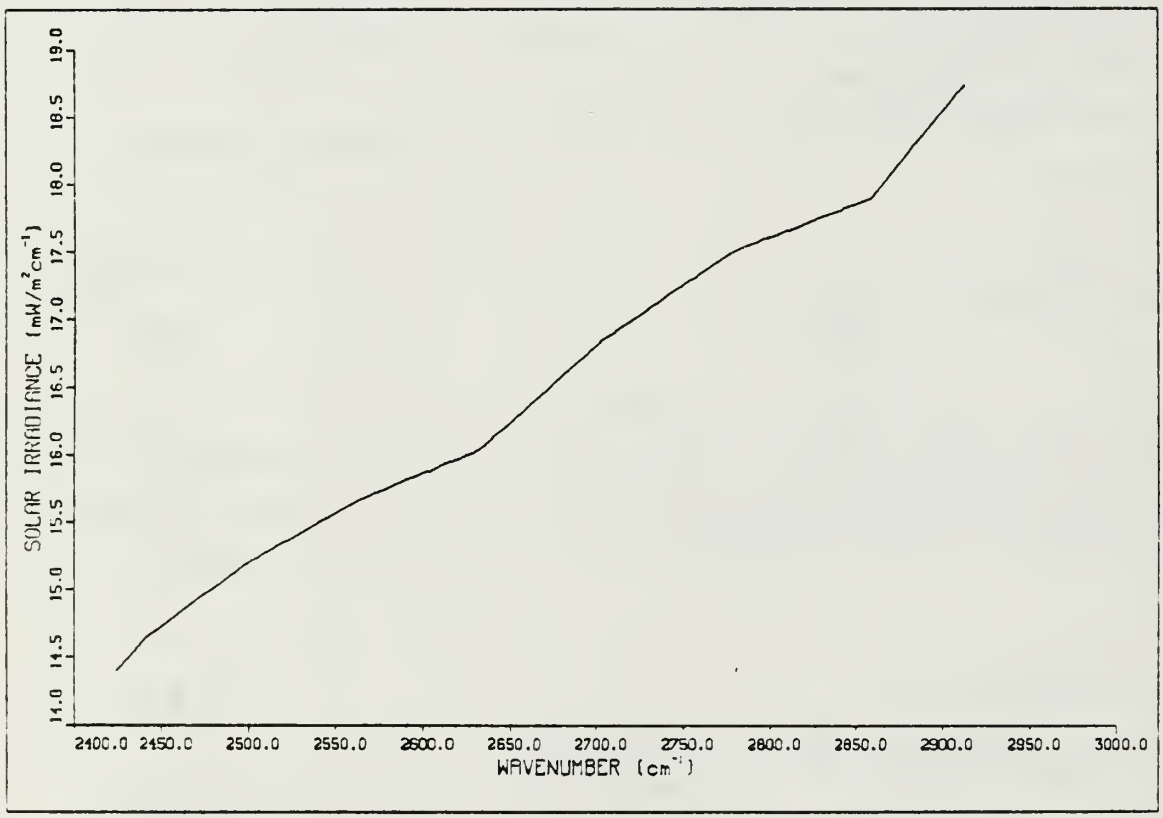

Fig. B.1 Solar spectral irradiance for NOAA-9 and NOAA-10 channel 3 spectral bands.

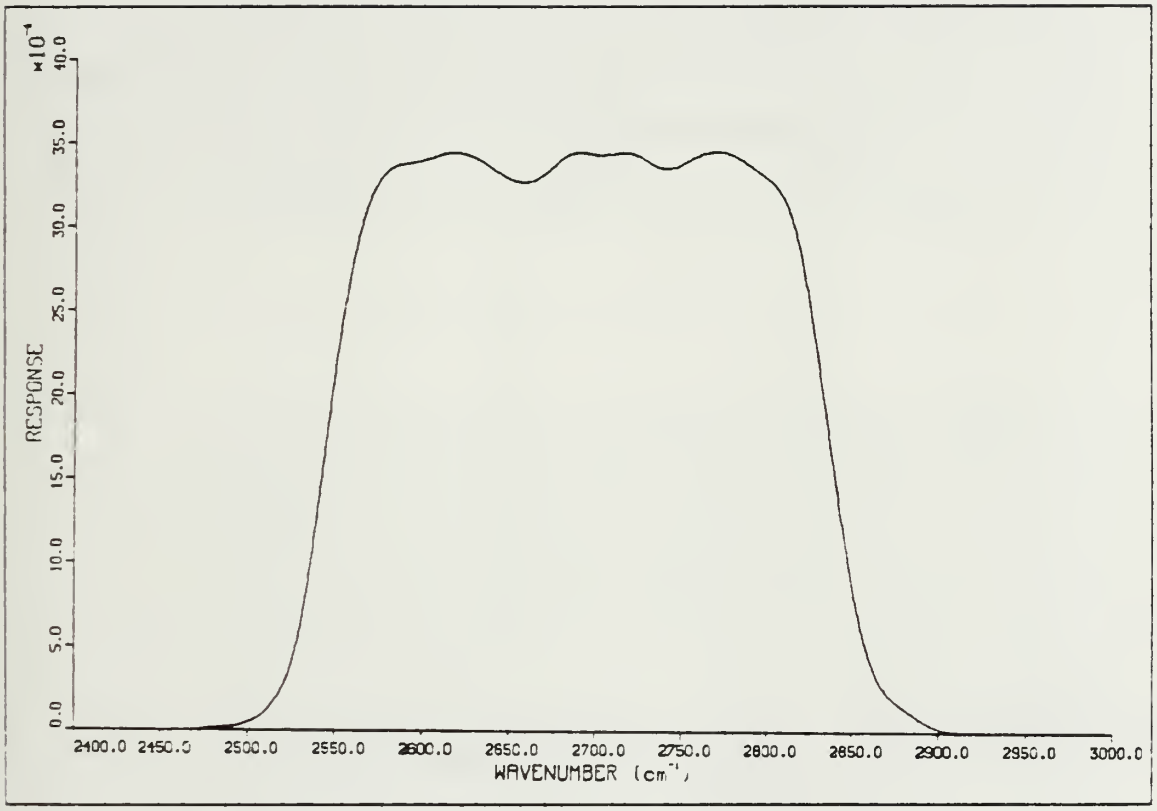

Fig. B.2 Channel 3 (NOAA-9) normalized spectral response.

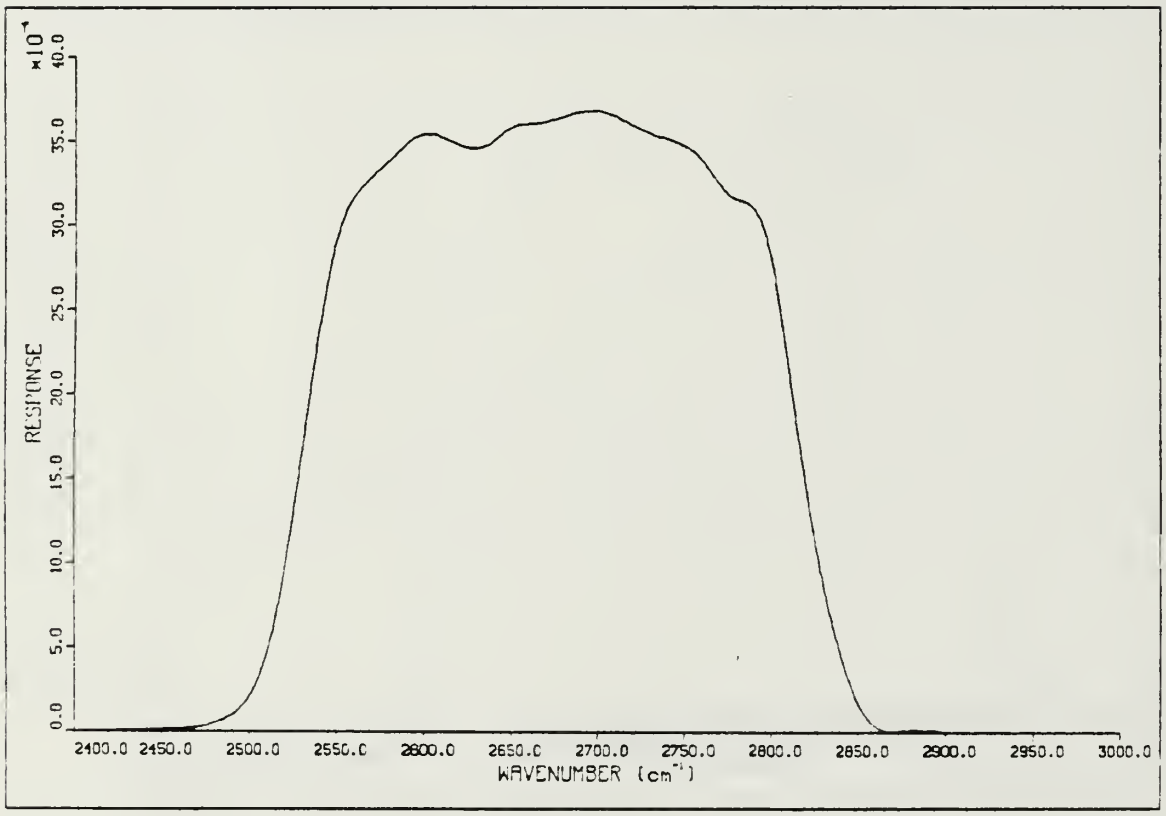

Fig. B.3 Channel 3 (NOAA-10) normalized spectral response.

APPENDIX C
SATELLITE IMAGES

This appendix combines all the images that were analyzed and verified in this thesis in one convenient location. Included with all analyses are the coincident visible and infrared images for comparison. Also included is an image of channel 3 brightness temperature. The analyses that were presented in Chapter IV are presented again here and the snow-covered areas are enhanced to show the difference between snow-covered and clear land. This illustrates the advantage of displaying land, snow, and clouds on a unique range of grayshade values. Any range of values can be enhanced as desired by the analyst and even various color enhancement schemes can be easily employed by displaying in this manner.

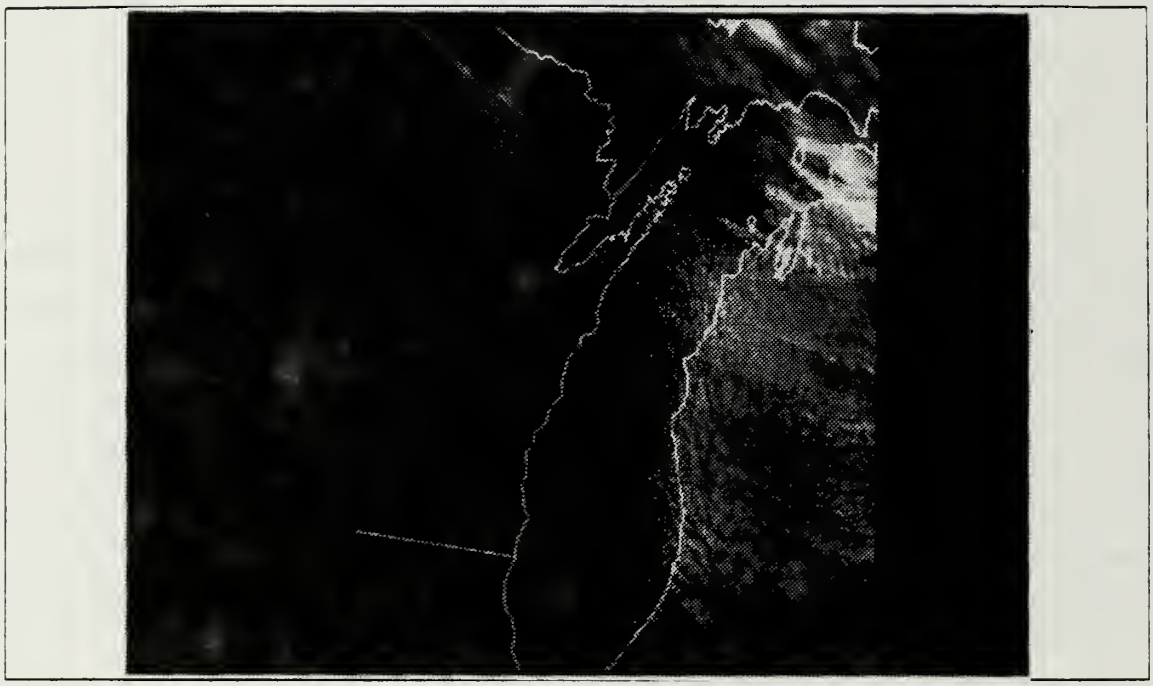

Fig. C.1 9 Nov 86 subscene 1, NOAA-9 AVHRR channel 1 reflectance.

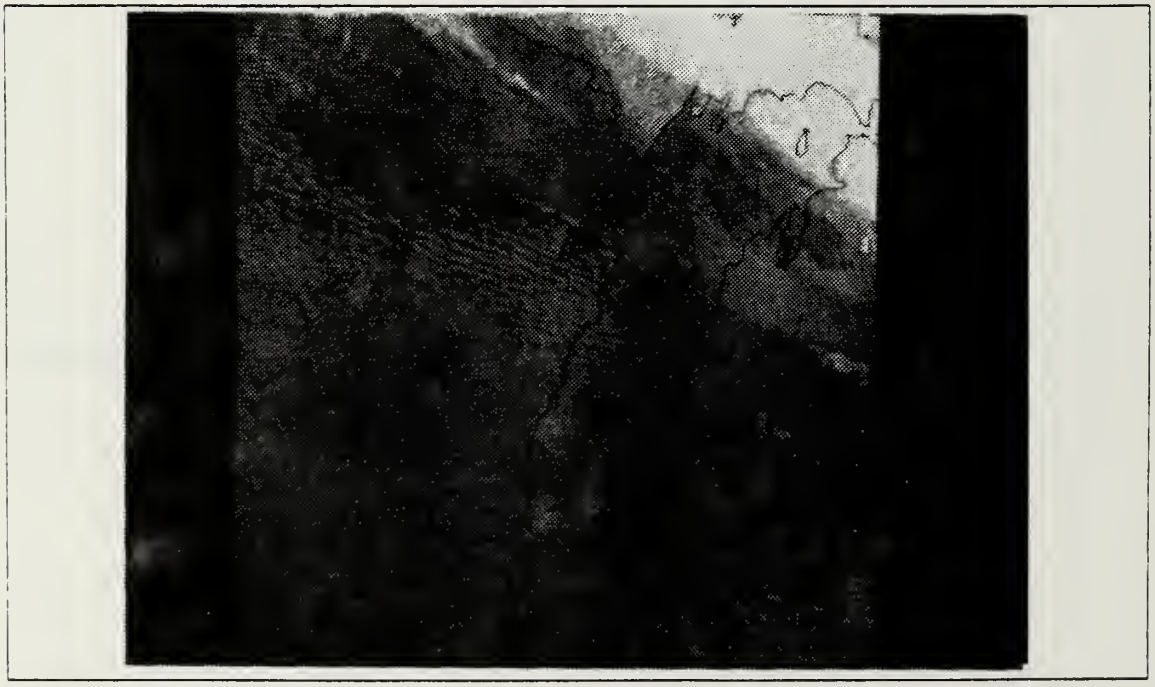

Fig. C.2 9 Nov 86 subscene 1, NOAA-9 AVHRR channel 3 brightness temperature.

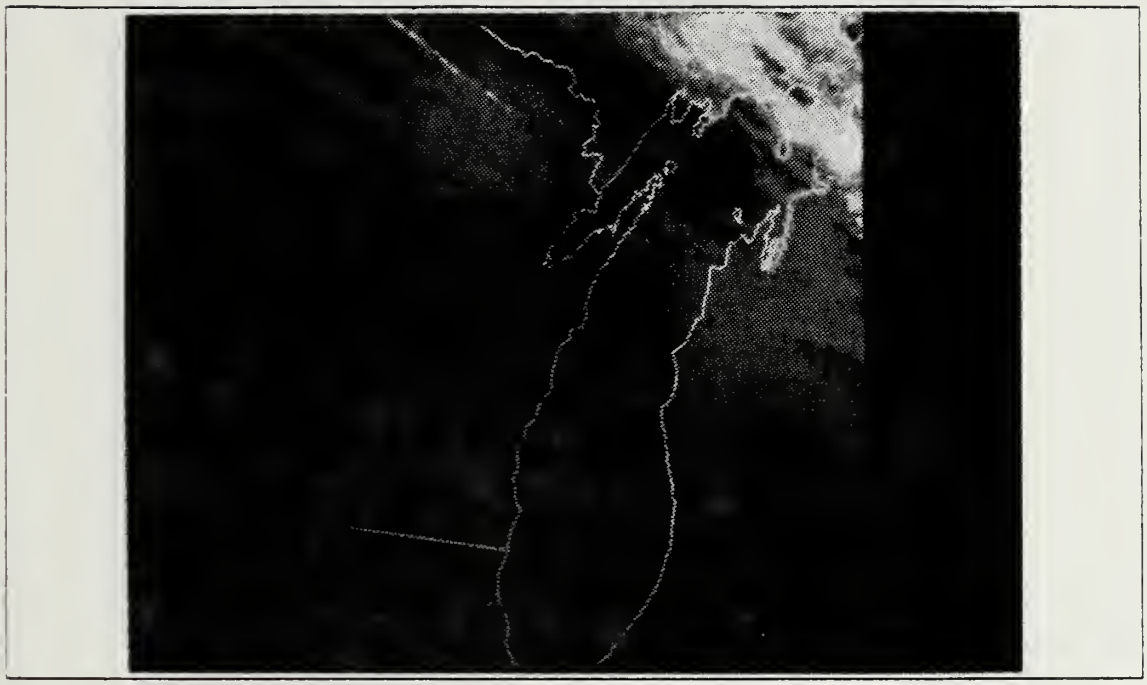

Fig. C.3 9 Nov 86 subscene 1, NOAA-9 AVHRR channel 4 brightness temperature.

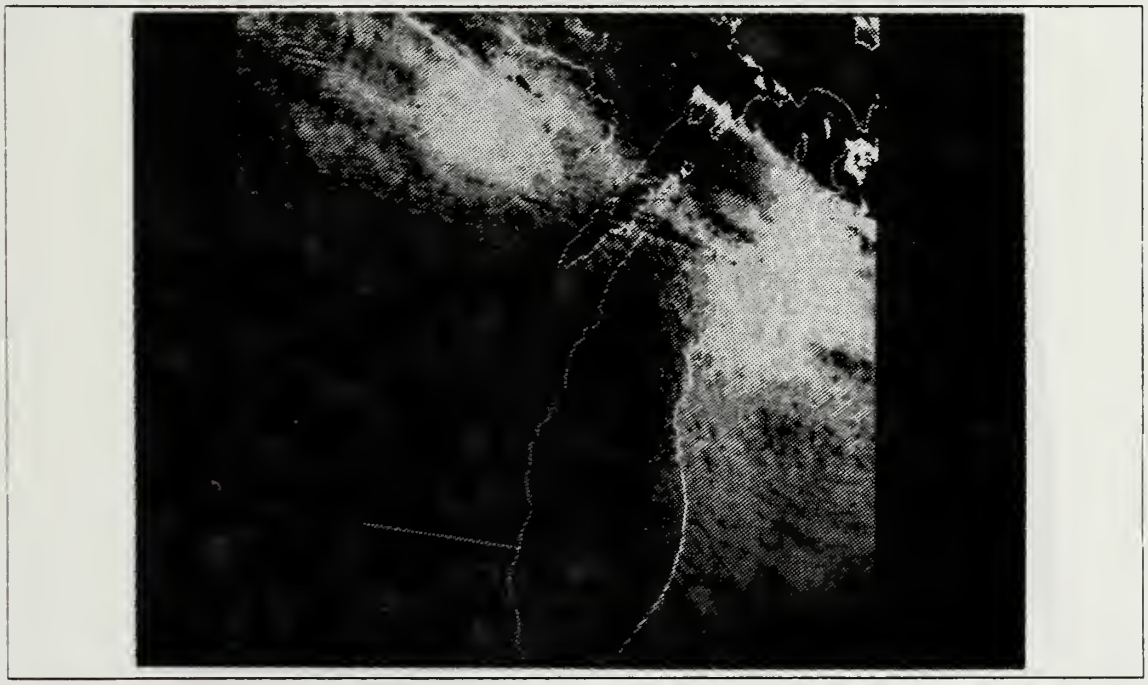

Fig. C.4 9 Nov 86 subscene 1, results of cloud cover analysis.

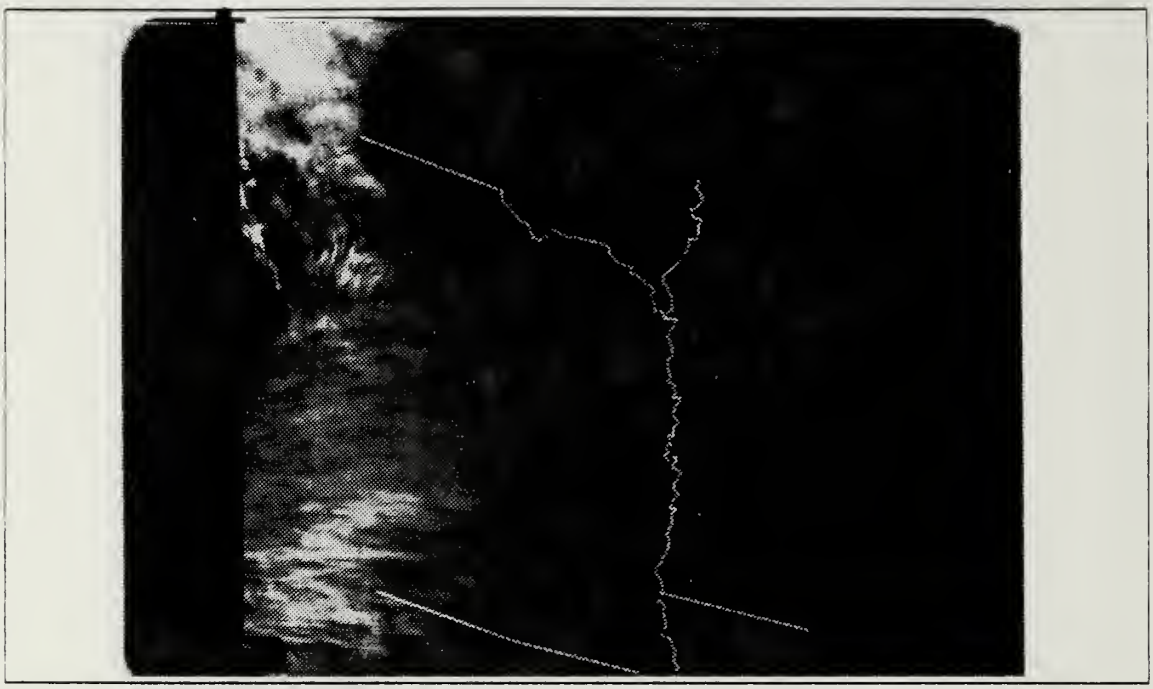

Fig. C.5 Same as Fig. C.1 for 9 Nov 86 subscene 2.

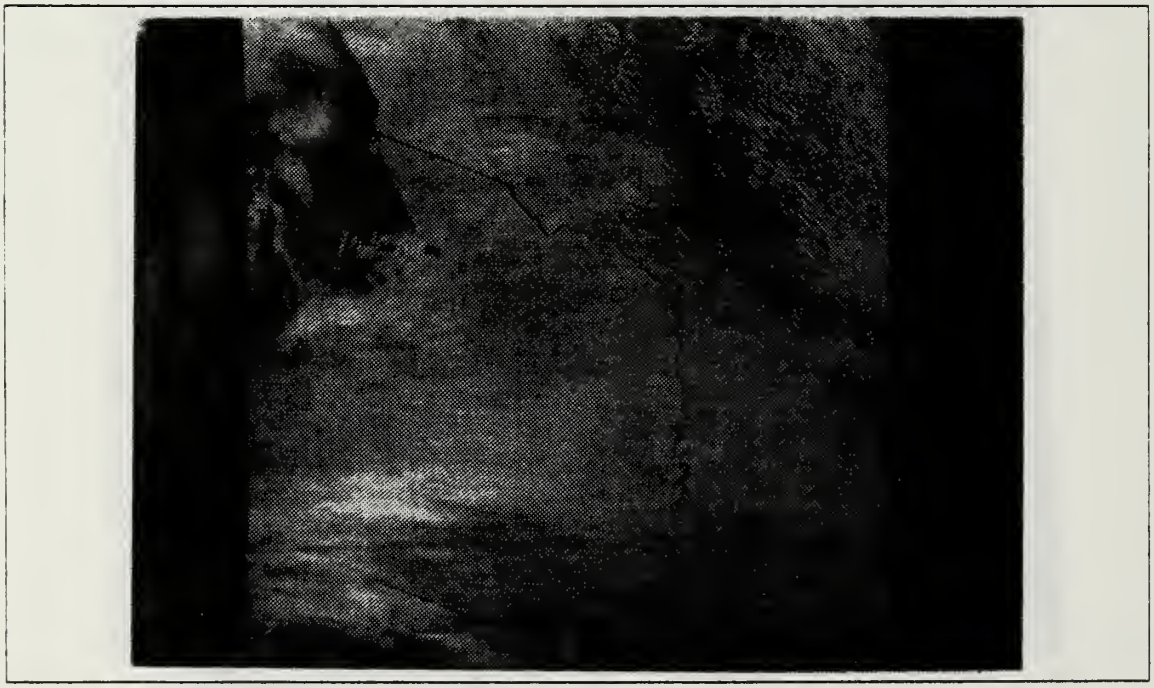

Fig. C.6 Same as Fig. C.2 for 9 Nov 86 subscene 2.

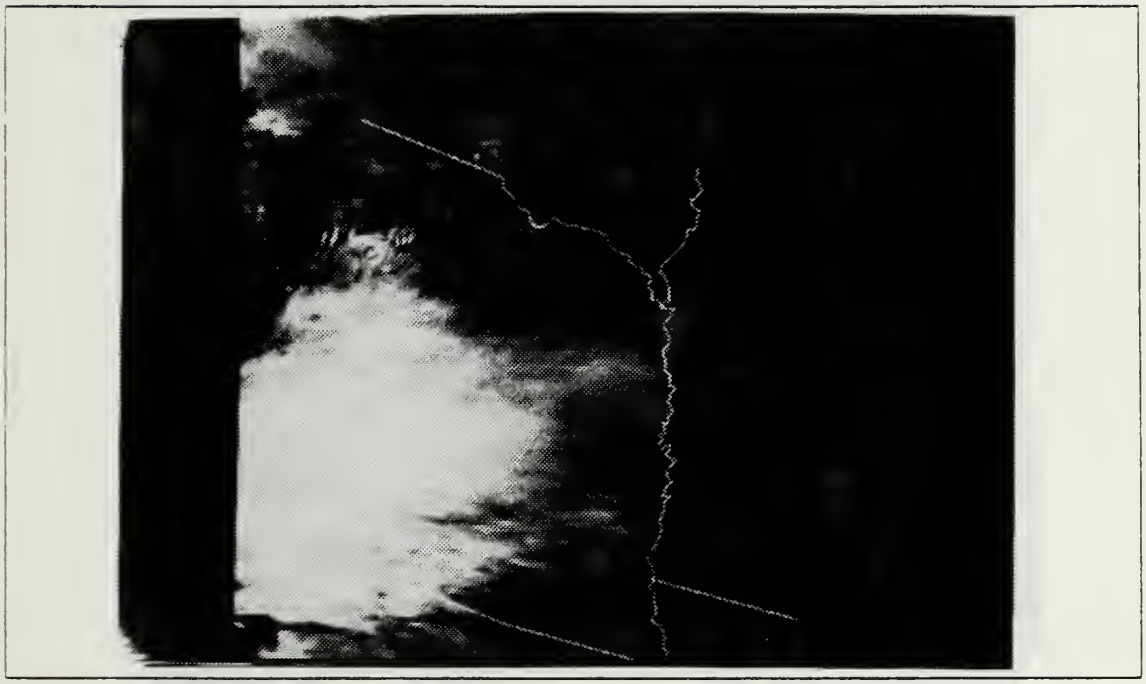

Fig. C.7 Same as Fig. C.3 for 9 Nov 86 subscene 2.

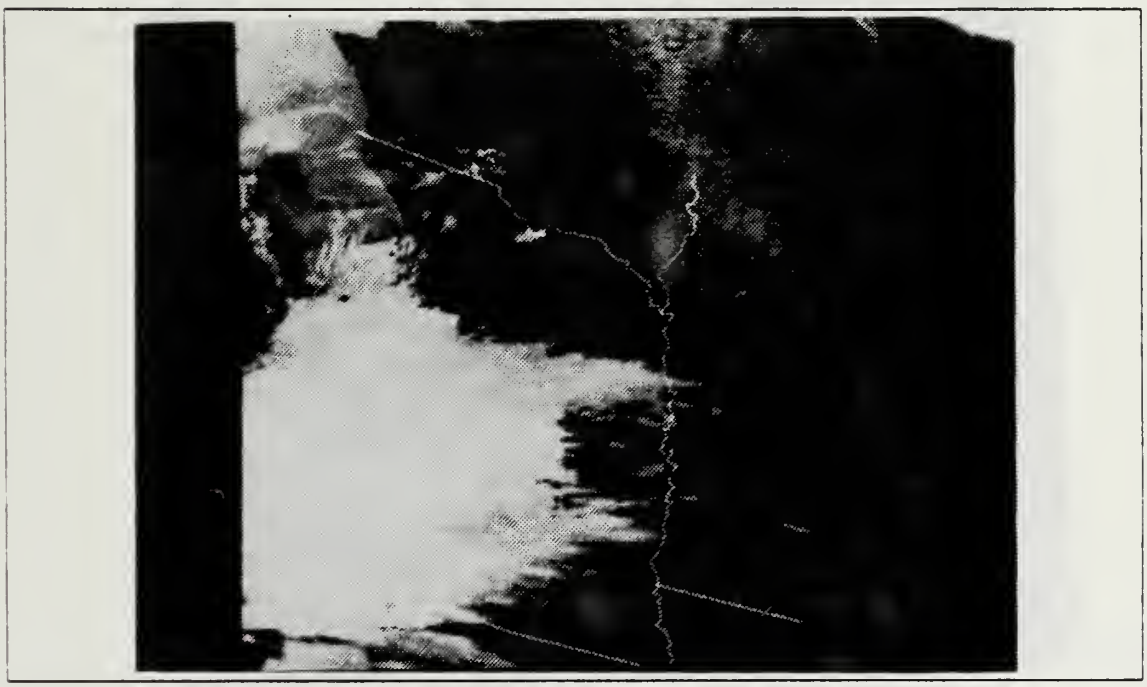

Fig. C.8 Same as Fig. C.4 for 9 Nov 86 subscene 2.

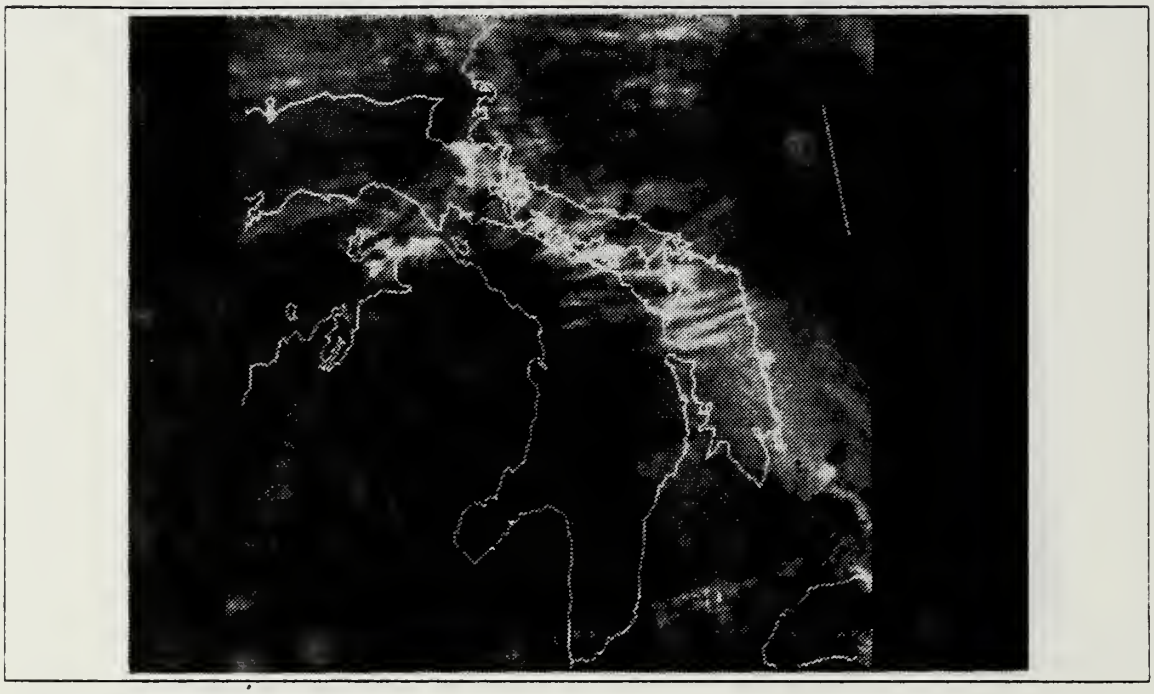

Fig. C.9 Same as Fig. C.1 for 10 Nov 86 subscene 1.

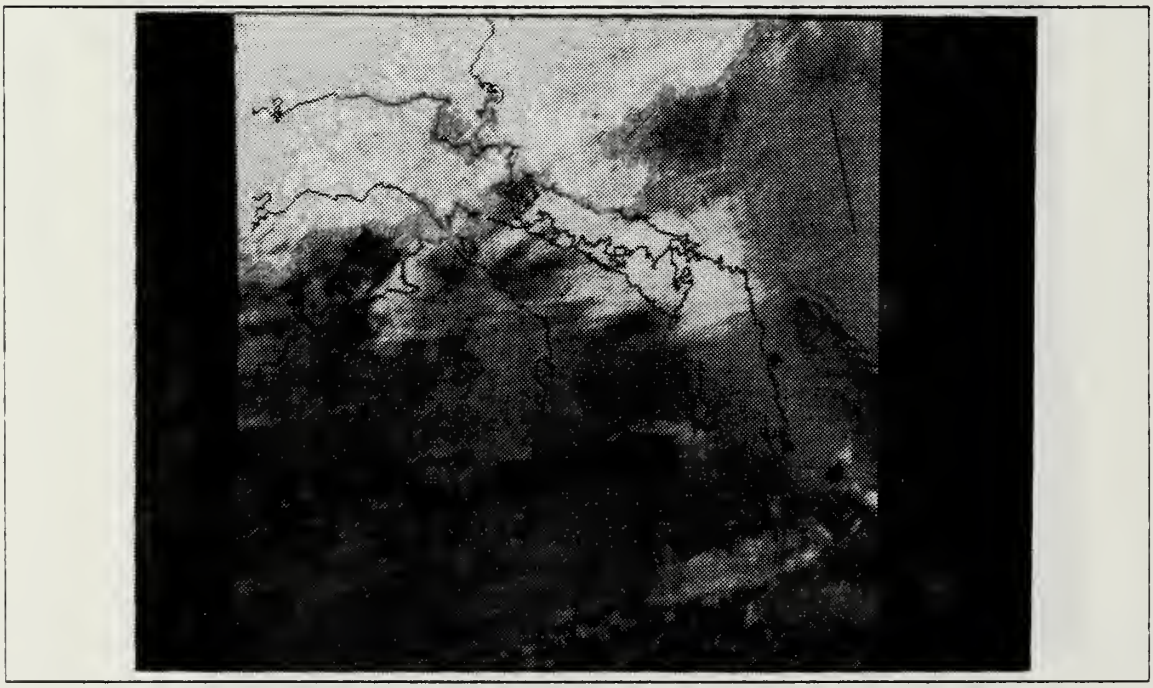

Fig. C.10 Same as Fig. C.2 for 10 Nov 86 subscene 1.

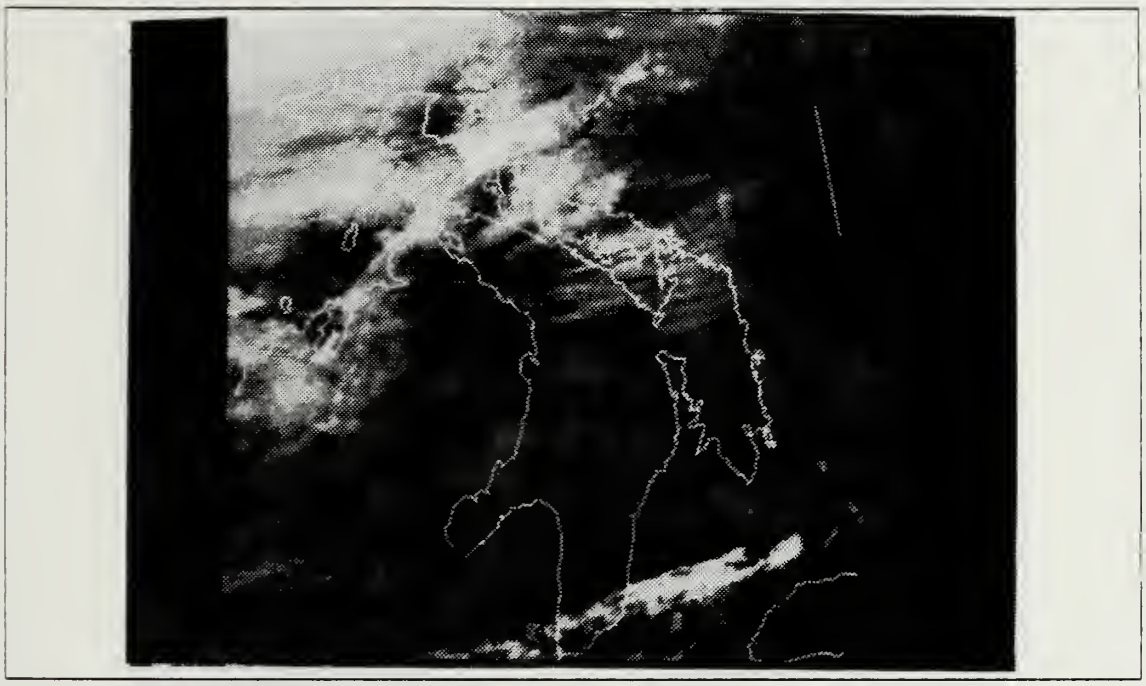

Fig. C.11 Same as Fig. C.3 for 10 Nov 86 subscene 1.

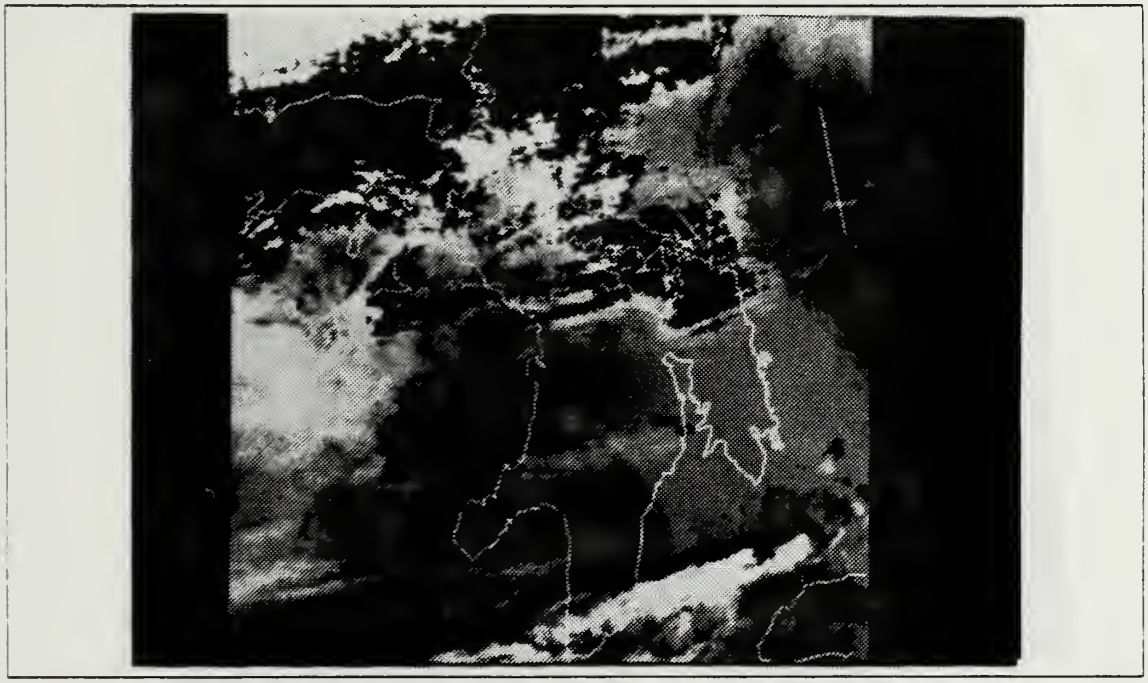

Fig. C.12 Same as Fig. C.4 for 10 Nov 86 subscene 1.

Fig. C.13 Same as Fig. C.1 for Case 1.

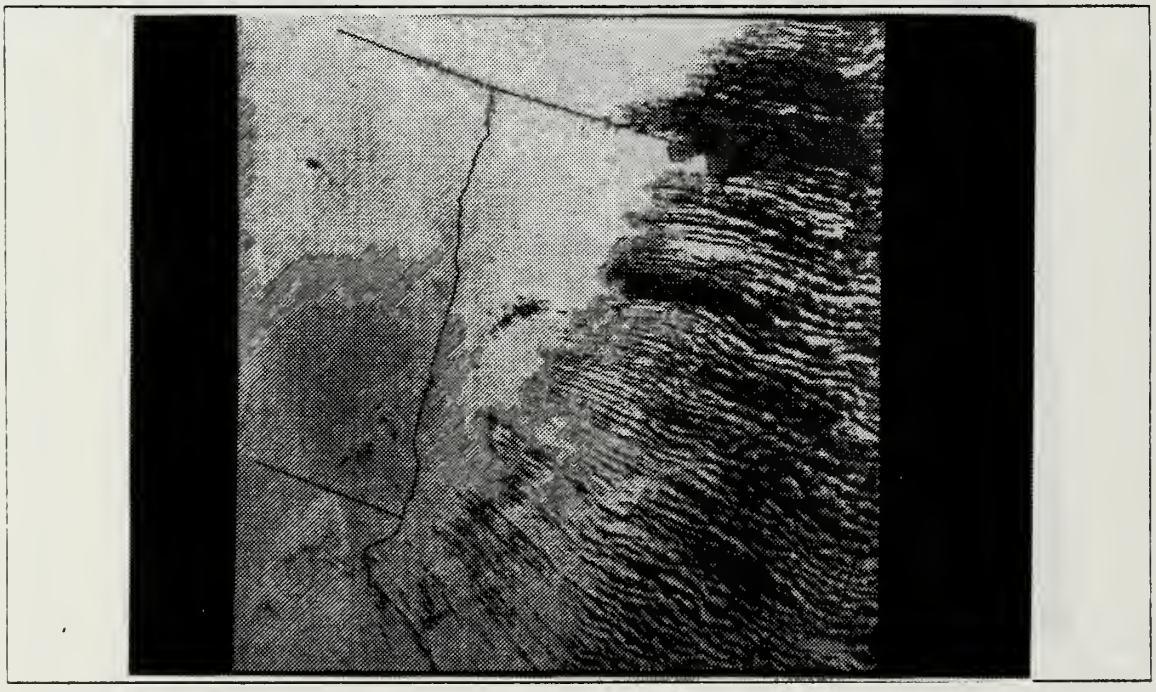

Fig. C.14 Same as Fig. C.2 for Case 1.

Fig. C.15 Same as Fig. C.3 for Case 1.

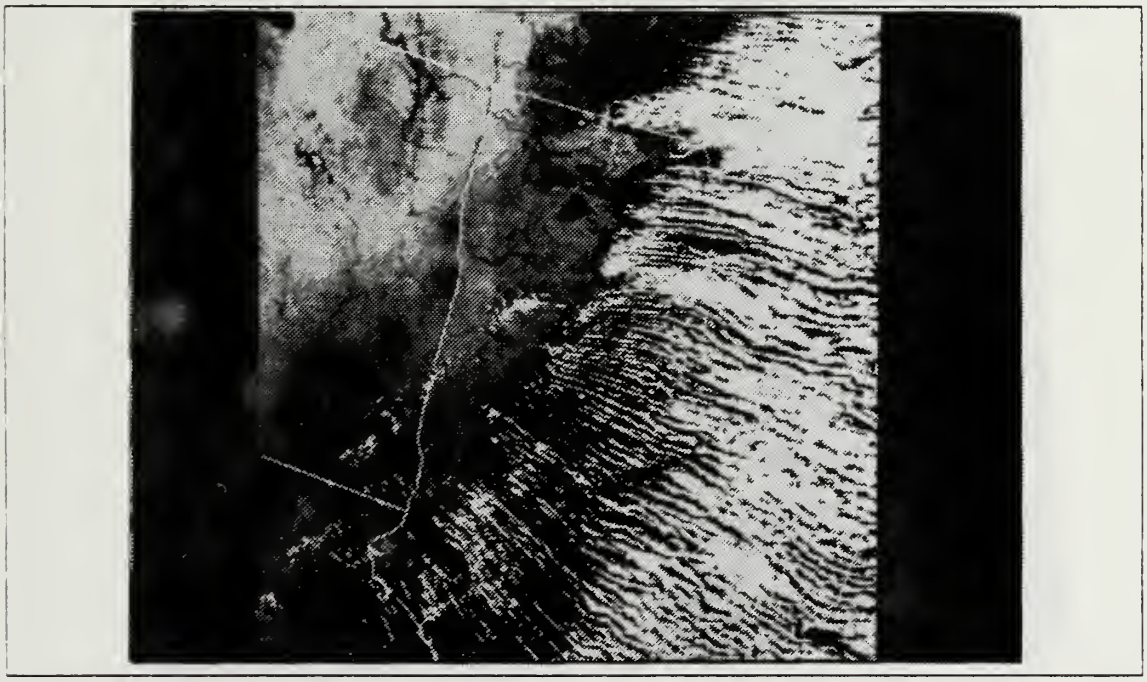

Fig. C.16 Same as Fig. C.4 for Case 1.

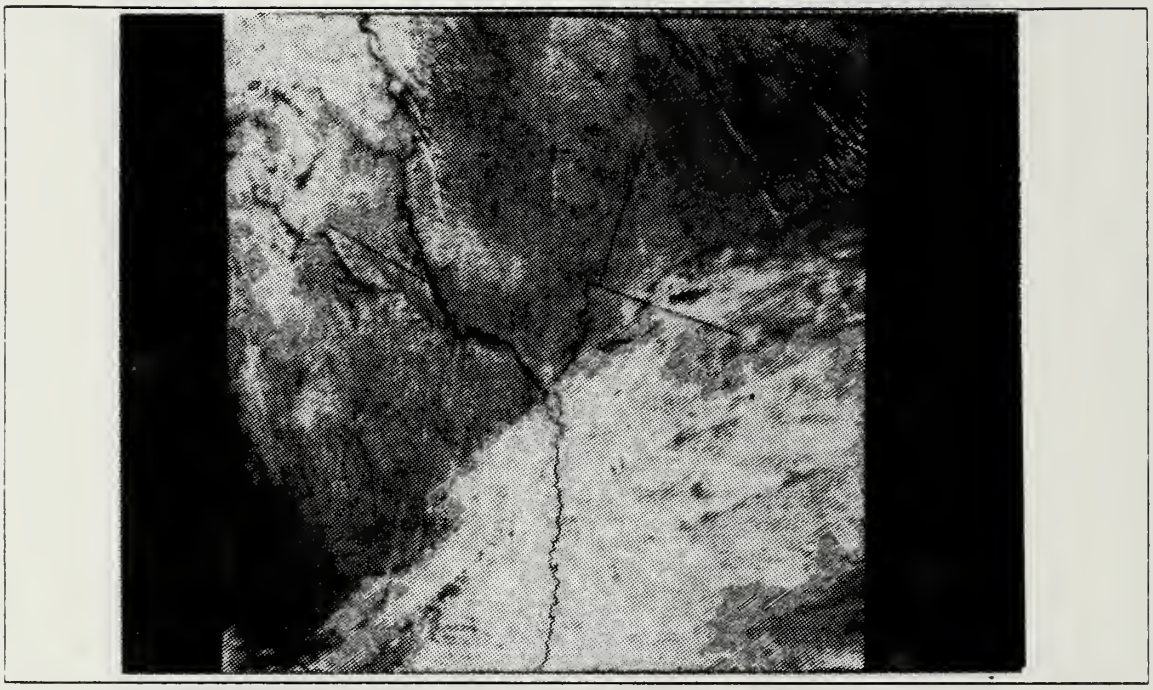

Fig. C.17 Same as Fig. C.1 for Case 2.

Fig. C.18 Same as Fig. C.2 for Case 2.

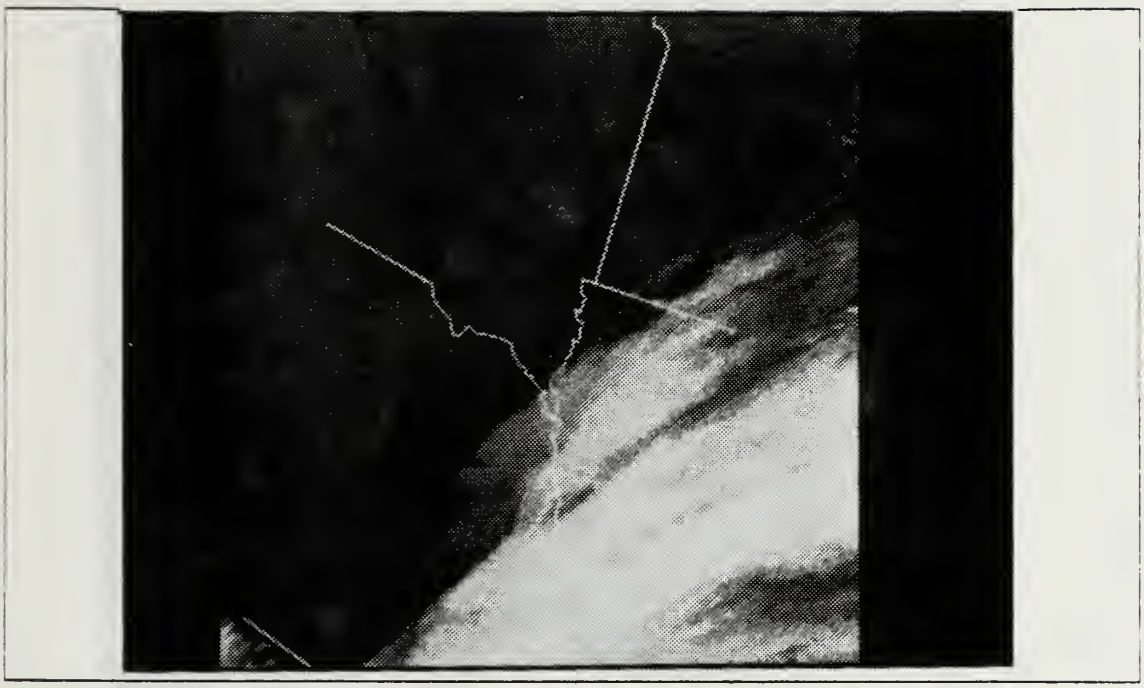

Fig. C.19 Same as Fig. C.3 for Case 2.

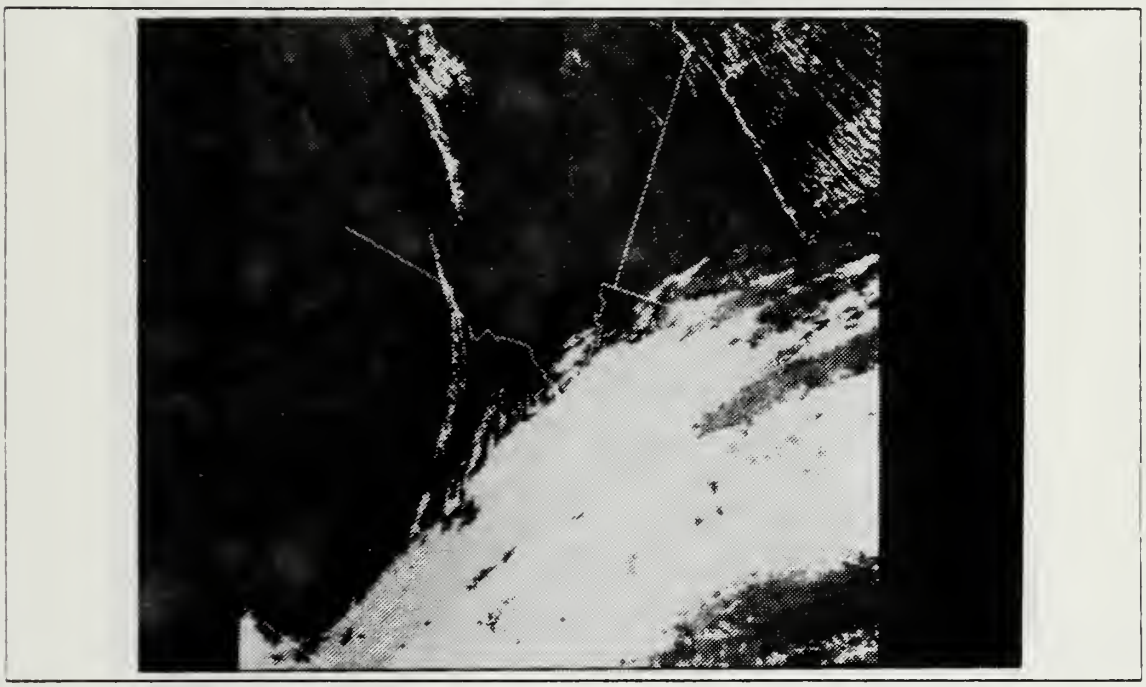

Fig. C.20 Same as Fig. C.4 for Case 2.

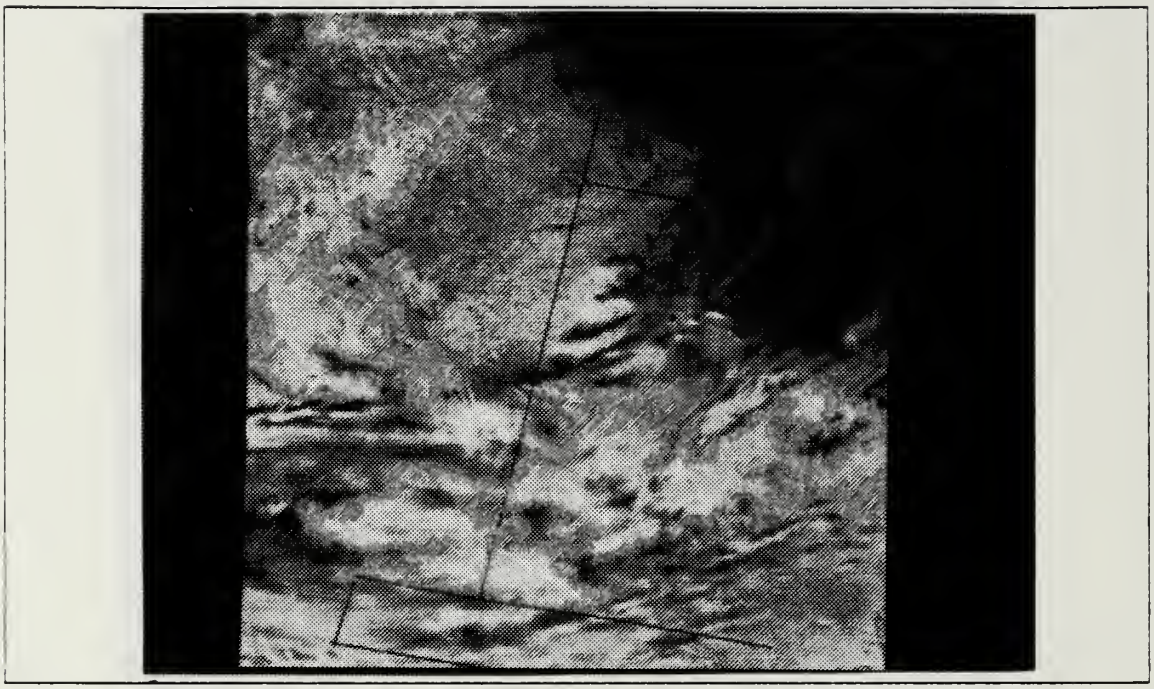

Fig. C.21 Same as Fig. C.1 for Case 3.

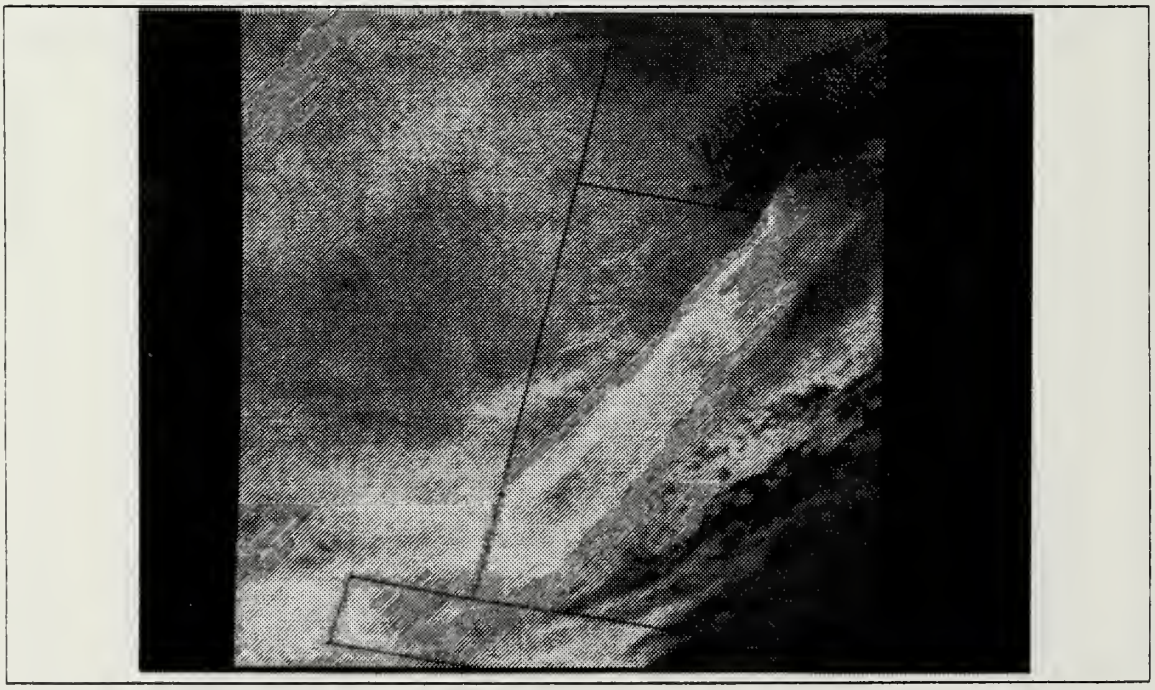

Fig. C.22 Same as Fig. C.2 for Case 3.

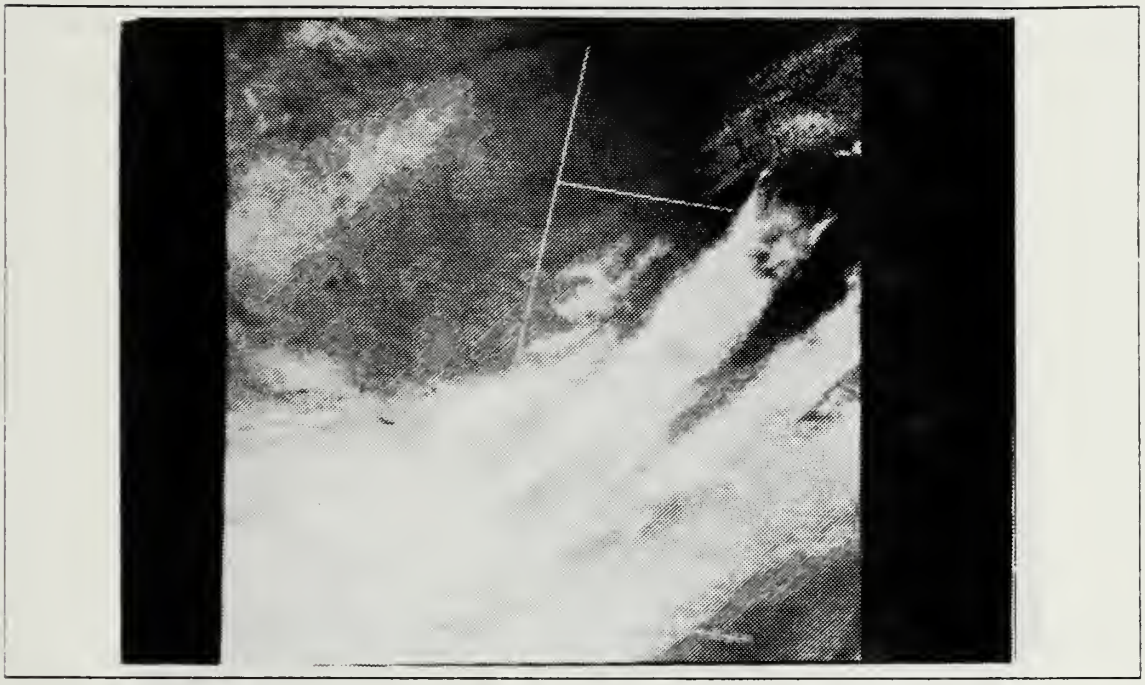

Fig. C.23 Same as Fig. C.3 for Case 3.

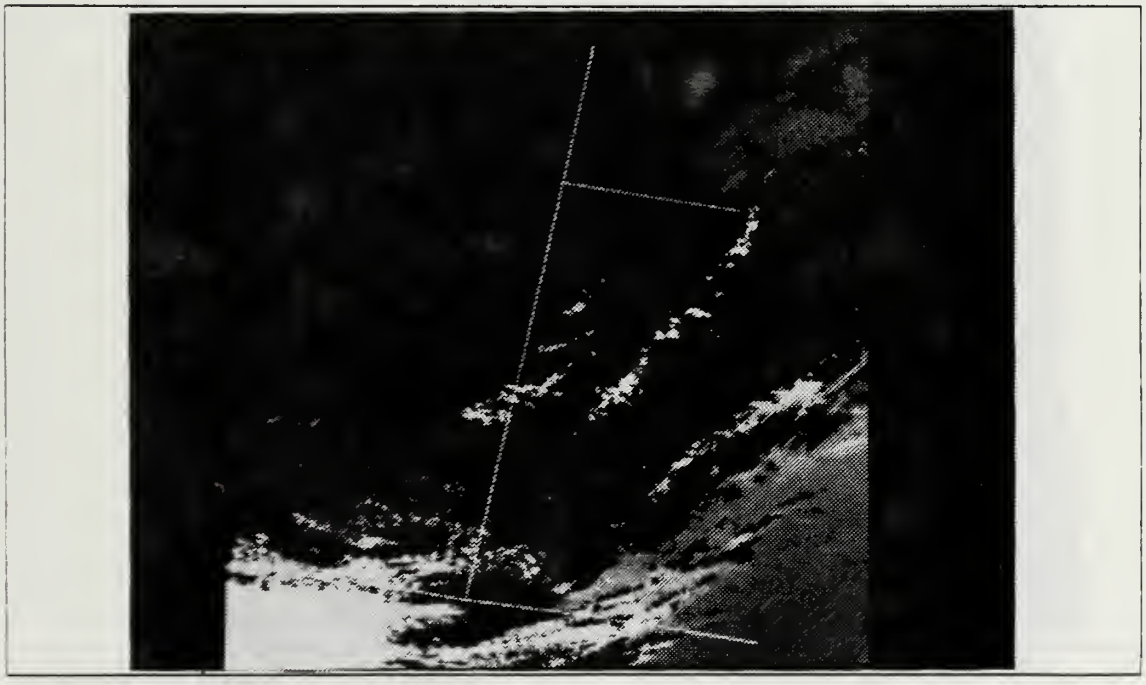

Fig. C.24 Same as Fig. C.4 for Case 3.

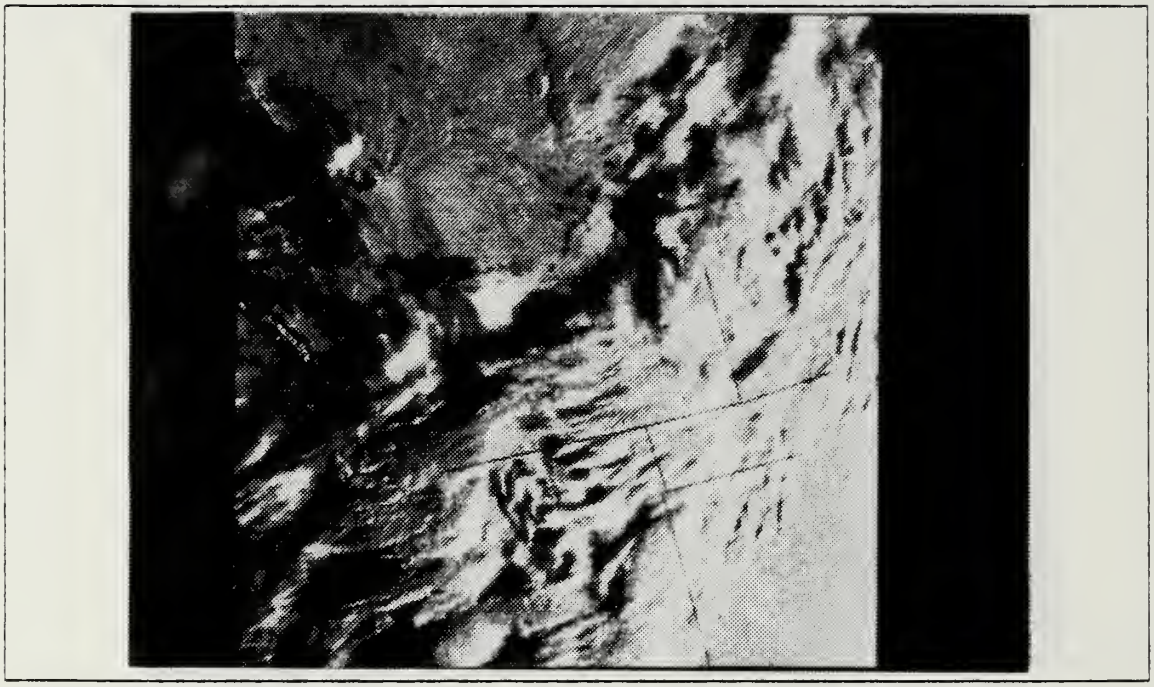

Fig. C.25 Same as Fig. C.1 for Case 4.

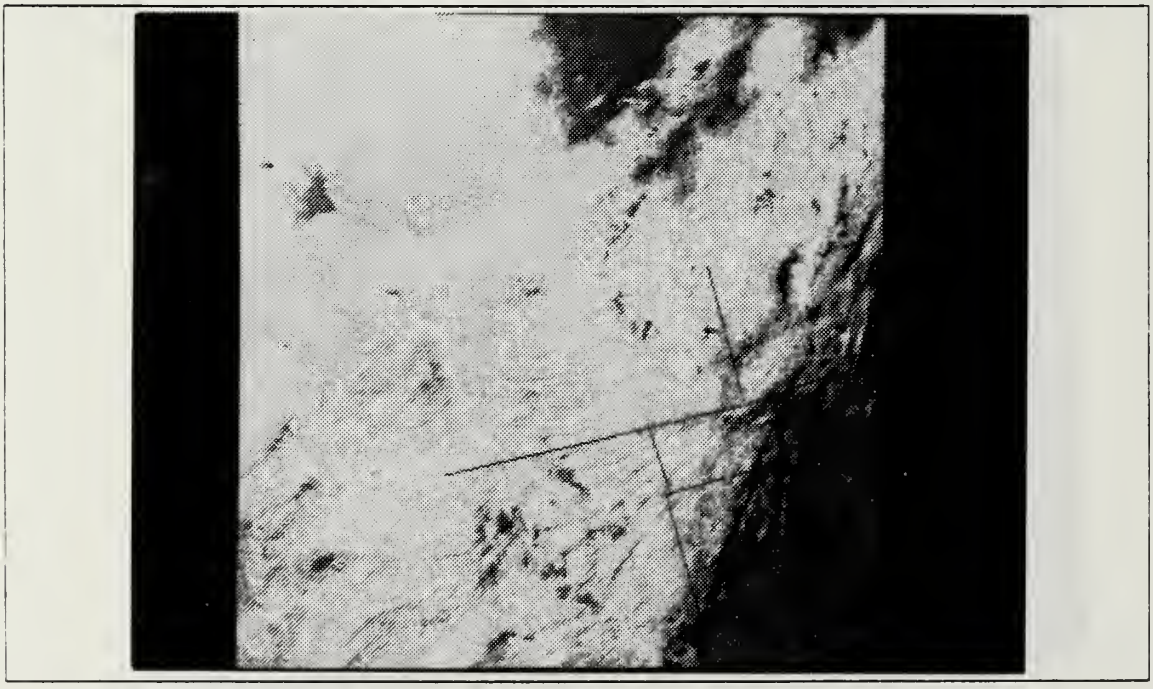

Fig. C.26 Same as Fig. C.2 for Case 4.

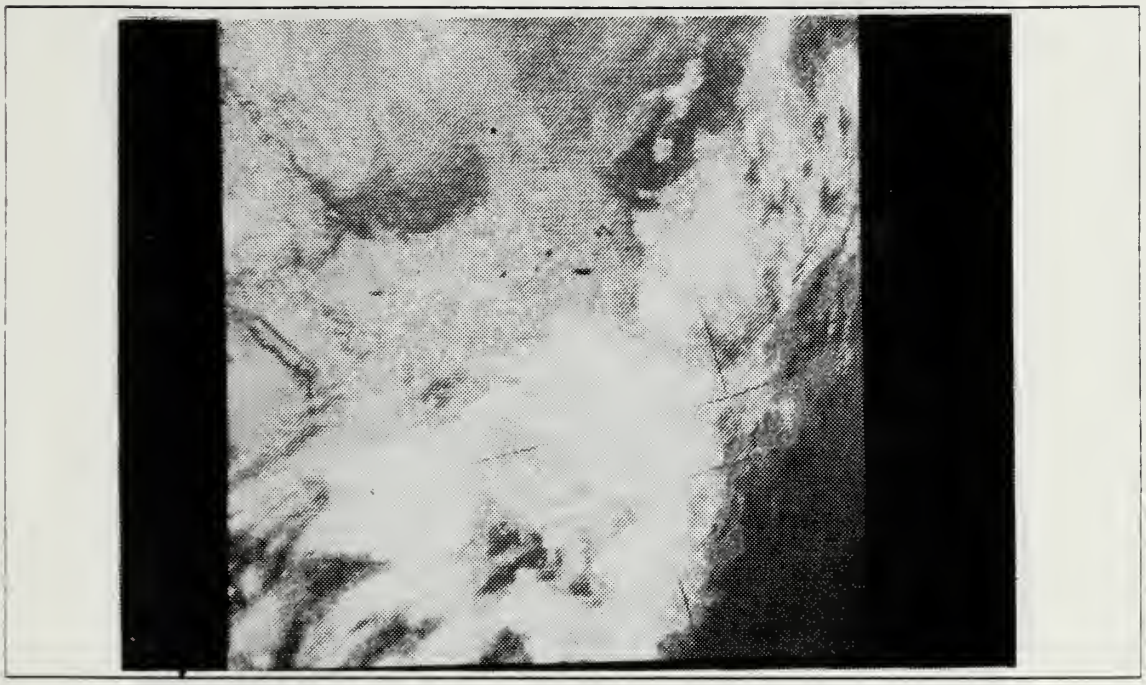

Fig. C.27 Same as Fig. C.3 for Case 4.

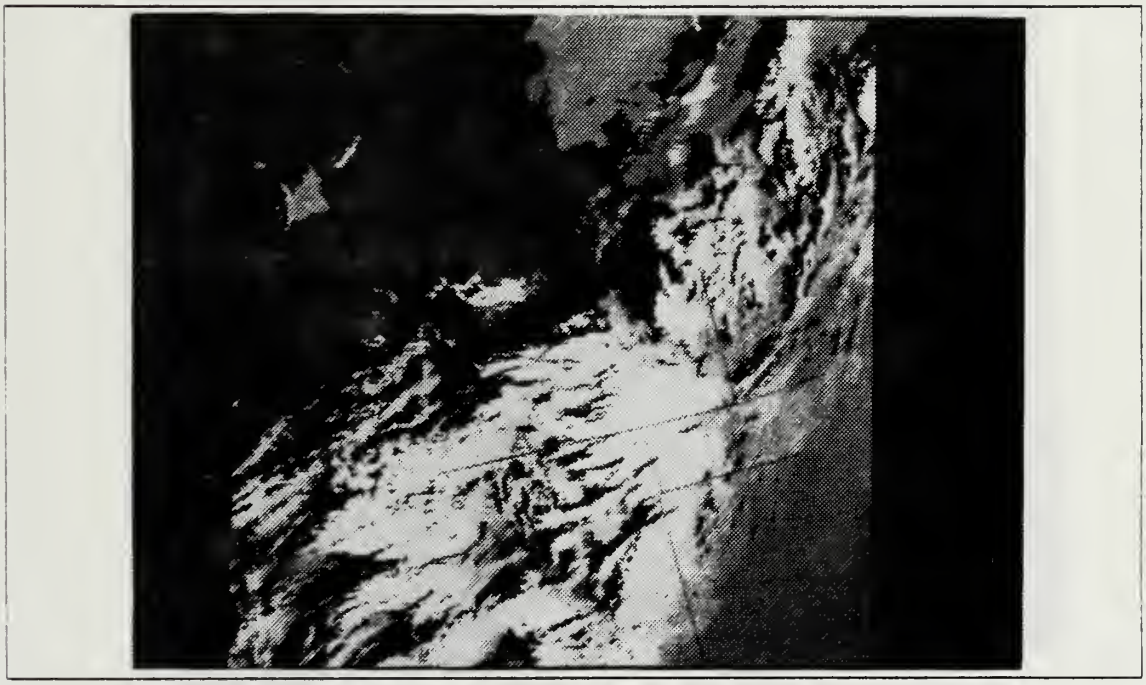

Fig. C.28 Same as Fig. C.4 for Case 4.

Fig. C.29 Same as Fig. C.1 for Case 5.

Fig. C.30 Same as Fig. C.2 for Case-5.

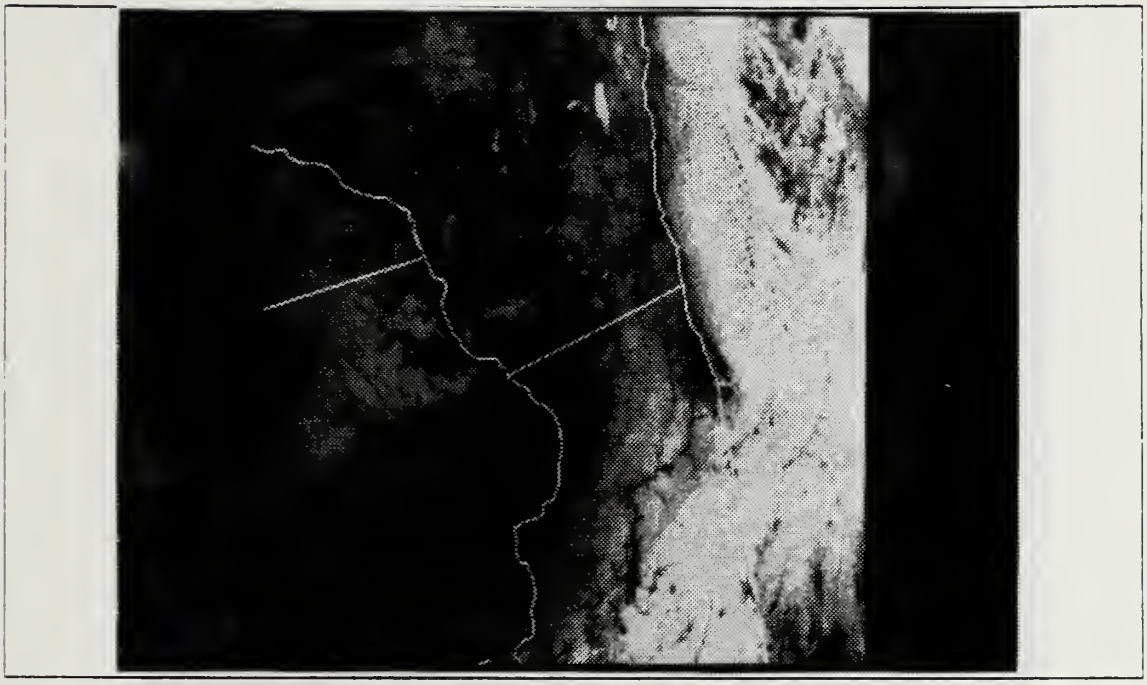

Fig. C.33 Same as Fig. C.1 for Case 6.

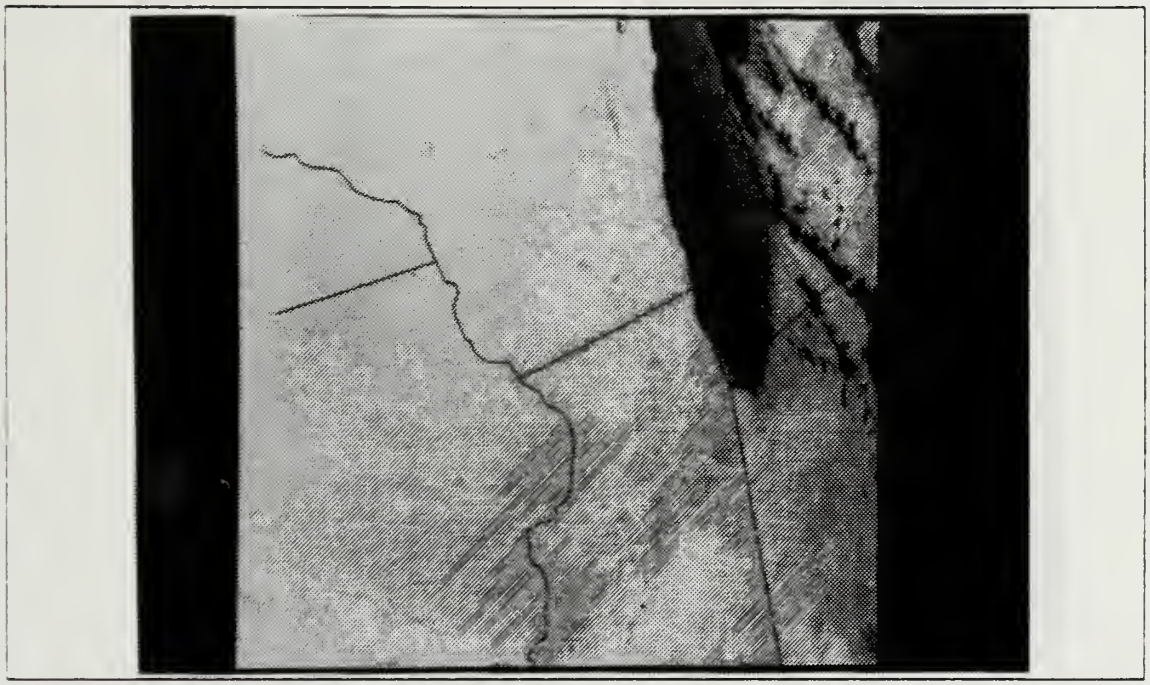

Fig. C.34 Same as Fig. C.2 for Case 6.

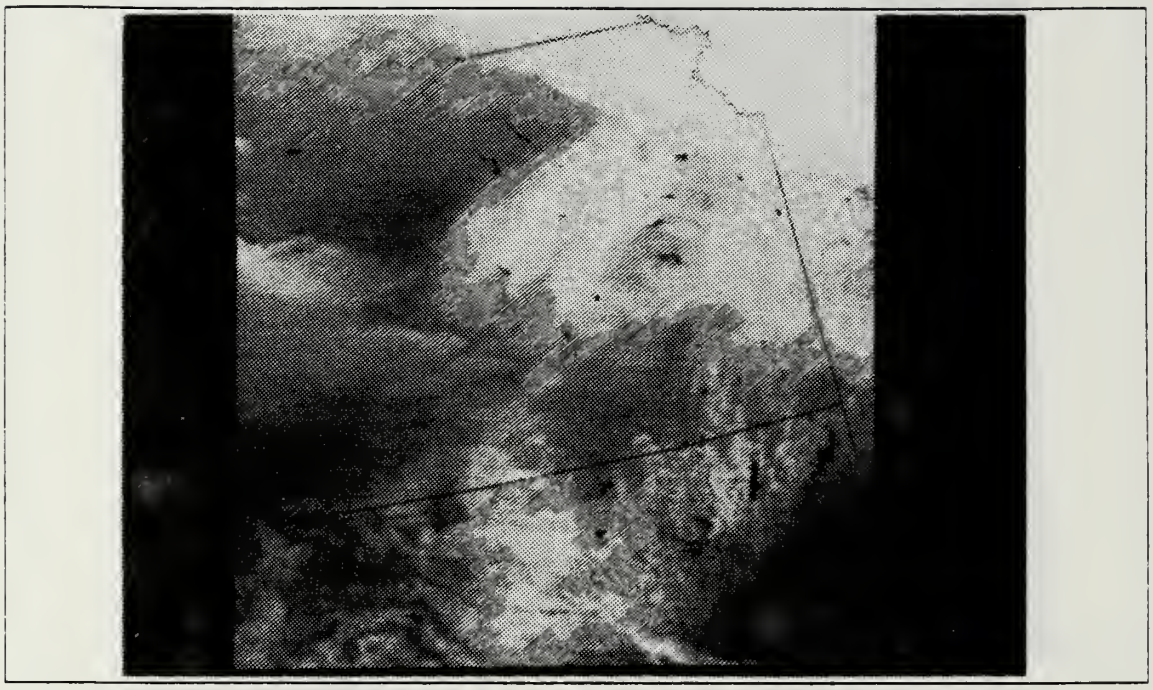

Fig. C.31 Same as Fig. C.3 for Case 5.

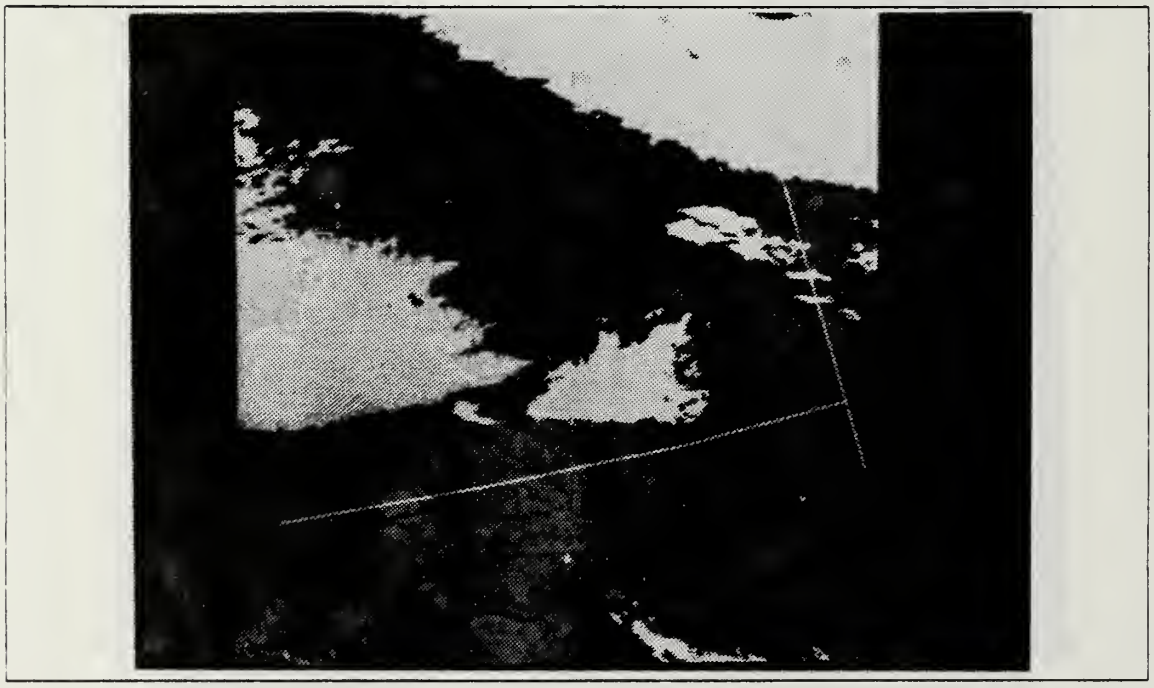

Fig. C.32 Same as Fig. C.4 for Case 5.

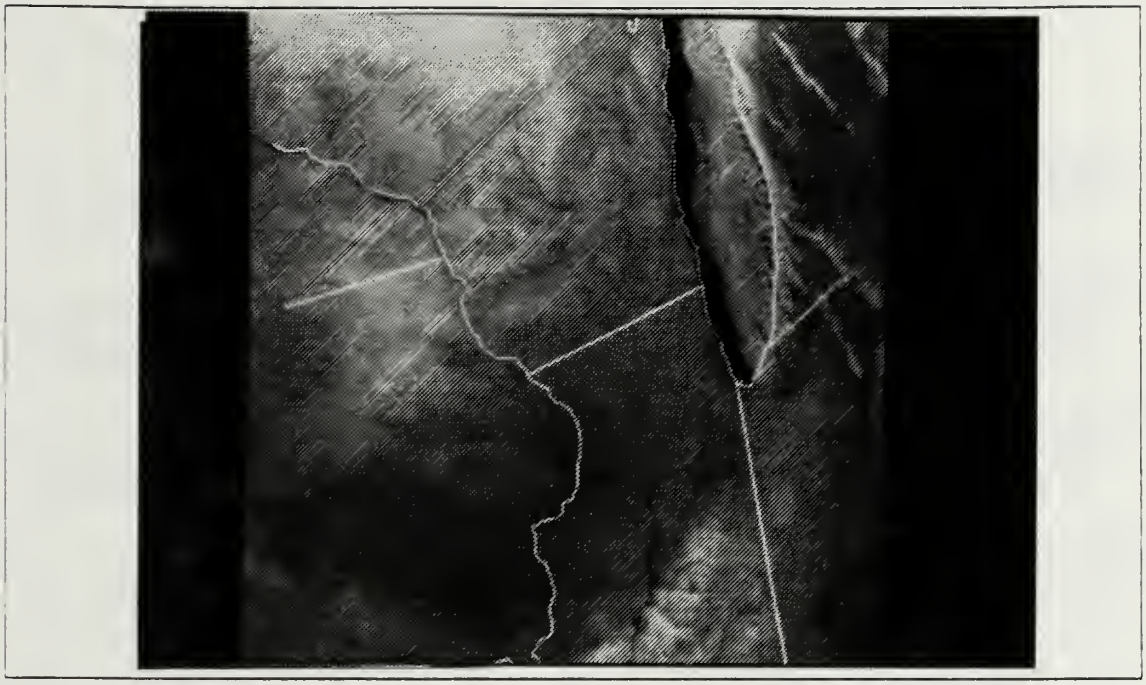

Fig. C.35 Same as Fig. C.3 for Case 6.

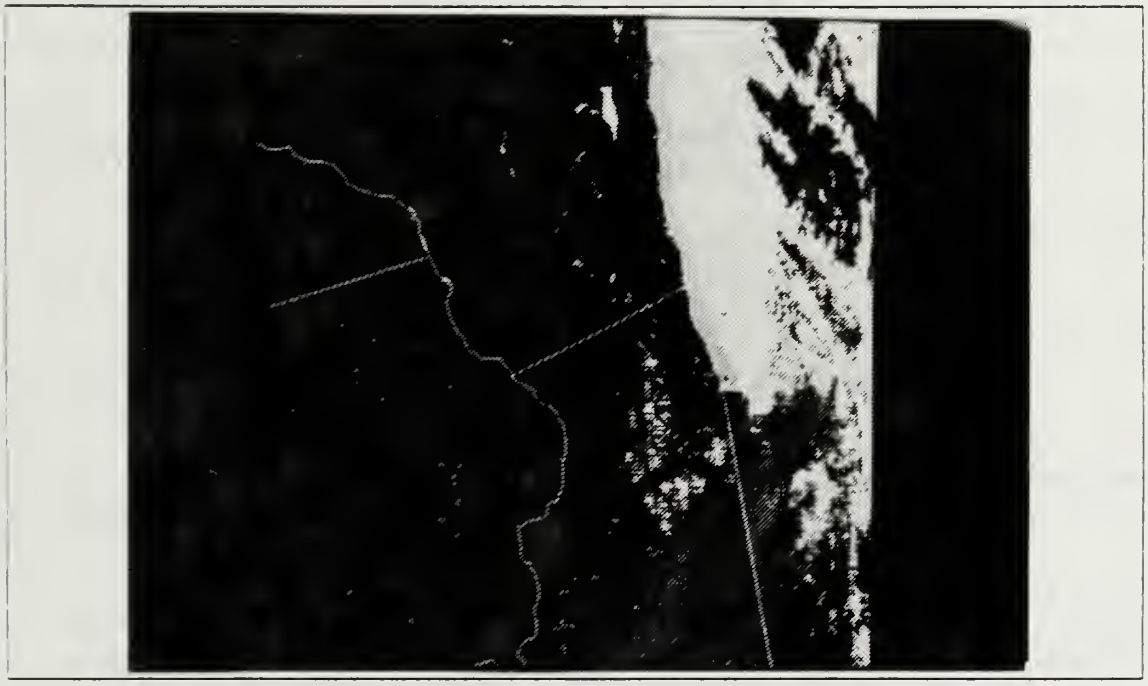

Fig. C.36 Same as Fig. C.4 for Case 6.

LIST OF REFERENCES

Arking, Albert and Jeffrey D. Childs, 1985: Retrieval of cloud cover parameters from multispectral satellite images. *J. Climate Appl. Meteor.*, **24**, 322-333.

Bunting, James T., Francis R. Valovcin, and Thomas J. Keegan, 1977: Meteorological Satellite Measurements and Applications. Air Force Geophysics Laboratory Tech. Rep. 77-0035, 17 pp.

Bunting, James T. and Robert P. d'Entremont, 1982: Improved cloud detection utilizing Defense Meteorological Satellite Program near infrared measurements. Air Force Geophysics Laboratory Tech. Rep. 82-0027, 91 pp.

Bunting, J. T. and K. R. Hardy, 1984: Cloud identification and characterization from satellites. *Satellite Sensing of a Cloudy Atmosphere: Observing the Third Planet.* (Ann Henderson-Sellers, Ed.), Taylor & Francis, London and Philadelphia, pp 203-240.

Bunting, James T., 1986: Personal communication. Air Force Geophysics Laboratory, Hanscom AFB, MA.

Fye, Falko K., 1978: The AFGWC Automated Cloud Analysis Model. Air Force Global Weather Central Tech. Mem. 78-002, 97 pp.

Gerald, Curtis F. and Patrick O. Wheatley, 1984: *Applied Numerical Analysis (Third Edition)*. Addison-Wesley Publishing Co., Inc., Reading, MA, pp. 191-196.

Hansen, James E. and James B. Pollack, 1970: Near-infrared light scattering by terrestrial clouds. *J. Atmos. Sci.*, **27**, 265-281.

Kidder, Stanley Q. and Huey-Tz'u Wu, 1984: Dramatic contrast between low clouds and snow cover in daytime 3.7μm imagery. *Mon. Wea. Rev.*, **112**, 2345-2346.

Lauritson, Levin, Gary J. Nelson, and Frank W. Porto, 1979: Data extraction and calibration of TIROS-N/NOAA radiometers. NOAA Technical Memorandum NESS 107, U.S. Dept. of Commerce, Washington, D.C., Appendix B.

Ruff, Irwin and Arnold Gruber, 1983: Multispectral identification of clouds and earth surfaces using AVHRR radiometric data. *Preprints Fifth Conf. on Atmospheric Radiation*, American Meteorological Society, Baltimore, MD, 31 October - 4 November 1983.

Shettle, E. P. and J. A. Weinman, 1970: The transfer of solar irradiance through inhomogeneous turbid atmospheres evaluated by Eddington's approximation. *J. Atmos. Sci.*, **27**, 1048-1055.

Stephens, Graeme L., 1981: The transfer of 3.7μm radiation through model cirrus clouds. *Preprints Fourth Conf. on Atmospheric Radiation*, American Meteorological Society, Toronto, Ont, Canada, 16 - 18 June 1981.

Taylor, V. R. and L. L. Stowe, 1984: Atlas of reflectance patterns for uniform earth and cloud surfaces (NIMBUS-7 ERB--61 Days). NOAA Tech. Rep. NESDIS-10, U. S. Dept. of Commerce, Washington, D.C., 66 pp.

Thekaekara, M. P., R. Kruger, and C. H. Duncan, 1969: Solar irradiance measurements from a research aircraft. *Appl. Opt.*, **8**, 1713-1732.

Warren, Stephen G. and Warren J. Wiscombe, 1980: A model for the spectral albedo of snow. II: Snow containing atmospheric aerosols. *J. Atmos. Sci.*, **37**, 2734-2745.

Wash, Carlyle H., Laura A. Spray, and Lang C. Chou, 1985: Satellite cloud and precipitation analysis using a minicomputer. NPS-63-85-003, Naval Postgraduate School, Monterey, CA, 90 pp.

Welch, Ronald M., Stephen K. Cox, and John M. Davis, 1980: Solar radiation and clouds. *Meteor. Monogr.*, No. 39, Amer. Meteor. Soc., 96 pp.

Wiscombe, Warren J. and Stephen G. Warren, 1980: A model for the spectral albedo of snow. I: Pure snow. *J. Atmos. Sci.*, **37**, 2712-2733.

INITIAL DISTRIBUTION LIST

		No. Copies
1.	Defense Technical Information Center Cameron Station Alexandria, VA 22304-6145	2
2.	Library, Code 0142 Naval Postgraduate School Monterey, CA 93943-5002	2
3.	USAFETAC/LD Air Weather Service Technical Library Scott AFB, IL 62225-5000	1
4.	Air Force Geophysics Laboratory AFGL/LYS Attn: Dr. J. T. Bunting Hanscom AFB, MA 07131-5000	2
5.	Headquarters Air Force Global Weather Central AFGWC/SDDC Offutt AFB, NE 68113-5000	1
6.	Headquarters Air Force Global Weather Central AFGWC/CC Offutt AFB, NE 68113-5000	1
7.	Headquarters Air Weather Service AWS/CC Scott AFB, IL 62225-5000	1
8.	Air Force Institute of Technology AFIT/CIR Wright-Patterson AFB, OH 45433-5000	1
9.	Capt. Robert C. Allen, Jr. Headquarters Air Force Systems Command AFSC/DLWS Andrews AFB, MD 20334-5000	5
10.	Professor Philip A. Durkee (63De) Naval Postgraduate School Monterey, CA 93943-5000	5
11.	Professor Carlyle H. Wash (63Wx) Naval Postgraduate School Monterey, CA 93943-5000	5

12.	Professor Thomas H. Vonder Haar (63Tv) Naval Postgraduate School Monterey, CA 93943-5000	1
13.	Professor Robert J. Renard (63Rd) Naval Postgraduate School Monterey, CA 93943-5000	1
14.	Department of Meteorology Reference Library Naval Postgraduate School Monterey, CA 93943-5000	1
15.	Naval Environmental Prediction Research Facility Reference Library Monterey, CA 93943-5000	1